Ph.D. DEGREE in

Environmental and Energy Engineering Science

CYCLE XXXIV

HIGHLY LUMINESCENT Eu(III) COMPLEXES AS PROBES FOR BIOMOLECULAR SENSING

PhD Candidate: Martina Sanadar

Supervisor: Prof. Andrea Melchior

Co-Supervisor: Prof. Marilena Tolazzi

2022

Dedication

Dedicated to my mother and father.

Hvala vam što ste mi pružili najbolje u životu.

"Considerate la vostra semenza:

fatti non foste a viver come bruti,

ma per seguir virtute e canoscenza"

(Dante Alighieri, Inferno, Canto XXVI)

Acknowledgements

Undertaking this PhD has been a truly life-changing experience for me. Thank you Jana for starting it all!

First, I would like to say a very big thank you to my supervisor Prof. Andrea Melchior for his support, continuous guidance and meticulous suggestions. Many thanks also to Prof. Marilena Tolazzi, my co-supervisor, for the opportunity, support and encouragement.

I also would like to thank all the co-authors, which contributed to the publications related to this thesis. This manuscript would not have been possible without your priceless contribution and brilliant work. Special thanks to Prof. Fabio Piccinelli and Dr. Chiara De Rosa, from Luminescent Materials Laboratory of University of Verona, for receiving me in your research group and teaching me a lot.

I am also grateful to Dr. Célia Bonnet for hosting me in her Metal complexes and MRI research group, at the CNRS – Orleans, France. It was an honour and a real pleasure working with you. Special thanks to Harlei and Tea for making there beautiful memories together.

Thanks to the PhD students that have been in the Thermodynamics and Modelling research group with me: Gina, Matteo and Daniele, for the company and support. I wish the best to Maria and Anđela, the new PhD candidates in our research group. Thanks to the "PhD for relax" group: Lucrezia, Veronica and Vahid. I will always remember our summertime and aperitivi, the scientific and personal support. I am grateful for the good moments my friends!

To my beloved Alberto, I would like to express my thanks for being such a good mate during this journey. Thank you, my love, for always knowing what to say to me and for being by my side whenever I need a guiding hand.

Most importantly, thanks to my family. I na kraju, najveću zaslugu za ono što sam postigla pripisujem svojim roditeljima. Shvaćam da ste žrtvovali mnoge stvari za mene, i zato hvala. Nadam se da sam vas učinila ponosnim roditeljima.

Co-Authorship Statement

This thesis is generated from the collaboration of our research group, Thermodynamics and Modelling (Polytechnic Department of Engineering and Architecture, University of Udine, Italy), Fabio Piccinelli's Luminescent Materials Laboratory (Department of Biotechnology of the University of Verona, Italy), Alejandro Giorgetti's Applied Bioinformatics Laboratory (Department of Biotechnology, University of Verona, Italy) and with Alex Duerkop (Institute of Analytical Chemistry, Chemo - and Biosensors, University of Regensburg, Germany).

Potentiometric, calorimetric (ITC titrations) and spectrophotometric (UV-Vis titrations) studies, as well as ESI-MS and elemental analyses were done at the University of Udine. Computational studies (DFT) on the complexes. Have been also performed by the group of Udine. Luminescence data analysis by Excel was developed in Udine.

The ligands syntheses and most of the luminescence studies have been performed at the University of Verona. During several visits at the research group of the University of Verona I had the pleasure collaborate in the organic synthesis and some luminescence experiments. I kindly acknowledge Dr. Chiara De Rosa for her effort and work. Part of the sensing experiments were done in the laboratory of prof. Duerkop in the University of Regensburg, Germany.

Molecular Dynamics Simulations have been done in the University of Verona by the Applied Bioinformatics Laboratory.

Sommario

L'applicazione di composti luminescenti basati su ioni lantanidi è estremamente attrattiva grazie alle loro caratteristiche spettroscopiche peculiari: bande strette di emissione, ampio intervallo tra bande di assorbimento ed emissione, tempi di vita degli stati eccitati molto maggiori dei comuni composti organici fluorescenti.

Tuttavia, la fotoluminescenza degli ioni lantanidi in soluzione è molto debole, a causa dei loro bassi coefficienti di assorbimento. Per incrementarla si possono impiegare complessi di tali ioni con leganti organici con alta capacità di assorbimento della luce incidente, e di trasferiscono l'energia assorbita al centro metallico. Utilizzando un opportuno cromoforo nel legante, si aumenta l'intensità di emissione dei lantanidi con il cosiddetto fenomeno chiamato "effetto antenna".

I più interessanti per il campo dell'imaging biomolecolare sono complessi di Eu(III) e Tb(III), a causa della loro bassa sensibilità dello stato eccitato agli spegnimenti vibrazionale causati da oscillatori come OH, NH o CH.

In questo progetto di dottorato si è seguito un approccio multidisciplinare per la progettazione, sintesi e caratterizzazione di nuovi complessi di Europio(III) basati su una struttura di base" chirale costituita dal frammento1,2-diamminocicloesano (DACH). Tali complessi sono stati applicati per la rilevazione di importanti bioanaliti presenti nel liquido extracellulare, quali bicarbonato, albumina e citrato.

Abstract

The application of luminescent lanthanide-based compounds became extremely attractive thank to their unique spectroscopic properties: sharp emission bands, broad absorption and excitation spectra, a very long excited state lifetime rather than those of conventional organic fluorophores.

The fluorescence of lanthanide salts is weak because of the low energy absorption of the metallic ion. Hence, organic chelated complexes of lanthanides are commonly used, where an organic chromophore is used as a sensitizer for lanthanide center luminescence. The antenna chromophore absorbs light with a high molar absorptivity, and transfers the excited state energy to the lanthanide center that consequently emits. This phenomenon is called "antenna effect".

The most used candidates in biological imaging are Eu(III) and Tb(III) complexes, due to the low sensitivity of their excited state to the vibrational quenching effects caused by OH, NH, or CH oscillators.

In this PhD project, a multidisciplinary approach was used in order to project and synthesize new Eu(III) complexes, starting from a chiral 1,2-Diaminecyclohexane (DACH) backbone. Solution speciation studies revealed that the complexes were stable and further tested for sensing application of relevant bio-analytes present in the extracellular fluid such as bicarbonate, albumin and citrate.

Table of contents

List of abbreviations

ACN	Acetonitrile
BSA	Bovine Serum Albumin
$CDCl_3$	Deuterated chloroform
DACH	1,2-diaminocyclohexane
DIBAL	Diisobutylaluminium hydride
DCM	Dichloromethane
DFT	Density Functional Theory
EA	Elemental analysis
EF	Extracellular fluid
emf	Electromotive force
ESI-MS	Electrosptray ionization mass spectrometry
EST	Equilibrium speciation tool
EtOH	Ethanol
HCO_3^-	Bicarbonate
IC_{50}	Half maximal inhibitory concentration
ITC	Isothermal titration calorimetry
Ln	Generic lanthanide
MeOH	Methanol
MOPS	3-(N-morpholino)propanesulfonic acid
MRI	Magnetic Resonance Imaging
NMR	Nuclear Magnetic Resonance
SA	Serum Albumin
TEA	Triethanolamine
TFA	Trifluoroacetic acid
TLC	Thin Layer Chromatography
Trp	Tryptophan
UV	Ultraviolet light
Vis	Visible light

List of figures

Chapter 1 – Introduction

Chapter 3 – Experimental

Chapter 4 –Protonation and complex formation

List of tables

Chapter 1 – Introduction

Chapter 4 – Protonation and complex formation

Chapter 5 – Luminescent sensing of bio-analytes

Chapter 1

Introduction

1.1 Introduction to the lanthanides

1.1.1 History and Relevance

When they were discovered in the 18th century, the Lanthanides were found as oxides, which were then called "earths".[1] At that time, these minerals appeared to be scarce, and so these newly discovered elements were called "rare earths". Actually, these elements are quite abundant and can be found all around the world.[2] Most of these reserves are located in China, and are estimated at some 44 million metric tons.[3] The United States also has significant reserves, estimated to amount to 1.5 million metric tons. After China, the major rare earth countries based on reserve volume are Vietnam, Brazil, and Russia.[4]

The history of the individual rare-earth element is complex and confused, mainly because of their chemical similarity, but the real Lanthanide chemistry started in Scandinavia. In 1794 Johan Gadolin, a Finnish chemist, physicist and mineralogist, was the first to succeeded in obtaining an "earth" (oxide) from a black mineral, lately named as gadolinite; he called the earth yttria.[5] From then, many lanthanide oxides were separated from this mineral. Nevertheless, at that time, it was usual to fall into mistakes due to the unreliable atomic masses and many newly discovered elements were not one element but mixtures of up to six different rare earth. In 1869, Mendeleev was not able to position the lanthanides in the periodic table because of the lack of an acceptable atomic theory and a set of elements for comparison.[6]

It was not until the 20th century when the physicist Henry Moseley, experimentally confirmed by the X-Ray spectroscopy,[7] that there were 15 elements going from lanthanum to lutetium. The last lanthanide found, the radioactive promethium, was discovered in 1947.[8] Promethium is also the rarest, occurs only in trace quantities in natural materials, as it has no long-lived or stable isotopes.[4]

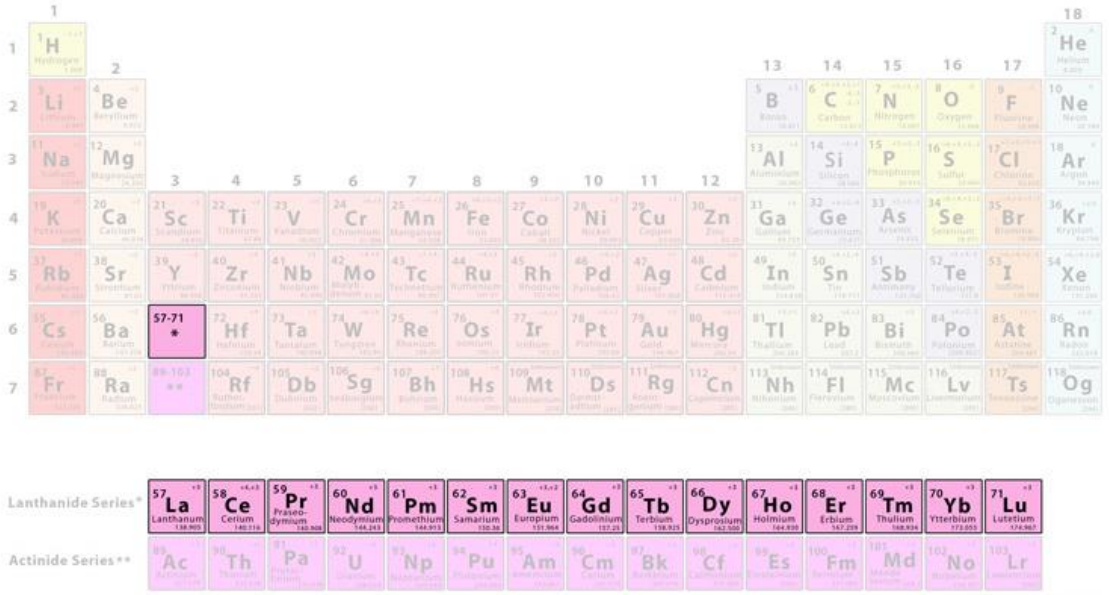

Figure 1.1 *The periodic table of elements. The lanthanide series is highlighted at the bottom of the periodic table*

The lanthanide elements form the largest subgroup in the periodic table, composed by 15 elements, ranging from lanthanum (atomic number 57) to lutetium (atomic number 71) (Figure 1.1). They are called *f*-block elements due to the gradual filling of the last electron in *f* orbitals of the antepenultimate shell. The lanthanide series can be extended with the elements scandium (atomic number 21) and yttrium (atomic number 39), since they have similar chemical properties; the enlarged series is then called rare earths.

The rare earths fall into the 50th percentile of the elemental abundance. Nowadays, China is the world's largest producer of rare earth elements with the 82 percent of the total minerals extracted (112.000 tonnes of rare earth oxides).[9]

Today, the rare-earth elements play a central role in numerous key-technologies (electronics, electric mobility, energy storage and production, optics, magnets, medicine, etc.)[10–14] and their global demand is expected to increase in the next years. However, their availability and price are expected to be serious issues in the next years, and, for this reason, they have been included by the European Commission in the "critical raw materials" list.[15]

For example, the Chinese monopoly allowed recently the increase of the prices for various rare earth materials leading to a major change in the dynamics of the rare earth markets.[16] However, if the demand continues to rise and no recycling of the produced rare earths will be carried out, the price and availability will probably be serious issues in the next years. In view of the limited reserves and high value of rare earth metals, recycling of these elements from end-of-life consumer goods is likely to become more important.[17,18]

1.2 General properties of lanthanides

1.2.1 Electronic configuration

The chemistry of the lanthanides is dominated by the +3 oxidation state with an electronic configuration of [Xe] $4f^n$ (n=0-14). The only exceptions are Ce^{4+}, Eu^{2+}, Sm^{2+}, Yb^{2+} and Tb^{4+} due to the presence of an empty, half-full or full 4*f* shell.[19] The 4*f* orbitals are well shielded by the xenon core, transforming the valence 4*f* orbitals into inner orbitals. This phenomenon is a crucial point both for chemical and spectroscopic properties of the lanthanide metal ions. The lanthanide(III) ions exhibit a close chemical resemblance across the periodic series, due to the small and regular decrease in their ionic radii due to a poor shielding effect of the 4*f* electrons. This phenomenon is called lanthanide contraction (Figure 1.2).[20,21]

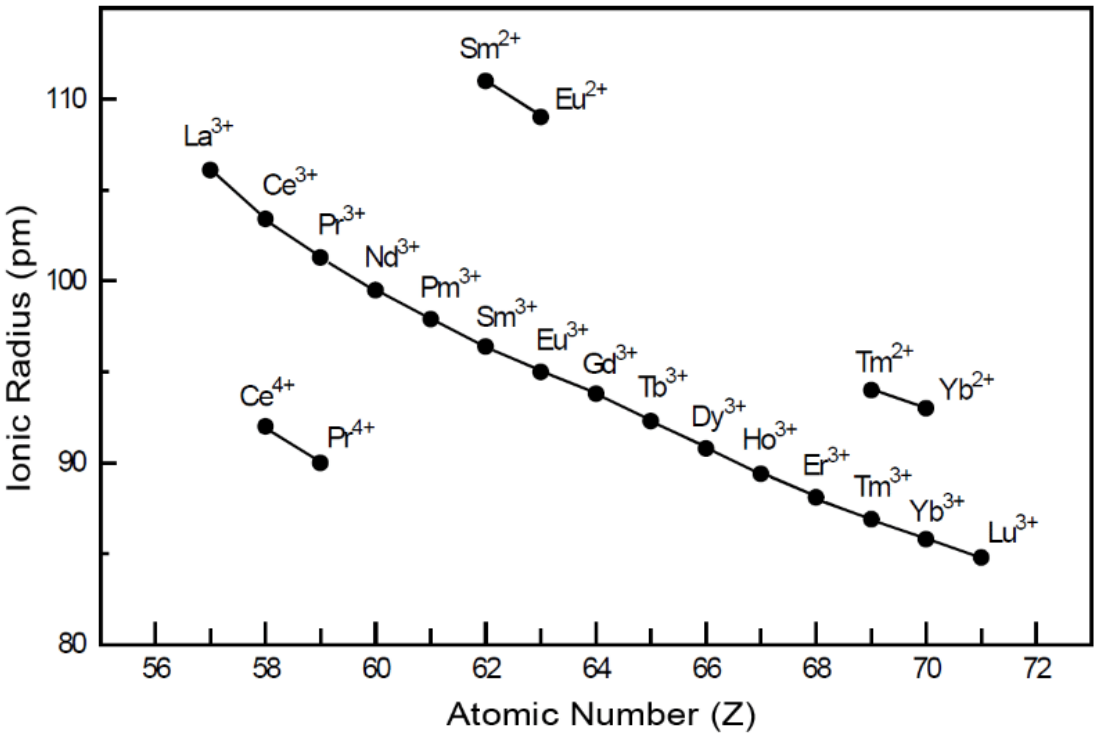

Figure 1.2 *Ionic radii throughout the lanthanide series* [22]

The lanthanides are characterized by filling the 4*f* orbitals gradually along the series. From praseodymium (Pr) to lutetium (Lu), orbitals are filled following the Aufbau principle. Lanthanum (La) and cerium (Ce), the first two lanthanides, present an exception to the Aufbau principle, by filling the 5*d* orbital before the 4*f*. It is related to the 5*d* subshell that have lower energy than the 4*f*. Differently for gadolinium (Gd), whose energy necessary to add an electron to the 5*d* orbital is lower instead of breaking the stable half filling of the 4*f* orbital.

All trivalent lanthanide ions are paramagnetic due to unpaired 4*f* electrons. La(III) and Lu(III) are exceptions, presenting $4f^0$ and $4f^{14}$ electronic configurations respectively (Table 1.1). Gd(III) presents seven unpaired electrons ($4f^7$) which confers high magnetic moment, making his complexes suitable for magnetism-related applications, such as MRI.[23,24]

Table 1.1 *Ground state electronic configurations of the lanthanide (Ln) atoms and their most common ions shown in correct order of orbital filling*

Atomic number	Name	Symbol	Electronic configuration (Ln)	Electronic configuration (Ln^{3+})
57	Lanthanum	La	[Xe]$5d^1$ $6s^2$	[Xe]$4f^0$
58	Cerium	Ce	[Xe]$4f^1$ $5d^1$ $6s^2$	[Xe]$4f^1$
59	Praseodymium	Pr	[Xe]$4f^3$ $6s^2$	[Xe]$4f^2$
60	Neodymium	Nd	[Xe]$4f^4$ $2s^2$	[Xe]$4f^3$
61	Promethium	Pm	[Xe]$4f^5$ $6s^2$	[Xe]$4f^4$
62	Samarium	Sm	[Xe]$4f^6$ $6s^2$	[Xe]$4f^5$
63	Europium	Eu	[Xe]$4f^7$ $6s^2$	[Xe]$4f^6$
64	Gadolinium	Gd	[Xe]$4f^7$ $5d^1$ $6s^2$	[Xe]$4f^7$
65	Terbium	Tb	[Xe]$4f^9$ $6s^2$	[Xe]$4f^8$
66	Dysprosium	Dy	[Xe]$4f^{10}$ $6s^2$	[Xe]$4f^9$
67	Holmium	Ho	[Xe]$4f^{11}$ $6s^2$	[Xe]$4f^{10}$
68	Erbium	Er	[Xe]$4f^{12}$ $6s^2$	[Xe]$4f^{11}$
69	Thulium	Tm	[Xe]$4f^{13}$ $6s^2$	[Xe]$4f^{12}$
70	Ytterbium	Yb	[Xe]$4f^{14}$ $6s^2$	[Xe]$4f^{13}$
71	Lutetium	Lu	[Xe]$4f^{14}$ $5d^1$ $6s^2$	[Xe]$4f^{14}$

The increase in Ln(III) solvation is one of the consequences of lanthanide contractions as one moves along the series. Indeed, the decrease in the ionic radius results in an increase in the charge density and greater polarity of these cations, which produces an increase of the number of solvent molecules in the second sphere of coordination.[25]

1.2.2 Coordination chemistry

Trivalent lanthanide ions Ln(III) have high charge density and high ionization potentials, consequently these ions are hard Lewis acids in terms of hard-soft acid-base theory, with therefore a preference for ligands with high electronegative donor sites (hard Lewis bases, such as O > N > S).[26] The nature of such bonding results in the predominant nature of ionic interactions. Water molecules and hydroxide ions tend also to be particularly strong ligands for Ln(III).

The discovery of lanthanides high coordination numbers arose in 1965 with the progress of X-ray diffraction techniques. Unlike transition metals, lanthanides do not have a specific coordination number. Thus, the coordination number of lanthanides can only be derived from X-ray diffraction studies and cannot be predicted by the absorption spectrum or the color. Lanthanides tend to have high coordination numbers compared to transition metals, since they are large and highly positively charged.[27]

Coordination numbers range from 3 to 12 in the solid state and are largely determined by the ionic radius of the cation and the charge and steric requirements of the ligand(s), with 8 and 9 being the most common in solution. The lanthanide ions can complete its coordination sphere with solvent molecules or anions (such as water or chloride), when the number of donating atoms in the ligand is too little or their electronic density is too low. Observation of high coordination number is due to lack of any directional bonding character and large ionic size, resulting in poor stereochemical preferences and consequently the coordinating ligands in the complex occupy positions that minimize the steric repulsions between them. Therefore, the coordination environment around the Ln(III) center often cannot be regarded as an idealized coordination polyhedron.[28]

The nature of donor atoms determines the coordination properties of the ligand. Since the lanthanide ions tend to bind hard bases, they present a strong affinity towards hard bases like neutral (ethers)[29] or negatively-charged (carboxylates)[30] O and N donors.[31–34] Therefore, amines and carboxylic acid groups are often used in lanthanide complexation.[35]

In the solid state, the most common coordination geometries of the Ln(III) complexes can be seen in Figure 1.3, as the square anti-prismatic, trigonal dodecahedral, tricapped trigonal prismatic and capped square antiprismatic.[36]

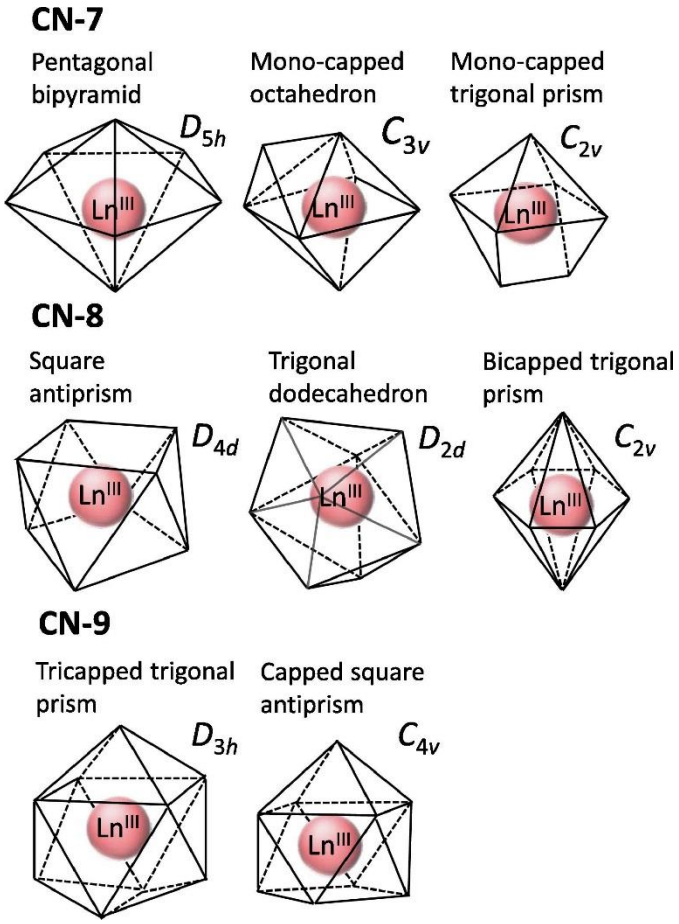

Figure 1.3 *Most common coordination geometries of Ln(III) ions in the solid state*[36]

However, resolving the coordination structure of Ln-ligand complexes in solution is challenging, experimentally or even computationally, since solution structures have more vibrational and rotational degrees of freedom than solids that are partially restrained in space. Coordination numbers are determined by ligand size, also by the number of donor atoms that may pack round the metal, or, in the case of bulky ligands, the interactions between distant groups that decide how many ligands may bind to the metal ion. Coordination numbers up to 8 or 9 are common with monodentate ligands, however using multidentate ligands may produce values as high as 12.[27]

The ligand coordination to a metal ion in solution arises in competition with the solvation of the species involved in the reaction, which is the highest for the cation. Therefore, the binding strength of a solvent towards the Ln(III) ion is a major factor in determining the thermodynamics of ligand coordination in such medium.[37]

In the first coordination sphere the binding conformation of the ligand, as well as ligand atomic speciation, must be determined since ligands will rearrange to a different conformation upon binding the Ln ion, and may change protonation state or react upon binding. Not only must the spatial positions of Ln ion/ligand/solvent/anion molecules with respect to each other be determined, but, due to the reactive nature of Ln(III) ions, chemical reactions can change the speciation. For example, coordinated water molecules can undergo hydrolysis and form Ln-hydroxides, or ligands can degrade upon binding the Ln ion.

In aqueous solutions, Ln(III) cations readily hydrolyse above ~ pH 6 to form hydroxo species[38]:

$$Ln^{3+}_{(aq)} + H_2O_{(l)} \rightleftharpoons Ln(OH)^{2+}_{(aq)} + H^{+}_{(aq)}$$

with reported log β_1 values ranging from -8.5 for $La(OH)^{2+}$ to -7.6 for $Lu(OH)^{2+}$.[39] Complex formation with organic ligands competes with hydrolysis, and the stability of Ln(III) complexes are typically measured using potentiometric or spectrophotometric methods, with results evaluated in terms of the equilibrium constant for the complexation reaction.

The most used ligands for the formation of strong Ln(III) complexes in solution are polyamino-polycarboxylates (Figure 1.4 and Figure 1.5), which present both, negatively-charged O- and neutral N-donor atoms. The Ln(III)–O bond distance is normally shorter than that of the Ln(III)–N bond.[40] Moreover, in aqueous solutions, ligands with negatively charged oxygen create complexes with high thermodynamic stability, resistant to hydrolysis.[41]

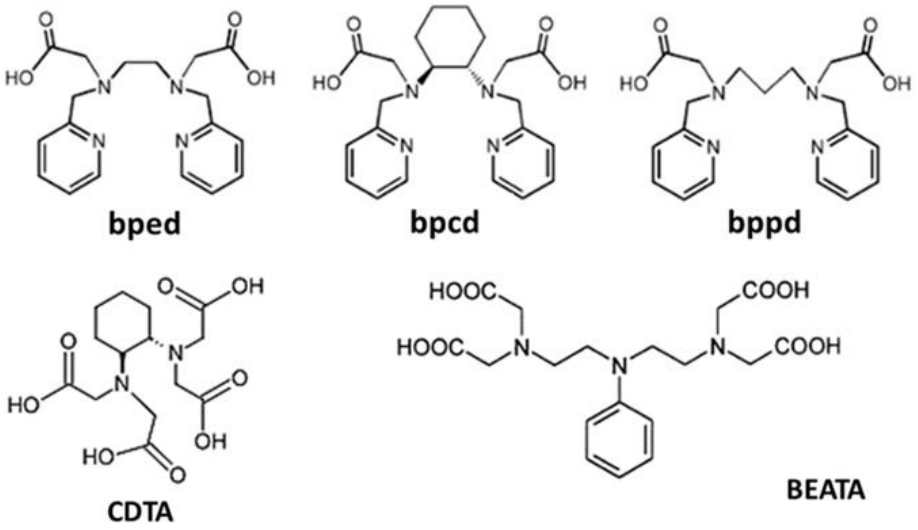

Figure 1.4 *Some open-chained polyamino-polycarboxylates ligands.* ***bped****: N,N′-bis(2-pyridylmethyl)ethylenediamine- N,N′-diacetate.* ***bpcd****: N,N′-bis(2-pyridylmethyl)-trans-1,2-diaminocyclohexane-N,N′-diacetic acid.* ***bppd****: bis(2-pyridylmeth- yl)-1,3-diaminopropane diacetate.* ***CDTA****: trans-1,2-diaminocyclohexane-N,N,N',N'-tetraacetic acid.* ***BEATA****: N,N-bis(2-aminoethyl)aniline-N,N,N′,N′-tetraacetic acid*

In addition, the ligand can be used to control thermodynamic and kinetic stability, solubility, responsiveness to the environment and photophysical properties.[25,42]

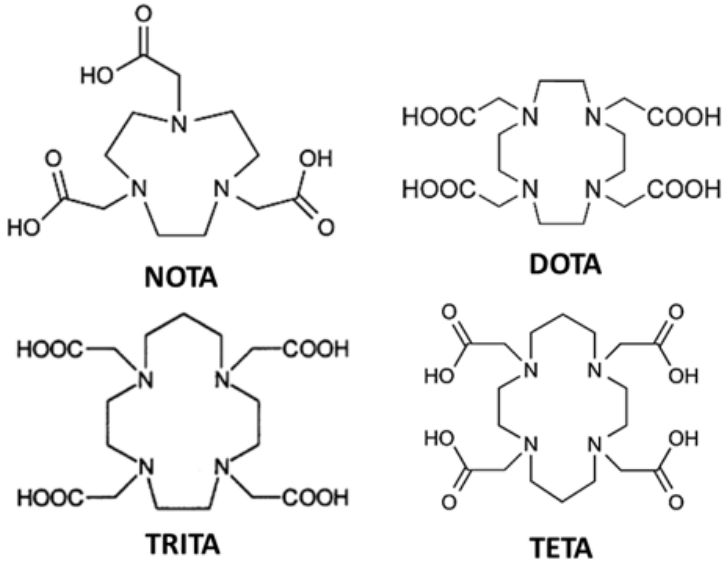

Figure 1.5 *Some macrocyclic polyamino-polycarboxylates ligands.* ***NOTA****: 1,4,7-triazacyclononane-1,4,7-triacetic acid.* ***DOTA****: 1,4,7,10-tetraazacyclododecane-1,4,7,10-tetraacetic acid.* ***TRITA****: 1,4,7,10-tetraazacyclotetradecane-1,4,7,10-tetraacetic acid.* ***TETA****: 1,4,8,11-tetraazacyclotetradecane-1,4,8,11-tetraacetic acid*

1.2.3 Lanthanide spectroscopy

One characteristic and interesting aspect of the lanthanides is their unusual spectroscopic properties. Trivalent lanthanide cations show absorption and emission bands that correspond to *f-f* electronic transitions that are forbidden (Laporte rule, which states that the spectral lines associated with electric-dipole transition must arise from the states of opposite parity).[43,44] Because of this, the Ln(III) ions show these transitions with a very low molar extinction coefficient ($\varepsilon < 10\ M^{-1}\ cm^{-1}$), limiting the practical applications of the lanthanides.[45] Since the 4*f* orbitals are relatively insensitive to the ligand field, their emission spectra present line-like emission bands, mostly in the visible and near infrared ranges (Figure 1.6), peculiar of each element.

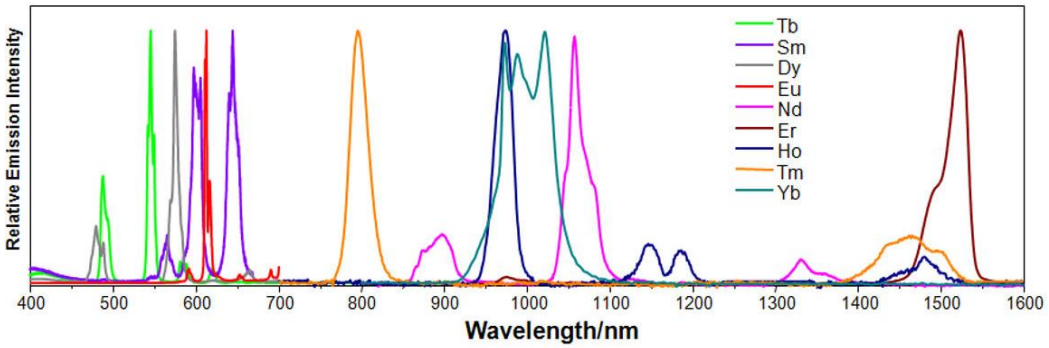

Figure 1.6 *Normalized emission spectra of some lanthanide*[46]

The photo-sensitization process was first discovered by Weissmann in 1942 when he observed that the intensity of Eu^{3+} ion was escalated in the presence of some organic compounds.[46] Based on the finding, organic ligands were designed for the preparation of strong luminescent Eu(III) complexes.

Therefore, to enhance the efficiency of the process, Ln(III) ions are usually chelated with ligands that have much broader and more intense absorption bands. When a strongly absorbing chromophore is used to "sensitize" Ln(III) emission the process is known as the *antenna effect* (Figure 1.7) and it is important in the design of bright luminescent lanthanide complexes. The chromophore is normally an aromatic or

unsaturated organic molecule that is either anionic or has a strong dipole moment to coordinate to the Ln(III) ion.

The mechanism of energy transfer from the organic ligand to the lanthanide ion was first proposed by Crosby and Whan.[46] Briefly, a light-harvesting organic ligand is excited and goes from the ground singlet state (S_0) to the singlet excited state (S_1). Then, the excited singlet state decays non-radiatively to a ligand triplet state via intersystem crossing (ISC). Then, the non-radiative energy transfer (ET) pathway from the triplet state of the ligand to the excited states of the Ln(III) ion with subsequent radiative transition to the ground state of the Ln(III) ion (Figure 1.7).

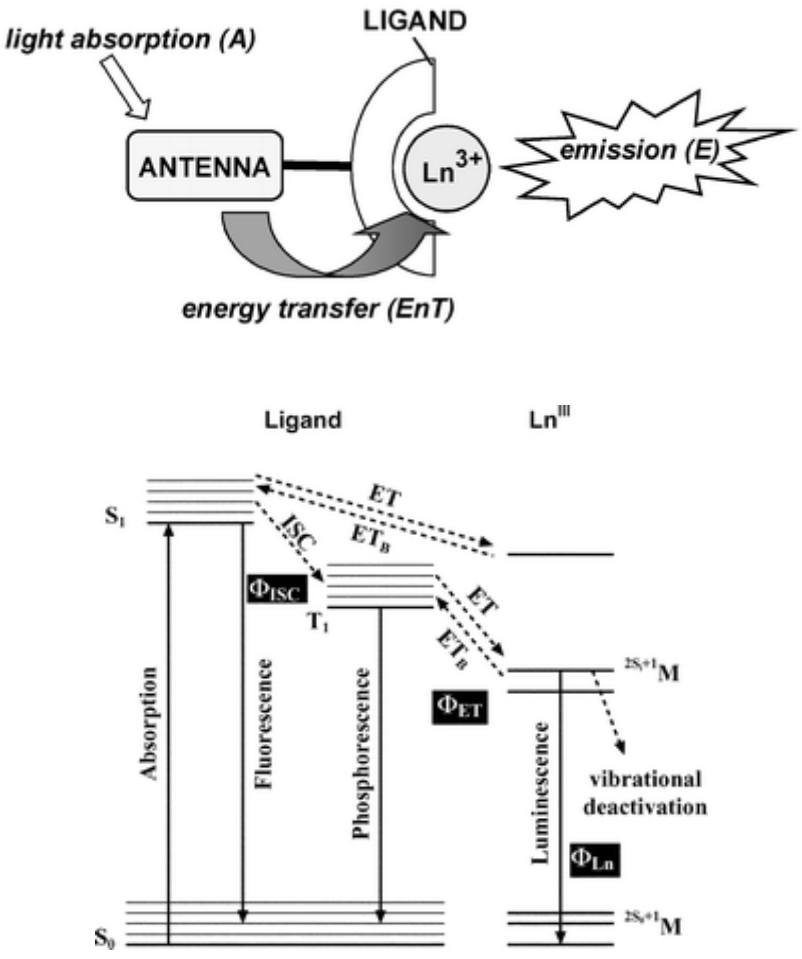

Figure 1.7 *(a) Scheme of the antenna effect;*[44] *(b) common pathway leading to lanthanide sensitization*[45]

The photosensitizing efficiency of the ligand can be quantified by the quantum yield (Φ), defined as the ratio of the number of photons emitted to the number of photons absorbed.[49] The total quantum yield (Φ_{tot}) can be obtained by the sum of the intersystem crossing (Φ_{ISC}), energy transfer (Φ_{ET}) and the lanthanide luminescence (Φ_{Ln}) (Equation 1.1):

$$\Phi_{tot} = \Phi_{ISC} \cdot \Phi_{ET} \cdot \Phi_{Ln} \qquad (1.1)$$

The known mechanism for the photosensitization of lanthanide complexes is shown, in Figure 1.7, where the components are represented in their corresponding steps. The lower triplet state of the antenna have to present higher energy ($\Delta E \geq 1850$ cm^{-1})[41,50] than the highest luminescent state of the lanthanide cation, in order to avoid back energy transfer to the antenna's triplet state. Nevertheless, at the same time, the gap has to be as low as possible with the aim of assure the highest quantum yield.

High Φ_{tot} values can also lead to a large energy gap between the highest ground state level and the lowest excited energy level of the lanthanide ion. As shown in the adapted Dieke's diagram in Figure 1.8, the lanthanide ions that have the largest gaps are: Eu(III), Gd(III) and Tb(III). As a result, they present the strongest luminescence between the lanthanides. Gd(III) ion efficiently emits UV luminescence at about 310nm, making Gd(III) chelates impractical for biological applications.[51] In contrast, Sm(III) and Dy(III) display favorable emission wavelengths in the near-IR region.[52,53] However, their lower excited-state energies make them susceptible to energy dissipation through non-radiative processes, decreasing emission intensity and luminescence lifetimes.

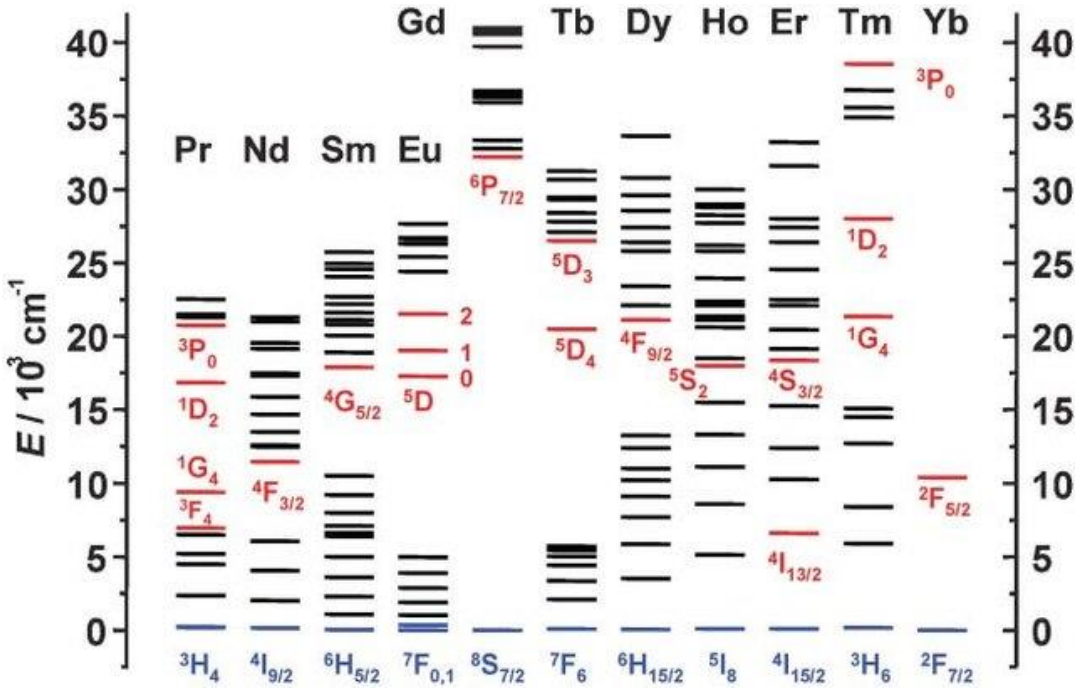

Figure 1.8 *Dieke diagram of partial energy levels of some trivalent lanthanide aqua ions. The main emissive levels are shown in red while the ground levels are drawn in blue*[54]

Ln(III) emission intensity is however sensitive to non-radiative deactivation processes such as energy back-transfer, thermal deactivation, and deactivation by vibrational coupling between the Ln(III) excited level and coordinated solvent molecules. In Figure 1.9 is depicted the electronic levels for Tb(III), Eu(III) and Yb(III), and the phonons for the water molecule O–H vibrations. The quenching of the $^5D_4$ Tb(III) and $^5D_0$ Eu(III) excited levels require vibrational coupling with 5–6, and 4–5 phonons, respectively, while the $^2F_{5/2}$ Yb(III) excited level only requires vibrational coupling with three phonons. The ease quenching of the Yb(III) excited level is one of the challenges to overcome in developing Yb(III) complexes for luminescence imaging.[55]

The extent of this quenching is inversely proportional to the energy gap between the emissive state and the ground state of the metal. The other quenchers of luminescence are the harmonics of N–H, C–H, and C=O stretching vibrations, but not as O–H oscillators.

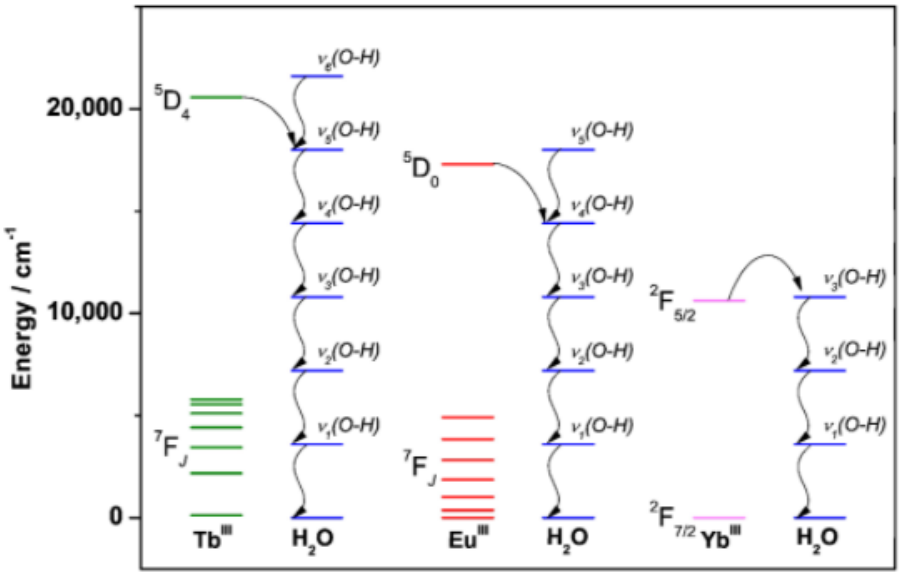

Figure 1.9 *Energy diagram showing the electronic levels of Tb(III) (green), Eu(III) (red), and Yb(III) (light pink), and the phonons for the water molecule O-H vibrations (blue)*[55]

Polydentate ligands not only increase the stability of the lanthanide complexes in solution but also allow the metal center to be protected from water molecules. Therefore, the luminescence of the lanthanide-based complexes is controlled by the denticity of the ligand. In the presence of linkers with low denticity, the lanthanides coordinate to solvent molecules, such as water, resulting in the deactivation of the Ln(III) excited states non-radiatively.

Eu(III) and Tb(III) complexes have further received significant attention due to several factors. The emission intensities are higher than those of Sm(III) and Dy(III) while displaying biologically appropriate emission wavelengths in the visible region (Figure 1.10). Moreover, Eu(III) and Tb(III) probes show long excited state lifetimes in the millisecond range, in contrast to nanosecond lifetimes of most organic fluorophores, making them extremely advantageous for time gated luminescence, which is crucial for its use for bio-sensing and bio-imaging applications (Figure 1.11).

As compared to the near-IR emitting lanthanides, Eu(III) and Tb(III) display less sensitivity to quenching by singlet oxygen and by vibrational energy transfer to X–H (X = C, N, O) of the surrounding ligands. The non-degeneracy of the $^5D_0$ emissive states of Eu(III) give a well-defined spectrum for facile interpretation. This is especially useful in the development of responsive probes.[56] These are important

features when these complexes are employed in biological applications, such as the sensing of biomarker molecules, as they have to display good performance in aqueous solution.

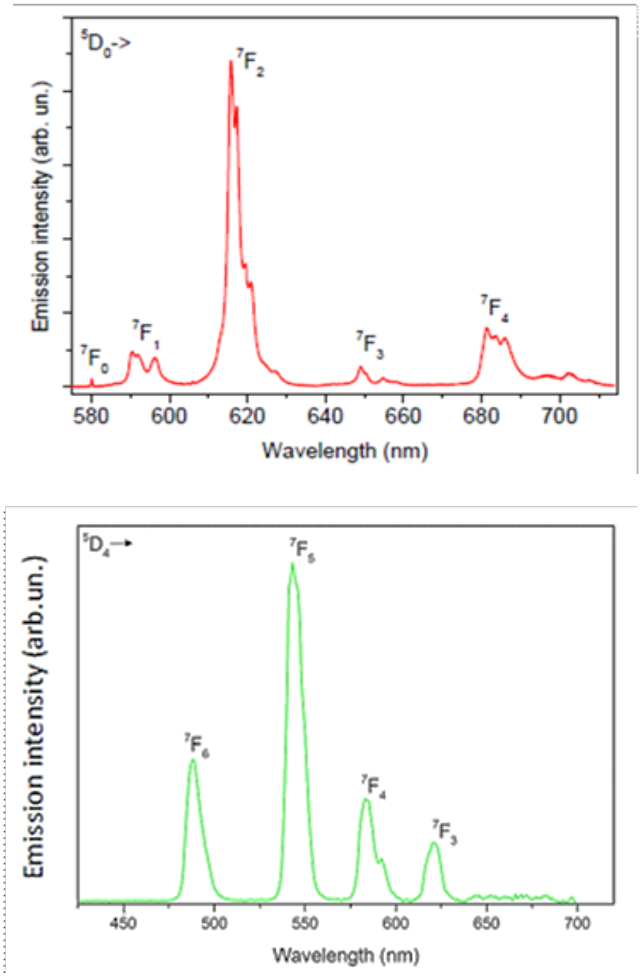

Figure 1.10 *Eu(III) (top) and Tb(III) (bottom) luminescent emission wavelengths, that emit red and green light, respectively*[50]

It should be also pointed out, that a specific excitation wavelength must be selected. Optical probes, which have excitation wavelength lower than 300 nm are useless, since the majority of the biomolecules strongly absorb UV light in that specific spectral range.[57]

In addition, when the emissive complex is chiral non-racemic, it may emit left and right circularly polarized light with different intensities. The phenomenon is called circularly polarized luminescence (CPL) and it is usually quantified through the

luminescence dissymmetry factor g_{lum}, defined as $g_{lum} = 2(I_L - I_R)/(I_L + I_R)$ (I_L and I_R being left- and right-polarized intensities, respectively).[58]

It follows immediately that $g_{lum} = \pm 2$ means complete polarization of the emitted light while 0 corresponds to an unpolarized beam. While isolated organic chiral molecules or macromolecules typically display glum values of $10^{-3} - 10^{-2}$, lanthanide complexes show values of 0.1 – 1,[59] with 1.38 being the highest value ever reported so far for a lanthanide complex.[60]

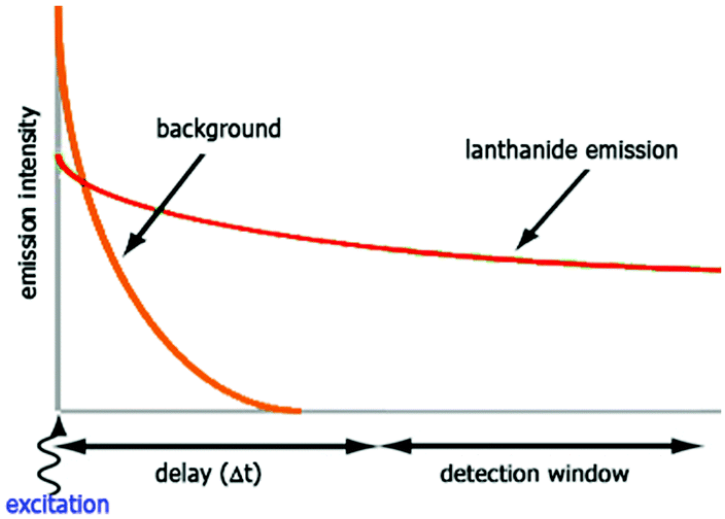

Figure 1.11 *Graphic description of the time-delay (or time-gated) measures*[61]

1.3 Luminescent trivalent lanthanide complexes

1.3.1 Design of Lanthanide(III) Chelates

Luminescent lanthanide complexes attracted much attention because of their stable emission colours, induced by the photo-antenna effect through the photo-excited energy transfer from aromatic ligands to Ln(III) ions.

The main aim in designing luminescent lanthanide complexes is to find a structure that retains the incorporated lanthanide ion brightly luminescent while keeping the material intact. More specifically, the complex should be water soluble, non-toxic, kinetically inert, photostable and thermodynamically stable, especially if it is used for in vivo experiments.

The chelating effect indicates that the reaction to produce the chelate is more advantageous in terms of energy than the reaction to produce the monodentated complex. It is mainly caused by two factor, one is the entropy increase effect, which increase due to the need for less ligand molecules caused by chelating. The other is the role of enthalpy, the same multi-dentate ligand reduces the mutual repulsion of ligands in different sites, which will affect the coordination pattern of ligands and the stability of complexes.[37,62]

The chelate effect resolves to prevent decomposition and to promote highly stable coordination compounds. Another key feature is that the Ln(III) ion needs to be as close as possible in space to the chromophore, in order to optimise the efficiency of the ligand to metal energy transfer step, and so is best coordinated to the lanthanide ion by an integral donor, typically a pyridine nitrogen or an anionic oxygen atom.[63] Thus, tridentate ligands or those having many coordinating sites designed with the energy donor levels are necessary for the stable complexation with metals in solutions with efficient energy transfer. These ligands strongly coordinate to Ln(III) and are soluble in water and solvents.[42]

They are categorized into three groups: macrocyclic ligands, tri-/tetra-pods and helicate systems. Tetrapod- and caged-style such as ethylenediaminetetraacetate (EDTA) derivatives sensitized strong *f-f* emissions not only for Eu(III) and Tb(III), but also Sm(III) and Dy(III).[64] Additionally, carboxylate in molecules acts as coordination site as well as aids water solubility in their complexes. Some related compounds with Gd(III) ions are useful MRI reagents[65–67] or in biosensing.[68]

In addition, more the lanthanides are heavier with a higher charge density, causing complexes formation with higher stability than the lighter ones.[69] As an example, the stability constants of some Ln(III) with ethylene-diaminetetraacetic acid (EDTA) and diethylenetriaminepentaacetic acid (DTPA) (Figure 1.12) in Table 1.2, where an increasing trend on the stability constants with increasing atomic number can be observed.

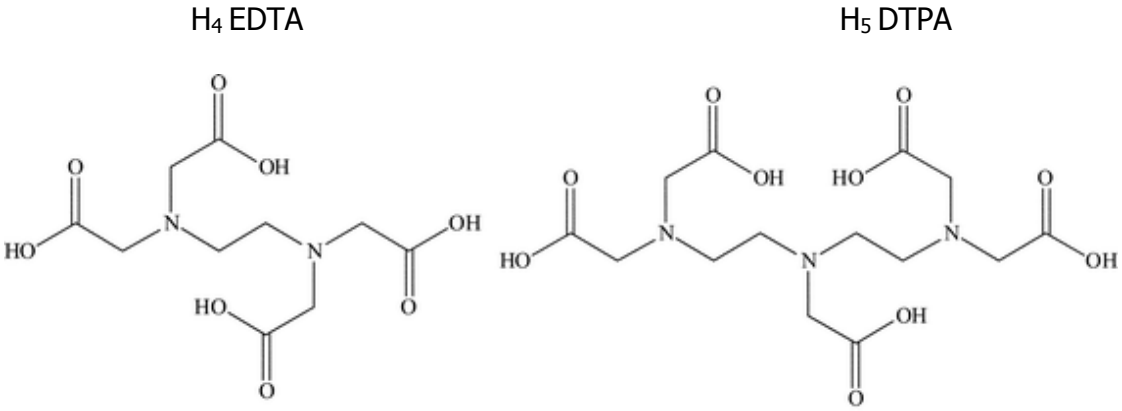

Figure 1.12 *Structure of H_4EDTA: ethylenediaminetetraacetic acid and H_5DTPA: diethylenetriaminepentaacetic acid*

Table 1.2 *Stability constants (logβ) of some Ln^{3+} in aqueous solution (T = 298.15 K, μ = 0.1 M NaCl) with $EDTA^{4-}$ and $DTPA^{5-}$. Charges omitted for clarity*

	La	Nd	Sm	Eu	Gd	Tb	Dy	Ho	Er	Tm	Yb	Lu
EDTA	15.4	16.5	17.1	17.3	17.3	17.9	18.2	18.6	18.8	19.3	19.4	19.8
DTPA	19.4	21.6	22.3	22.3	22.4	22.7	22.8	22.7	22.7	22.7	22.6	22.4

μ: *Ionic strength, properly defined in Chapter 3.*

The stability of the complex is a key requirement in most of the applications to avoid the release of the toxic free Ln(III) ions ions.[33,50,70] Much of the development of ligands for Ln(III) ions has stemmed from their use in Gd^{3+} contrast agents for Magnetic Resonance Imaging (MRI). All of the currently approved Gd^{3+} contrast agents use complexes with chelating or macrocyclic ligands such as DTPA (Magnevist®), DOTA (Dotarem®) and HP-DO3A (ProHance®) (Figure 1.13).

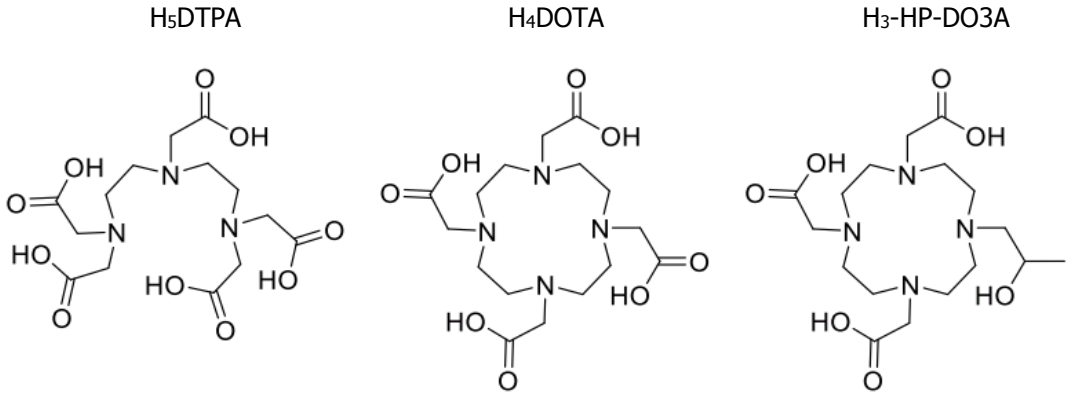

Figure 1.13 *Ligands for Gd^{3+}-based MRI contrast agents*

The nature of these ligands offers favorable binding due to the chelate effect and those with macrocycles further increase the stability by reducing the entropic penalty caused by ligand rearrangement upon metal binding. This can be observed by comparing the binding constants of $[Gd(DTPA)]^{2-}$ and $[Gd(DOTA)]^{-}$ (log K = 22.3 and 24.7, respectively).[71]

In luminescent sensing applications, chelation is needed to ensure a high thermodynamic stability, selectivity and kinetic inertness at physiological pH (~7.4). The latter features are especially important in biological media where *transmetallation* (i.e. the exchange of the lanthanide ion with endogenous cations usually present at high concentrations) can occur. This is especially true in the case of the abundant Zn^{2+} and Ca^{2+} ions. In particular, the latter presents an ionic radius similar to Ln^{3+} ions and therefore they can interfere with physiological processes.[34,72–74] As a consequence, low complex stability could give rise to the release in solution of free toxic metal ion.[75] Also, the ligand can be designed to define the number of coordination sites available for labile water molecules, which can be replaced by the analyte.

Given the hard-acid nature of lanthanide ions, hard bases, such as carboxylic acids, amides, and pyridines, are used as ligands. Macrocycles (such as DOTA derivatives) and open nona- or octa-dentate chelates (such as DTPA derivatives) functionalized with suitable *antennas*, are usually employed for luminescent applications. Increasing the rigidity of the chelate itself can further minimize energy loss through

other X–H (X = C, N, O) vibrations of the chelate, since the pathway and degree of energy loss are dependent on the environment surrounding of the excited center.[76]

1.3.2 Luminescent sensing of bio-analytes

Luminescent molecular probes have attracted interest and focus thanks to their high sensitivity with wide range in detection of specific bio-analytes. Usually, they are detected due to significant changes in the luminescence intensity or wavelength. The definition of a bio-analyte is simple: "Any substance undergoing bioanalysis".

Luminescent lanthanide complexes have gained increasing attention in bioanalytical studies, especially those of Eu(III) and Tb(III) ions. By careful design of the ligand, stable Ln(III) complexes can be devised for rapid and reversible bio-analyte binding, providing a luminescence response that is fast and sensitive. The creation of Ln(III)-based bio-analyte receptors is driven by the need for new sensing and imaging tools for biological, clinical and drug discovery research. A variety of Ln(III) complexes have been developed for binding and sensing anions, cations and bio-analytes in aqueous media, and these have been summarized effectively in some comprehensive reviews.[50,76–79]

For example, protonation/deprotonation of the antenna moieties can give to noticeable changes in the energy absorption and/or transfer to the metal, and consequently a noticeable change on the emission intensity (Figure 1.12). The determination of pH in cells and tissues, crucial for many physiological activities, can be detected with pH dependence sensors,[80–83] and pH-regulated Ln(III) complexes for imaging application.[84–87]

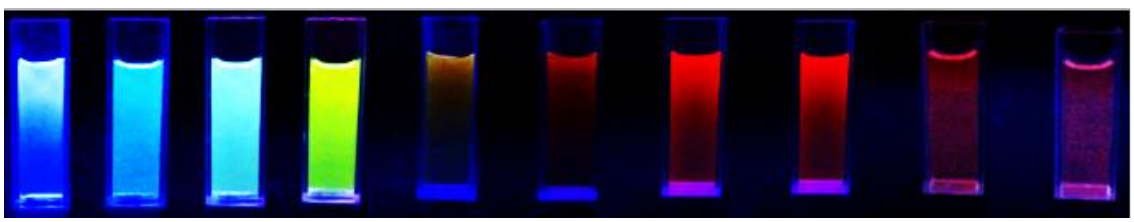

Figure 1.14 *Emission color changes of Eu(III) and Tb(III) complex mixture in aqueous solution from pH 3 (left) to pH 12 (right)*[88]

A bio-analyte can bind directly the metal center, with the displacement of one or more inner-sphere water molecules. This causes a variation of the lanthanide coordination environment and to a change in the emission intensity, form in the spectra and lifetime of the complex (Figure 1.13 a). The variation of the emission spectral form after anion binding offers the opportunity for ratiometric analysis. Also, coordinated water molecules promote an efficient deactivation of the Ln(III) excited state, *via* non-radiative energy transfer to vibrational modes of the O–H groups. When coordinated water is displaced after binding of a certain bio-analyte (such as lactate,[89,90] HPO_4^{2-},[91,92] HCO_3^-,[93–95] and citrate[90]) the deactivation of the excited state becomes less efficient, resulting in the enhancement of emission intensity, lifetime, and spectral shape induced by changes in the Ln(III) coordination environment.

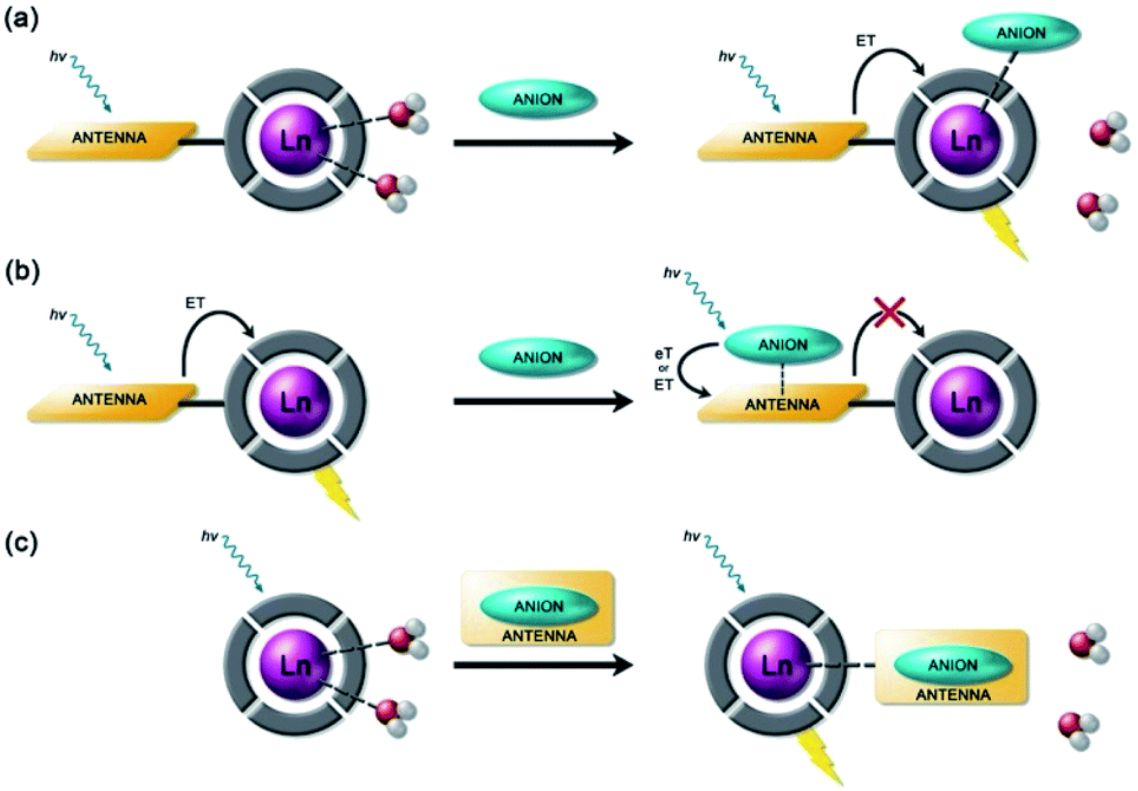

Figure 1.15 *Representation of lanthanide(III) sensing mechanisms for anion detection: (a) anion coordination to the metal center with displacement of inner-sphere water molecules; (b) anion interaction with the antenna causing luminescence quenching; (c) binding of an anion that have a sensitizer, which "switches" on the luminescence*[96]

Alternatively, the bio-analyte could interact with the complex *via* non-covalent interaction (e.g. via π–π stacking with the antenna), electrostatic interactions, or

hydrogen bonding (Figure 1.13 b). This could potentially lead to a quenching of the singlet or triplet excited state of the antenna, by an energy or charge transfer mechanism, causing a decrease in Ln(III) emission intensity.[98,99] Lastly, a less common signaling mechanism foresees the "switching on" of Ln(III) emission upon bio-analyte binding, that however possesses an appropriate chromophore group (Figure 1.13 c). This implies the matching of anion's triplet excited state energy with the Ln(III) excited state, along minimal back energy transfer.[99,100] This approach can lead to high selectivity towards a target anion; however, there is a need of a suitable chromophore.

Nevertheless, the bio-analyte recognition in water is challenging for some reasons: they possess a wide range of geometries, could be pH sensitive ($H_2PO_4^-/HPO_4^{2-}$, HCO_3^-/CO_3^{2-})[101,102] and have high hydration energies.[103] The nature and abundance of potentially interfering species in aqueous media under investigation must be considered, such as competing anions and cations, or biomolecules as proteins and nucleic acids.[104] In the literature, Ln(III) complexes were proposed for the detection of amino acids,[105,106] proteins[107,108] and nucleic acids.[109,110] The detection of such species is relevant for the study of biological processes, such as enzymatic activity,[111–113] measuring tumor biomarkers[114,115] and gene therapy[116,117] among others.

While the majority of lanthanide-based luminescent sensors respond to bio-analytes through change in spectral form and emission intensity and lifetime, recent research is evaluating chiroptical properties.[118,119] CPL spectroscopy combines the sensitivity of luminescence and the specificity of chiroptical response, and one can envision that the advancement on polarized microscopy will accelerate the use of CPL of lanthanide complexes either in combination with or independent of optical imaging techniques.[50] Induced CPL upon binding to chiral Ln(III) complexes is particularly useful to signal selectively the presence of chiral species in solution, such as certain proteins[60] or chiral ions (e.g., sialic acid[120] or lactate[119]). In the latter case, it was shown that a chiral Tb(III) complex was able to differentiate between D- and L-lactate.[119] Each of these examples illustrates how the chemistry of bio-analyte recognition using lanthanide complexes in aqueous media has progressed, allowing real-life applications to be exploited.

1.4 Bibliography

[1] H. Tariq, A. Sharma, S. Sarkar, L. Ojha, R. P. Pal, V. Mani, *Asian-Australasian J. Anim. Sci.* **2020**, *33*, 373–381.
[2] F. Xie, T. A. Zhang, D. Dreisinger, F. Doyle, *Miner. Eng.* **2014**, *56*, 10–28.
[3] J. T. T. da Silva, I. C. Bicalho, G. P. Ribeiro, C. H. Ataíde, *Miner. Eng.* **2020**, *155*, 106402.
[4] V. Balaram, *Geosci. Front.* **2019**, *10*, 1285–1303.
[5] P. Dinér, *Nat. Chem.* **2016**, *8*, 192.
[6] M. Laing, *J. Chem. Educ.* **2008**, *85*, 63.
[7] G. Lente, *ChemTexts* **2019**, *5*, 17.
[8] S. Cotton, *Lanthanide and Actinide Chemistry*, John Wiley & Sons, Ltd, **2006**.
[9] Z. Chen, *J. Rare Earths* **2011**, *29*, 1–6.
[10] X. Song, M. H. Chang, M. Pecht, *JOM* **2013**, *65*, 1276–1282.
[11] J. C. G. Bünzli, A. S. Chauvin, *Handb. Phys. Chem. Rare Earths* **2014**, *44*, 169–281.
[12] S. P. Fricker, *Chem. Soc. Rev.* **2006**, *35*, 524–533.
[13] A. De Bettencourt-Dias, *Dalt. Trans.* **2007**, 2229–2241.
[14] F. T. Edelmann, *Chem. Soc. Rev.* **2012**, *41*, 7657–7672.
[15] S. Bobba, S. Carrara, J. Huisman, F. Mathieux, C. Pavel, *Eur. Comm.* **2020**, DOI 10.2873/58081.
[16] N. A. Mancheri, B. Sprecher, G. Bailey, J. Ge, A. Tukker, *Resour. Conserv. Recycl.* **2019**, *142*, 101–112.
[17] T. Dutta, K. H. Kim, M. Uchimiya, E. E. Kwon, B. H. Jeon, A. Deep, S. T. Yun, *Environ. Res.* **2016**, *150*, 182–190.
[18] B. E. Johnson, P. H. Santschi, C. Y. Chuang, S. Otosaka, R. S. Addleman, M. Douglas, R. D. Rutledge, W. Chouyyok, J. D. Davidson, G. E. Fryxell, et al., *Environ. Sci. Technol.* **2012**, *46*, 11251–11258.
[19] P. Di Bernardo, A. Melchior, M. Tolazzi, P. L. Zanonato, *Coord. Chem. Rev.* **2012**, *256*, 328–351.
[20] S. Sairenji, S. Akine, T. Nabeshima, *Dalt. Trans.* **2016**, *45*, 14902–14906.
[21] M. Seitz, A. G. Oliver, K. N. Raymond, *J.Am.Chem.Soc.* **2007**, *129*, 11153–11160.
[22] M. Atanassova, V. Kurteva, *RSC Adv.* **2016**, *6*, 11303–11324.
[23] P. Caravan, J. J. Ellison, T. J. McMurry, R. B. Lauffer, *Chem. Rev.* **1999**, *99*, 2293–2352.
[24] B. Sitharaman, B. D. Jacobson, Y. Z. Wadghiri, H. Bryant, J. Frank, *J. Appl. Phys.* **2013**, *113*, DOI 10.1063/1.4796183.
[25] E. Bentouhami, G. M. Bouet, J. Meullemeestre, F. Vierling, M. A. Khan, *Comptes Rendus Chim.* **2004**, *7*, 537–545.
[26] D. Écija, J. I. Urgel, A. P. Seitsonen, W. Auwärter, J. V. Barth, *Acc. Chem. Res.* **2018**, *51*, 365–375.
[27] S. A. Cotton, *Comptes Rendus Chim.* **2005**, *8*, 129–145.
[28] T. M. Fyles, *Can. J. Chem.* **1987**, *65*, 884–891.
[29] S. Kannan, M. A. Moody, C. L. Barnes, P. B. Duval, *Inorg. Chem.* **2008**, *47*, 4691–4695.
[30] H. Kitano, Y. Onishi, A. Kirishima, N. Sato, O. Tochiyama, *Radiochim. Acta* **2006**, *94*, 541–547.
[31] M. G. B. Drew, M. R. S. Foreman, M. J. Hudson, K. F. Kennedy, *Inorganica Chim. Acta* **2004**, *14*, 4102–4112.
[32] P. Di Bernardo, P. L. Zanonato, A. Melchior, R. Portanova, M. Tolazzi, G. R. Choppin, Z. Wang, *Inorg. Chem.* **2008**, *47*, 1155–1164.
[33] A. Bianchi, L. Calabi, F. Corana, S. Fontana, P. Losi, A. Maiocchi, L. Paleari, B. Valtancoli, *Coord. Chem. Rev.* **2000**, *1*, 309–393.
[34] C. S. Bonnet, S. Laine, F. Buron, G. Tircsó, A. Pallier, L. Helm, F. Suzenet, É. Tóth, *Inorg. Chem.* **2015**, *54*, 5991–6003.
[35] J. A. McCleverty, T. J. Meyer, in *Compr. Coord. Chem. II From Biol. to Nanotechnology.*, Elsevier: Amsterdam, **2003**, pp. 25–39.
[36] P. P. Ferreira da Rosa, Y. Kitagawa, Y. Hasegawa, *Coord. Chem. Rev.* **2020**, *406*, 213153.
[37] P. Di Bernardo, A. Melchior, M. Tolazzi, P. L. Zanonato, *Coord. Chem. Rev.* **2012**, *256*,

328–351.
[38] C. F. B. and R. S. Mesmer, *The Hydrolysis of Cations*, John Wiley & Sons, Ltd, **1977**.
[39] F. S. Richardson, *Chem. Rev.* **1982**, *82*, 541–552.
[40] A. Trzesowska, R. Kruszynski, T. J. Bartczak, *Acta Crystallogr. B.* **2005**, *61*, 429–434.
[41] E. G. Moore, A. P. S. Samuel, K. N. Raymond, *Acc. Chem. Res.* **2009**, *42*, 542–552.
[42] A. E. Martell, R. D. Hancock, R. J. Motekaitis, *Coord.Chem.Rev.* **1994**, *133*, 39–65.
[43] J. H. V. Vleck, *J. Phys. Chem.* **1937**, *41*, 67–80.
[44] S. F. Mason, *Inorganica Chim. Acta* **1984**, *94*, 88.
[45] R. C. Leif, L. M. Vallarino, M. C. Becker, S. Yang, *Cytom. Part A* **2006**, *69A*, 767–778.
[46] H. Uh, S. Petoud, *Comptes Rendus Chim.* **2010**, *13*, 668–680.
[47] R. Ferreira, P. Pires, B. De Castro, R. A. Sá Ferreira, L. D. Carlos, U. Pischel, *New J. Chem.* **2004**, *28*, 1506–1513.
[48] F. Gutierrez, C. Tedeschi, L. Maron, J. P. Daudey, R. Poteau, J. Azema, P. Tisnès, C. Picard, *Dalt. Trans.* **2004**, *0*, 1334–1347.
[49] G. A. Crosby, J. N. Demas, J. B. Callis, *J. Res. Natl. Bur. Stand. Sect. A, Phys. Chem.* **1972**, *76A*, 561–577.
[50] M. C. Heffern, L. M. Matosziuk, T. J. Meade, *Chem. Rev.* **2014**, *114*, 4496–4539.
[51] I. Hemmilä, V. Laitala, *J. Fluoresc. 2005 154* **2005**, *15*, 529–542.
[52] A. N. Gusev, V. F. Shul'Gin, S. B. Meshkova, M. Hasegawa, G. G. Alexandrov, I. L. Eremenko, W. Linert, *Polyhedron* **2012**, *47*, 37–45.
[53] M. A. Mahmoud, E. T. Abdel-Salam, N. F. Abdel Aal, Z. M. Showery, S. A. Sallam, *J. Coord. Chem.* **2019**, *72*, 749–769.
[54] J.-C. Bünzli, C. Piguet, *Chem. Soc. Rev.* **2006**, *34*, 1048–1077.
[55] J. H. S. K. Monteiro, *Mol.* **2020**, *25*, DOI 10.3390/molecules25092089.
[56] K. Binnemans, *Coord. Chem. Rev.* **2015**, *295*, 1–45.
[57] R. van Grondelle, *Faraday Discuss.* **2018**, *207*, 513–521.
[58] F. Zinna, L. Di Bari, *Chirality* **2015**, *27*, 1–13.
[59] G. Muller, *Dalt. Trans.* **2009**, 9692.
[60] J. L. Lunkley, D. Shirotani, K. Yamanari, S. Kaizaki, G. Muller, *J. Am. Chem. Soc.* **2008**, *130*, 13814–13815.
[61] E. Mathieu, A. Sipos, E. Demeyere, D. Phipps, D. Sakaveli, K. E. Borbas, *Chem. Commun.* **2018**, *54*, 10021–10035.
[62] Y. Ma, Y.-S. Yang, Y.-H. Jiang, Y.-X. Li, M. Liu, Z.-F. Li, H.-L. Han, Y.-P. Yang, X.-L. Xin, Q.-H. Jin, *RSC Adv.* **2017**, *7*, 41651–41666.
[63] A. K. R. Junker, L. R. Hill, A. L. Thompson, S. Faulkner, T. J. Sørensen, *Dalt. Trans.* **2018**, *47*, 4794–4803.
[64] S. Petoud, S. M. Cohen, J.-C. G. Bünzli, K. N. Raymond, *J. Am. Chem. Soc.* **2003**, *125*, 13324–13325.
[65] L. Götzke, G. Schaper, J. März, P. Kaden, N. Huittinen, T. Stumpf, K. K. K. Kammerlander, E. Brunner, P. Hahn, A. Mehnert, et al., *Coord. Chem. Rev.* **2019**, *386*, 267–309.
[66] C. Xie, H.-F. Chau, J.-X. Zhang, S. Tong, L. Jiang, W.-Y. Fok, H.-L. Lung, S. Zha, R. Zou, J. Jiao, et al., *Adv. Ther.* **2019**, *2*, 1900068.
[67] J. C. Frías, J. Soriano, S. Blasco, E. García-España, A. Rodríguez-Rodríguez, D. Esteban-Gómez, F. Carniato, M. Botta, C. Platas-Iglesias, M. T. Albelda, *Inorg. Chem.* **2020**, *59*, 7306–7317.
[68] S. Mizukami, R. Takikawa, F. Sugihara, Y. Hori, H. Tochio, M. Wälchli, M. Shirakawa, K. Kikuchi, *J. Am. Chem. Soc.* **2008**, *130*, 794–795.
[69] M. Regueiro-Figueroa, D. Esteban-Gómez, A. de Blas, T. Rodríguez-Blas, C. Platas-Iglesias, *Chemistry* **2014**, *20*, 3974–3981.
[70] J. Ramalho, M. Ramalho, *Magn. Reson. Imaging Clin. N. Am.* **2017**, *25*, 765–778.
[71] W. P. Cacheris, S. K. Nickle, A. D. Sherry, *Inorg. Chem.* **1987**, *26*, 958–960.
[72] J. C. G. Bünzli, A. S. Chauvin, C. D. B. Vandevyver, S. Bo, S. Comby, *Ann. N. Y. Acad. Sci.* **2008**, *1130*, 97–105.
[73] J. M. Idée, M. Port, I. Raynal, M. Schaefer, S. Le Greneur, C. Corot, *Fundam. Clin. Pharmacol.* **2006**, *20*, 563–576.
[74] C. S. Bonnet, É. Tóth, *Curr. Opin. Chem. Biol.* **2021**, *61*, 154–169.

[75] A. Pałasz, P. Czekaj, *Acta Biochim. Pol.* **2000**, *47*, 1107–1114.
[76] J. C. G. Bünzli, C. Piguet, *Chem. Soc. Rev.* **2005**, *34*, 1048–1077.
[77] S. J. Butler, D. Parker, *Chem. Soc. Rev.* **2013**, *42*, 1652–1666.
[78] A. B. Aletti, D. M. Gillen, T. Gunnlaugsson, *Coord. Chem. Rev.* **2018**, *354*, 98–120.
[79] M. L. Aulsebrook, B. Graham, M. R. Grace, K. L. Tuck, *Coord. Chem. Rev.* **2018**, *375*, 191–220.
[80] S. Shuvaev, M. Starck, D. Parker, *Chem. – A Eur. J.* **2017**, *23*, 9974–9989.
[81] J. C. G. Bünzli, *Chem. Rev.* **2010**, *110*, 2729–2755.
[82] X. Wang, H. Chang, J. Xie, B. Zhao, B. Liu, S. Xu, W. Pei, N. Ren, L. Huang, W. Huang, *Coord. Chem. Rev.* **2014**, *273–274*, 201–212.
[83] O. A. Blackburn, M. Tropiano, L. S. Natrajan, A. M. Kenwright, S. Faulkner, *Chem. Commun.* **2016**, *52*, 6111–6114.
[84] G. Chen, N. J. Wardle, J. Sarris, N. P. Chatterton, S. W. A. Bligh, *Dalt. Trans.* **2013**, *42*, 14115–14124.
[85] L. Zhang, A. F. Martins, P. Zhao, Y. Wu, G. Tircsó, A. D. Sherry, *Angew. Chemie* **2017**, *129*, 16853–16857.
[86] R. Botár, E. Molnár, G. Trencsényi, J. Kiss, F. K. Kálmán, G. Tircsó, *J. Am. Chem. Soc.* **2020**, *142*, 1662–1666.
[87] P. Urbanovský, J. Kotek, F. Carniato, M. Botta, P. Hermann, *Inorg. Chem.* **2019**, *58*, 5196–5210.
[88] C. S. Bonnet, E. Tóth, *AJNR. Am. J. Neuroradiol.* **2010**, *31*, 401–409.
[89] Z. Wang, J. Gao, K. Zhang, Z. Mai, Q. Wang, *Opt. Mater. (Amst).* **2018**, *81*, 1–6.
[90] M. Leonzio, A. Melchior, G. Faura, M. Tolazzi, M. Bettinelli, F. Zinna, L. Arrico, L. Di Bari, F. Piccinelli, *New J. Chem.* **2018**, *42*, 7931–7939.
[91] R. S. Dickins, S. Aime, A. S. Batsanov, A. Beeby, M. Botta, J. I. Bruce, J. A. K. Howard, C. S. Love, D. Parker, R. D. Peacock, H. Puschmann, *J. Am. Chem. Soc.* **2002**, *124*, 12697–12705.
[92] S. Y. Huang, M. Qian, V. C. Pierre, *Inorg. Chem.* **2019**, *58*, 16087–16099.
[93] C. X. Zhao, X. P. Zhang, Y. Shu, J. H. Wang, *ACS Appl. Mater. Interfaces* **2020**, *12*, 22593–22600.
[94] F. Piccinelli, C. De Rosa, A. Melchior, G. Faura, M. Tolazzi, M. Bettinelli, *Dalt. Trans.* **2019**, *48*, 1202–1216.
[95] L. Bridou, L. G. Nielsen, T. J. Sørensen, *J. Rare Earths* **2020**, *38*, 498–505.
[96] J. Vaněk, P. Lubal, P. Hermann, P. Anzenbacher, *J. Fluoresc.* **2013**, *23*, 57–69.
[97] S. E. Bodman, S. J. Butler, *Chem. Sci.* **2021**, *12*, 2716–2734.
[98] E. A. Weitz, J. Y. Chang, A. H. Rosenfield, V. C. Pierre, *J. Am. Chem. Soc.* **2012**, *134*, 16099–16102.
[99] E. A. Mikhalyova, A. V. Yakovenko, M. Zeller, M. A. Kiskin, Y. V. Kolomzarov, I. L. Eremenko, A. W. Addison, V. V. Pavlishchuk, *Inorg. Chem.* **2015**, *54*, 3125–3133.
[100] H. Lei, J. Liu, J. Yan, S. Lu, Y. Fang, *ACS Appl. Mater. Interfaces* **2014**, *6*, 13642–13647.
[101] K. Gupta, A. K. Patra, *Eur. J. Inorg. Chem.* **2018**, *2018*, 1882–1890.
[102] D. G. Smith, R. Pal, D. Parker, *Chem. – A Eur. J.* **2012**, *18*, 11604–11613.
[103] M. J. Langton, C. J. Serpell, P. D. Beer, *Angew. Chemie Int. Ed.* **2016**, *55*, 1974–1987.
[104] P. Gale, T. Gunnlaugsson, F. P. Schmidtchen, *Chem. Soc. Rev* **2010**, *39*, 3916–3935.
[105] S. Shinoda, K. Yano, H. Tsukube, *Chem. Commun.* **2010**, *46*, 3110–3112.
[106] T. Wu, J. Kessler, P. Bouř, *Phys. Chem. Chem. Phys.* **2016**, *18*, 23803–23811.
[107] S. S. Shinoda, H. Tsukube, S. Shinoda, H. Tsukube, *Analyst* **2011**, *136*, 431–435.
[108] X. Wang, X. Wang, Y. Wang, Z. Guo, *Chem. Commun.* **2011**, *47*, 8127–8129.
[109] C. Zhao, Y. Sun, J. Ren, X. Qu, *Inorganica Chim. Acta* **2016**, *452*, 50–61.
[110] H. A. Azab, G. M. Khairy, N. Abd El-Ghany, M. A. Ahmed, *J. Photochem. Photobiol. A Chem.* **2019**, *374*, 1–9.
[111] F. Smrčka, P. Lubal, *Mol. 2020, Vol. 25, Page 4164* **2020**, *25*, 4164.
[112] S. H. Hewitt, S. J. Butler, *Chem. Commun.* **2018**, *54*, 6635–6647.
[113] C. M. Spangler, C. Spangler, M. Schäerling, *Ann. N. Y. Acad. Sci.* **2008**, *1130*, 138–148.
[114] O. Alptürk, O. Rusin, S. O. Fakayode, W. Wang, J. O. Escobedo, I. M. Warner, W. E.

Crowe, V. Král, J. M. Pruet, R. M. Strongin, *Proc. Natl. Acad. Sci. U. S. A.* **2006**, *103*, 9756–9760.
[115] X. Chen, H. Song, Z. Li, R. Liu, Y. Lv, *Anal. Chem.* **2021**, *93*, 13719–13726.
[116] R. Jastrząb, M. Nowak, M. Skrobańska, A. Tolińska, M. Zabiszak, M. Gabryel, Ł. Marciniak, M. T. Kaczmarek, *Coord. Chem. Rev.* **2019**, *382*, 145–159.
[117] G. D. Palmer, M. J. Stoddart, E. Gouze, J.-N. Gouze, S. C. Ghivizzani, R. M. Porter, C. H. Evans, *Gene Ther.* **2008**, *15*, 357–363.
[118] H. Y. Wong, W. S. Lo, K. H. Yim, G. L. Law, *Chem* **2019**, *5*, 3058–3095.
[119] M. Leonzio, A. Melchior, G. Faura, M. Tolazzi, M. Bettinelli, F. Zinna, L. Arrico, L. Di Bari, F. Piccinelli, *New J. Chem* **2018**, *42*, 7931.
[120] T. Wu, P. Bouř, *Chem. Commun.* **2018**, *54*, 1790–1792.

Chapter 2

Aim of the work

2.1 Aim

The selective detection and imaging of specific bioanalytes represents a fundamental component of several biomedical studies. Therefore, the need to satisfy the requirements of the modern bioanalysis and bioimaging is becoming of outstanding importance. Ln(III) complexes, mainly Eu(III) and Tb(III) complexes, have been exploited as sensors in physiological conditions for the detection of important bio-analytes due to the advantages highlighted in the introduction.

In this framework, the aim of this thesis was to obtain highly emissive Eu(III) complexes and characterize their ability to report different bio-analytes present in the interstitial extracellular fluid (i.e. hydrogen carbonate, serum albumin and citrate).

In the PhD work, water soluble Eu(III) complexes, based on the chiral 1,2-diaminocyclohexane (DACH) backbone, were studied for their application as luminescent sensors.

The speciation of Eu(III) complexes has been determined by potentiometric and spectrophotometric studies. Moreover, calorimetry and fluorimetry experiments were carried out to study the interaction with selected analytes. Theoretical calculations were used to get structural information on the complexes and their adducts with the analytes.

The study of the stability, speciation and structure of these luminescent Eu(III) complexes in water is important as it is essential to define the emissive species at a given pH (especially the physiological one). Also, the definition of the relative affinity for different analytes allows to assess the selectivity of the luminescent sensor in a complex matrix.

Chapter 3

Experimental

3.1 Procedures, techniques and characterization

3.1.1 Ligand and Complex Synthesis

All the library of water soluble ligands and Eu(III) complexes (Figure 3.1) are constituted by a chiral 1,2-diaminocyclohexane (DACH) moiety.

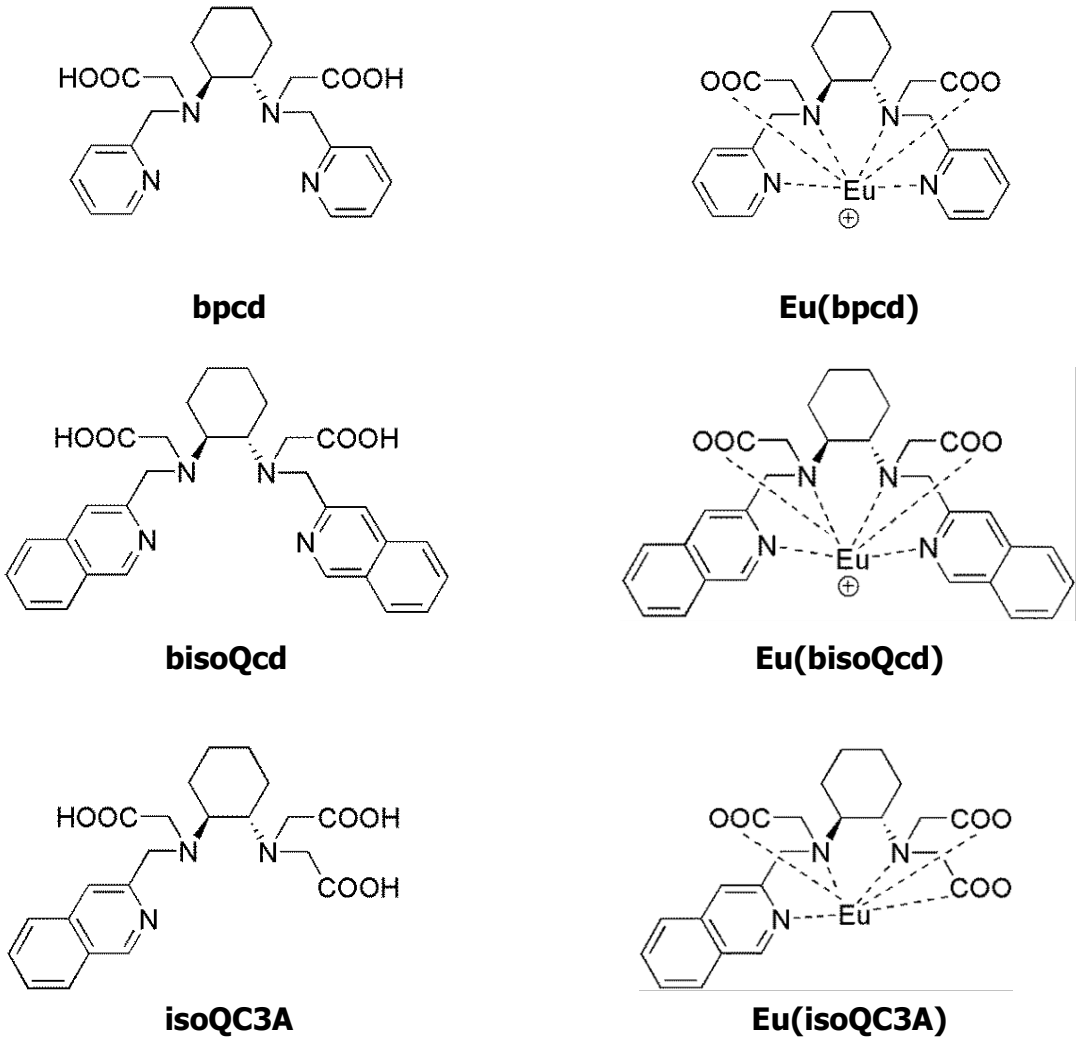

Figure 3.1 *Studied ligands and Eu-complexes, where bpcd = N,N′-bis(2-pyridylmethyl)-trans-1,2- diaminocyclohexane-N,N′-diacetic acid, bisoQcd = N,N′-bis(2-isoquinolinmethyl)-trans-1,2-diaminocyclohexane N,N′- diacetate) and isoQC3A = N-isoquinolyl-N,N′,N′-trans-1,2-cyclohexylenediaminetriacetate*

The bpcd and isoQC3A ligand and the relative Eu(III) complexes, have been previously synthesized and characterized in other works and PhD thesis.[1–3] Herein,

we recall the different synthetic route for diacetate bisoQcd and his triacetate analogous isoQC3A ligands.

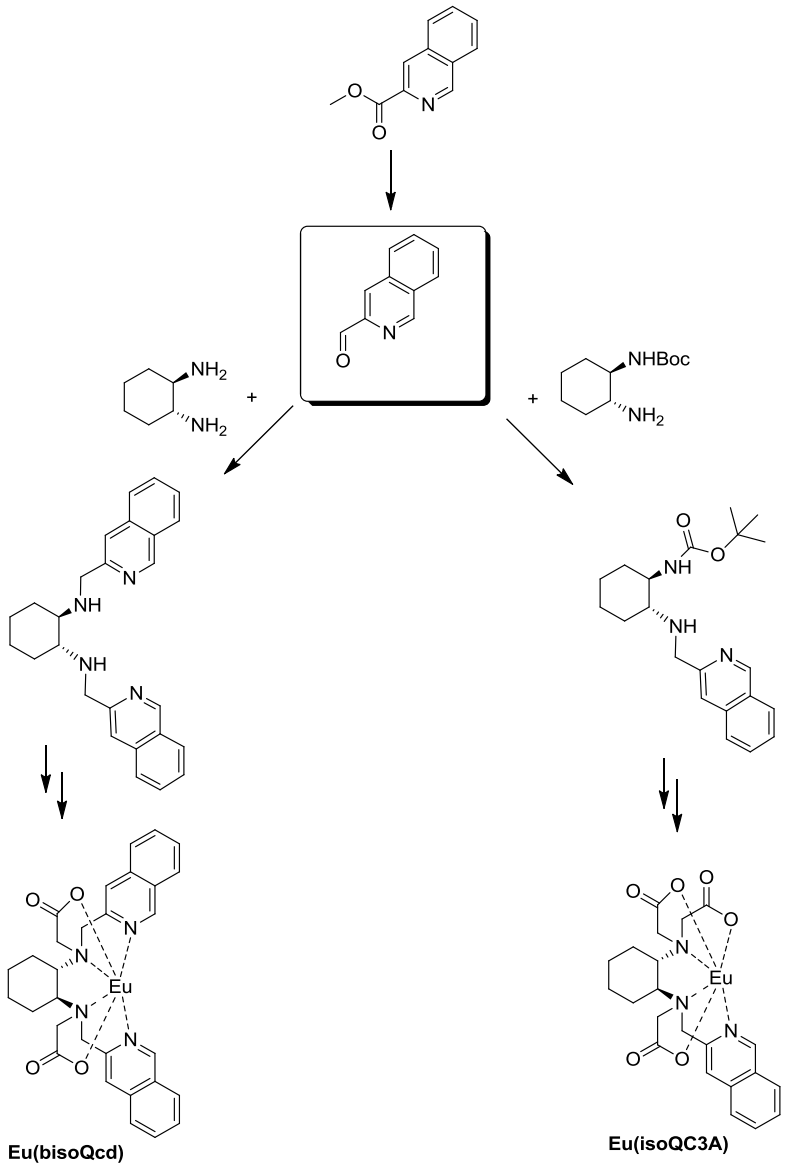

Figure 3.2 *Different synthetic route for bisoQcd and isoQC3A ligands*

3.1.2 Elemental analysis

Elemental analysis of final products, both ligands and complexes, and some of their intermediate have been carried out by using EACE 1110 CHNOS analyzer.

3.1.3 Electrospray ionization mass spectroscopy

The final products (ligands and complexes) and some of their intermediate products have been analysed by electrospray ionization mass spectrometry (ESI-MS) with a Finnigan LXQ Linear Ion Trap (Thermo Scientific, San Jose, CA, USA) operating in positive mode. Xcalibur software (Thermo Scientific) was used for data acquisition. A methanol solution of the sample was diluted and infused with a syringe pump, with flow rate of 10 µL/min into the ion source. The typical source conditions were transfer line capillary at 548.15 K; ion spray voltage at 4.70 kV; sheath, auxiliary and sweep gas (N_2) flow rates at 10, 5 and 0 arbitrary units, respectively. Helium was used as the collision damping gas in the ion trap set at 1 mTorr.

3.2 Determination of equilibrium constants

3.2.1 Principles and definitions

A chemical equilibrium is a condition in the course of a reversible chemical reaction, in which no net change in the amounts of reactants and products occurs. A reversible chemical reaction is one in which the products, as soon as they are formed, react to produce the original reactants.

The equation allows the calculation of the equilibrium constant, or the relative amounts of products and reactants present at equilibrium, from measured or derived values of standard free energies of substances.

The equilibrium constant (K) of a generic reaction (Equation 3.1 a) is a mathematical relationship that shows how the products concentrations vary with the concentration of the reactants (Equation 3.1 b). The experiments are therefore carried out at a constant temperature, using a thermostatic control apparatus. Moreover, the ionic strength of the solution was kept constant, using a sufficiently high concentration of an inert background electrolyte.

Since, the experiments were done at constant temperature and ionic strength, activities can be substituted by concentrations to give a modified K' (Equation 3.1 c) which, from now on, will be simply called K.[4]

$$bB + cC \rightleftharpoons dD + eE \qquad (3.1\ a)$$

$$K = \frac{a_D^d \cdot a_E^e}{a_B^b \cdot a_C^c} \qquad (3.1\ b)$$

$$K' = \frac{[D^d] \cdot [E^e]}{[B^b] \cdot [C^c]} = K \qquad (3.1\ c)$$

During the course of this thesis, for the equilibrium constant is going to be used two different terms: *K* (the above-defined stepwise equilibrium constant) and β (the cumulative overall equilibrium constant or formation constant). The first one is more intuitive and common, and sometimes will be used for comparison of the obtained results. The second one was used for computational purposes (required by the software used for the constants fitting) and will be defined after.

Successive stepwise formation constants of a generic protonation (K_1, K_2, K_3 and K_4) can be defined (Equations 3.2 a-d)[4] as:

$$L^{4-} + H^+ \rightleftharpoons LH^{3-}; \quad K_1 = \frac{[LH^{3-}]}{[L^{4-}] \cdot [H^+]} \qquad (3.2\ a)$$

$$LH^{3-} + H^+ \rightleftharpoons LH_2^{2-}; \quad K_2 = \frac{[LH_2^{2-}]}{[LH^{3-}] \cdot [H^+]} \qquad (3.2\ b)$$

$$LH_2^{2-} + H^+ \rightleftharpoons LH_3^-; \quad K_3 = \frac{[LH_3^-]}{[LH_2^{2-}] \cdot [H^+]} \qquad (3.2\ c)$$

$$LH_3^- + H^+ \rightleftharpoons LH_4; \quad K_4 = \frac{[LH_4]}{[LH_3^-] \cdot [H^+]} \qquad (3.2\ d)$$

Given the four overall protonation reactions for the same compound, β_1, β_2, β_3 and β_4 can be defined (Equations 3.3 a-d). In addition, the mathematical relation between *K* and *β* values are also shown in Equations 3.3 a-d. For simplicity, the logarithm of these constants is reported. The mathematical relation between *log K* and *log β* values are easily deduced from Equations 3.3 a-d.[4]

$$L^{4-} + H^+ \rightleftharpoons LH^{3-}; \quad \beta_1 = \frac{[LH^{3-}]}{[L^{4-}] \cdot [H^+]} = K_1 \qquad (3.3\ a)$$

$$L^{4-} + 2H^+ \rightleftharpoons LH_2^{2-} \; ; \quad \beta_2 = \frac{[LH_2^{2-}]}{[L^{4-}]\cdot[H^+]^2} = K_1 \cdot K_2 \qquad (3.3\ b)$$

$$L^{4-} + 3H^+ \rightleftharpoons LH_3^{-} \; ; \quad \beta_3 = \frac{[LH_3^{-}]}{[L^{4-}]\cdot[H^+]^3} = K_1 \cdot K_2 \cdot K_3 \qquad (3.3\ c)$$

$$L^{4-} + 4H^+ \rightleftharpoons LH_4 \; ; \quad \beta_4 = \frac{[LH_4]}{[L^{4-}]\cdot[H^+]^4} = K_1 \cdot K_2 \cdot K_3 \cdot K_4 \qquad (3.3\ d)$$

The thermodynamic equilibrium constant expression relates the activities (a unitless quantity that can be used in place of concentration. Since activities are unitless, they eliminate the units of all the quantities in the equilibrium constant expression, making the constant itself unitless all the time) of all of the species. The activity (ai) and the concentration (Ci) of a generic species Ci, are related when using Equation 3.4, where a is the activity of C, [C] is the concentration and γ is the activity coefficient of C; this last term is constant, when the ionic strength (μ) and temperature (T) of the system are kept under control.[4–8]

$$a_i = \gamma_i \cdot [C]_i \qquad (3.4)$$

In our experiments, T (298.15 K) and μ (0.1 M) were kept constant in order to have reliable thermodynamic data and to deal with concentrations instead of activities. Therefore, in the following concepts and equations, such as pH (Equation 3.5 a) and Nernst equation (Equation 3.6 a), the concentrations will be considerate instead of activities.

Thus, instead of Equation 3.5 a, Equation 3.5 b is going to be used (p[H] will be written as pH), and instead of Equation 3.6 a is going to be used Equation 3.6 b, where E is the observed electromotive force (emf), E^0 is the standard emf for the redox couple $S^{z+}/S^{(z-n)+}$, *n* is the number of electrons involved in the reduction of S, R is the gas constant and F is the Faraday constant. $E^{0'}$ is a modified standard emf (Equation 3.6 c), and it will be written as E^0 from now on.

$$pH = -log\ a_{H^+} \qquad (3.5\ a)$$

$$p[H] = -log[H^+] \qquad (3.5\ b)$$

$$E = E^0 + \frac{RT}{nF} ln \frac{a_{S^{z+}}}{a_{S^{(z-n)+}}} \qquad (3.6\ a)$$

$$E = E^{0\prime} + \frac{RT}{nF} ln \frac{[S^{z+}]}{[S^{(z-n)+}]} \qquad (3.6\ b)$$

$$E^{0\prime} = E^0 + \frac{RT}{nF} ln \frac{\gamma_{S^{z+}}}{\gamma_{S^{(z-n)+}}} \qquad (3.6\ c)$$

The Gibbs free energy of a system instead is defined as the enthalpy of the system minus the product of the temperature times the entropy of the system (Equation 3.7).

$$G = H - TS \qquad (3.7)$$

The Gibbs free energy of the system is a state function because it is defined in terms of thermodynamic properties that are state functions (Equation 3.8). The change in the Gibbs free energy of the system that occurs during a reaction is therefore equal to the change in the enthalpy of the system minus the change in the product of the temperature times the entropy of the system.

$$\Delta G = \Delta H - \Delta\ (TS) \qquad (3.8)$$

If the reaction is run at constant temperature, this equation can be written as follows (Equation 3.9):

$$\Delta G = \Delta H - T\Delta S \qquad (3.9)$$

The change in the free energy of a system that occurs during a reaction can be measured under any set of conditions. If the data are collected under standard-state conditions, the result is the standard-state free energy of reaction (ΔG^{o}). Enthalpy

(ΔH^0), free energy (ΔG^0) and entropy (ΔS^0) are related by the equation (Equation 3.10):

$$\Delta G^\circ = \Delta H^\circ - T\Delta S^\circ \qquad (3.10)$$

The beauty of the equation defining the free energy of a system is its ability to determine the relative importance of the enthalpy and entropy terms as driving forces behind a particular reaction. The change in the free energy of the system that occurs during a reaction measures the balance between the two driving forces, enthalpy and entropy, that determine whether a reaction is spontaneous.
It can be shown that the equilibrium constant is related to the thermodynamic function standard Gibbs free energy accompanying the reaction (Equation 3.11). The standard Gibbs free energy of the reaction, $\Delta G°$, which is the difference between the sum of the standard free energies of the products and that of the reactants, is equal to the negative natural logarithm of the equilibrium constant multiplied by the so-called gas constant R and the absolute temperature T:

$$\Delta G^\circ = -RT \ln K \qquad (3.11)$$

The Nernst equation describes the relationship between the cell potential at any moment in time and the standard-state cell potential (Equation 3.6).

If we rearrange the equation what we may obtain is (Equation 3.12):

$$nFE = nFE^\circ - RT \ln Q \qquad (3.12)$$

one can now compare it with the equation used to describe the relationship between the free energy of reaction at any moment in time and the standard-state free energy of reaction (Equation 3.13).

$$\Delta G = \Delta G^\circ + RT \ln Q \qquad (3.13)$$

These equations are similar because the Nernst equation is a special case of the more general free energy relationship. We can convert one of these equations to the other by taking advantage of the following relationships between the free energy of a reaction and the cell potential of the reaction when it is run as an electrochemical cell (Equation 3.14).

$$\Delta G^{o} = -nFE^{o} \qquad (3.14)$$

3.2.2 Acid-base titrations

All the equilibrium constants founded during this PhD work have been obtained owing potentiometric and spectrophotometric acid-base titrations. The potentiometry is one of the most frequently used method to determine the stability constants of complex species in solution, due to its great accuracy and precision. Although, the recommended ligand concentration for this technique is around 1-5 mM.[4] As a consequence, when reaching the required concentration was not possible (due to solubility problems) spectrophotometric acid-base titrations where done. The latter technique can also give additional information about the protonation and complexation sites when the chromophore moieties of the molecule are involved.

All acid-base titrations were performed in 0.1 M NaCl aqueous solution, in order to keep ionic strength constant. The titration cell was maintained at constant temperature (298.15 ± 0.1 K) thanks to a circulatory bath. The emf was collected by means of a combined glass electrode (Metrohm Unitrode 6.0259.100) connected to a computer-controled potentiometer (Amel Instruments, 338 pH Meter). The initial solution was bubbled with Argon while the system was reaching thermal equilibrium. Moreover, during experiments, a low Argon flux was maintained over the closed system in order to avoid CO_2 from reaching the solution. The aim is to eliminate the solved atmospheric CO_2, which would lead to a protolytic impurity since it may contaminate the alkali (Equation 3.15).[4,6,7,9]

$$CO_{2(aq)} + H_2O_{(l)} \rightleftharpoons H_2CO_{3(aq)} \qquad (3.15)$$

$$NaOH_{(aq)} + H_2CO_{3(aq)} \rightleftharpoons NaHCO_{3(aq)} + H_2O_{(l)}$$

The gas flux was also previously passed through a NaOH trap in order to capture the eventual CO_2 present. In the case of spectrophotometric titrations, a fibre-optic probe, with a 10 mm path length, connected to a computer-controlled Varian Cary 50 instrument, was immersed into the solution in order to record and collect absorbance data. NaOH was added via automatic burette (Metrohm Dosimat 665) manually (spectrophotometry) or automatically (potentiometry). The solution was continuously gently stirred by means of a magnetic stirrer (Figure 3.3).

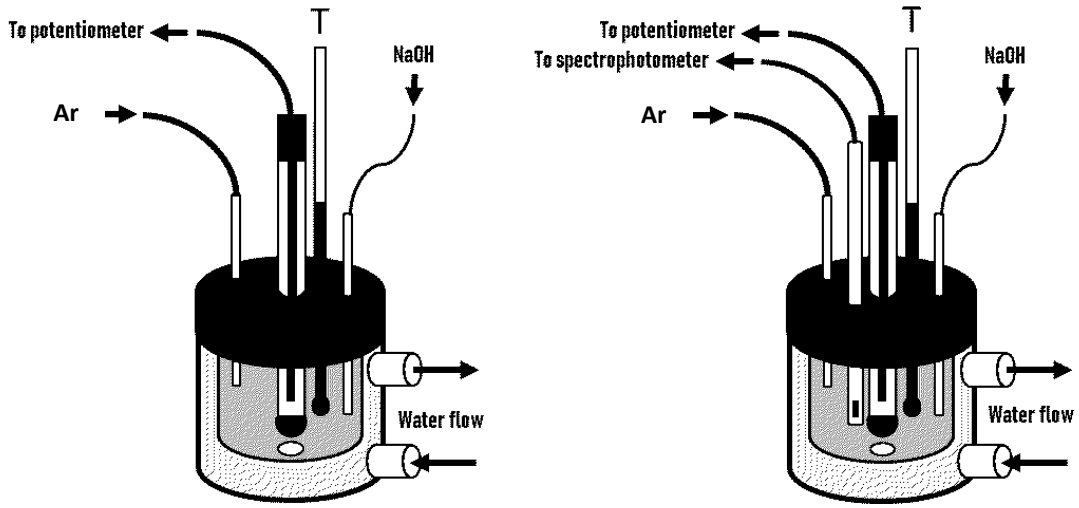

Figure 3.3 *Principle of the system for potentiometric (left) and spectrophotometric (right) acid-base titrations*

The electrode before each titration was calibrated (modified Nernst equation, Equation 3.6 b) performing an acid-base titration with standard HCl and NaOH 0.1 M stock solutions. In addition, carbon dioxide present in solution was checked by Gran method.[7] GLEE (glass electrode evaluation),[9] part of HyperQuad program, can be used to calculate the slope and the electrode standard potential linearizing the titration curve where E is the measured potential (Equation 3.16):

$$E = E^0 + s \log[H^+] \qquad (3.16)$$

The optimal case should show all the points fitted by two lines, with the first relative to the acid (beginning of titration) and the second relative to the base (end of titration) converging in a single point. This intersection gives an estimation of the equivalent volume, which should be the same for acid and base ideally, as shown in Figure 3.4.

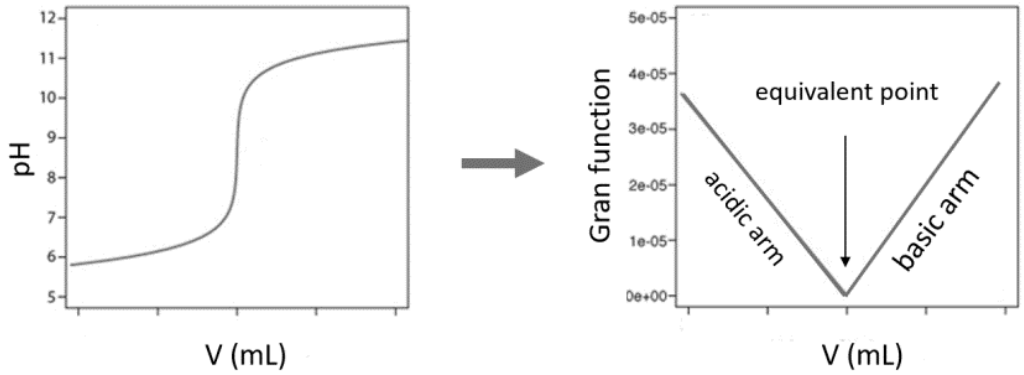

Figure 3.4 *Gran plot*

In case of base contamination, for example given from carbonate, it may happen that the alkaline region will be larger than the acid region. About it, the alkalinity level can be calculated:

$$\text{Alkalinity level } \% \quad = \frac{\text{Ve base} - \text{Ve acid}}{\text{Ve base}} * 100 \qquad (3.17)$$

Once calibrated, the system was prepared for the protonation studies after acidifying the system with HCl and adding the right amount of ligand. After this first acid-base titration, the solution was acidified again and the right amount of metal was added in order to prepare the system for the complexation experiments. In each titration, the solution was brought from an approximate pH value of 2.3 to about pH 11.5 by the addition of standard NaOH solution.

When needed, the program VLpH was used for the calibration of a glass electrode in terms of hydrogen ion concentration at very low pH, since deviations from the Nernst law are observed. The electrode response in that case is assumed to follow a modified Nernst law (Equation 3.18), in which E is a measured electrode potential, E^0 is the "standard" electrode potential, s is a slope factor and *jp* is a "junction potential" correction factor.

$$E = E^0 + s \log_{10}[H^+] + jp\,[H^+] \qquad (3.18)$$

The calibration process was done in two stages: after performing a "titration", by adding a strong acid of known concentration to a known quantity of background electrolyte solution and measured the electrode potential at each titration point. VLpH program was used to determine the calibration parameters, E^0, s, and *jp*. $[H^+]$ was calculated from the amount of acid added, and its strength.
After that, read a set of data points from an experimental titration curve (obtained using the same background electrolyte) and adjust the values such that they will appear to obey the Nernst Law (Equation 3.19).

$$E^{adj} = E - jp\,[H^+] = E^0 + s \log[H^+] \qquad (3.19)$$

3.2.3 Potentiometric acid-base titrations

Potentiometry is one of the most frequently used method to determine the stability constants of complex species in solution, because of its great accuracy and precision.[10] Potentiometry consists of measuring the potential between two electrodes in contact with the solution.[4] Not always is possible to find an indicator electrode sensible towards the desired analyte but, fortunately, the system in equilibrium can usually be studied by following a competing species. For instance, in the case of the formation of a lanthanide complex, there will be competition between the H^+ and lanthanide cations during the acid-base titration toward ligand complexation and, thus, it is possible to study the system by following the H^+ cations instead of the lanthanide ones. As we have already mentioned, in this work a

combined glass electrode has been used. It is both, the reference and the indicator electrode at the same time, and it is sensible towards the activity of H^+ cations.

Both the additions and the measurements where controlled by a personal computer. The inputs which defined the data acquisition where:

- Total volume injected
- Volume step (fix or variable) and number of lectures
- Dead time after the injection, before the reading
- Delay time between readings (same injection)
- Maximum drift accepted between readings (same injection)
- Maximum number of readings for the same injection

Stock solutions of NaOH and HCl were prepared by diluting 1.0 M standard solutions (Fluka Analytical) in ultrapure water (>18 MΩ·cm, ELGA Purelab UHQ). The ionic strength of all solutions was adjusted to 0.1 M with appropriate amounts of NaCl (Riedel-de Häen). Stock solutions of Eu(III) (80 mM) were prepared by dissolving the chloride salt (Sigma-Aldrich). The lanthanide content in the stock solutions was determined by titration with EDTA and xylenol orange as an indicator in acetate buffer.[11] Free acid concentration in lanthanide solutions were checked by Gran's method.[7]

Protonation constants of the bisoQcd and isoQC3A ligand was determined by acid–base potentiometric titrations. The titration cell was maintained at constant temperature (T = 298.15 K) with a circulatory bath and under an argon radial flux. The electromotive force (emf) data were collected by using a computer-controlled potentiometer (Amel Instruments, 338 pH Meter) connected to a combined glass electrode (Metrohm Unitrode 6.0259.100). The electrode was calibrated before each experiment by an acid–base titration with standard HCl and NaOH solutions. Titrations were performed by adding NaOH or HCl to ligand solutions (total ligand concentration, bisoQcd $C°_L$ = 0.72 mM and isoQC3A $C°_L$ = 0.75 mM) by a computer-controlled burette (Metrhom Dosimat 765).

The emf data collected, the concentrations of the initial species (HCl, ligand and, eventually, metal), the initial volume, the temperature and the calibration data obtained previously are introduced in the Hyperquad[12,13] program in order to obtain the speciation model which better fits the experimental data. This program calculations are essentially based on a non-linear least-squares refinement, which minimizes the error (U) in each run (i) between calculated and experimental emf (E), giving less weight (w) to the data near the equivalence point (Equation 3.20). E_{calc} is obtained from Equation 3.6 b, where the modified standard emf and a slope factor, used to correct the deviation from the expected slope, $\left(\frac{RT}{nF}\right)$ are obtained from the previous calibration.

$$U = \sum_i [w_i \, (E_{calc,i} - E_{exp,i})^2] \qquad (3.20)$$

3.2.4 Spectrophotometric acid-base titrations

Due to its high accuracy and precision, potentiometric acid-base titrations was the first choice for the study of systems in equilibrium. However, spectrophotometric acid-base titrations have been done when the performance of potentiometric ones was not possible.

The change in the UV-Vis absorbance along the acid-base titrations was used for the study of the chemical equilibria. In Eq. 3.21 it is reported the Lambert-Beer Law: A_λ, is the absorbance at a certain λ wavelength, d is the optical path, [S] is the concentration of the absorbing analyte S and ε_λ the molar absorbance at a certain λ wavelength. Nevertheless, this expression is valid at low concentrations (< 0.02 M) and when the absorbing species does not go through chemical changes.

$$A_\lambda = d \cdot [S] \cdot \varepsilon_\lambda \qquad (3.21)$$

As our Eu(III) complexes form more than one absorbing species with different molar absorbance, the total absorbance of the system can be expressed as a sum of the

separated contributions, as shown in Eq. 3.22, where *n* would be the number of different absorbing species formed.

$$A_\lambda = d \cdot ([S]_0 \cdot \varepsilon_{\lambda,0} + [S]_1 \cdot \varepsilon_{\lambda,1} + \cdots + [S]_n \cdot \varepsilon_{\lambda,n}) \qquad (3.22)$$

The investigated wavelength range depended on the chromophore moieties of the ligand. The titration cell usually contained the ligand (concentration typically 0.045 mM) and in the case of complexation studies an equimolar quantity of Eu(III).

The formation constants for the Eu(III) complex were determined by spectrophotometric UV–vis/pH titrations. Spectra of the solutions at variable pH were collected with a Varian Cary 50 spectrophotometer equipped with an optical fiber probe which was inserted in the titration cell (optical path: 1 cm). The cell containing the ligand (both bisoQcd and isoQC3A C°L = 0.045 mM) and an equimolar quantity of Eu(III) was titrated with NaOH and the pH corresponding to each spectrum was measured as described above.
Data have been elaborated by HypSpec[12,13] computer program to obtain the speciation model which best reproduces the experimental data. Calculations are based on a non-linear least-squares refinement but, in this case, it minimizes the error (U) in each run (i) between calculated and experimental absorbance (A) (Equation 3.23).

$$U = \sum_i \left(\frac{A_{calc,i} - A_{exp,i}}{A_{exp,i}} \right)^2 \qquad (3.23)$$

3.2.5 Isothermal titration calorimetry

Calorimetry is a well-known experimental technique used to measure the reaction heat of a chemical process. Isothermal calorimetry means that the reaction heats involved are studied in isothermal conditions, recording the heat exchange among the reaction vessel and a thermostatic bath. This technique can measure reaction

heats within the microjoule range, and it is therefore useful to study reactions involving very small quantities of reagents. A typical experiment consists of measuring the reaction heat generated when known volumes of titrant are added to a reaction cell containing the titrand. Isothermal calorimetry gained attention in chemical equilibrium studies since it offers the possibility of using a single technique to determine the thermodynamic properties (ΔG^0, ΔH^0 and ΔS^0) of a wide range of different types of interactions. These processes usually develop small amounts of reaction heats, but thanks to the sensitivity of this technique, it is suitable to determine the stability constants of very weak complexes.

TA Instruments TAMIII thermostat, equipped with a nanocalorimeter (Figure 3.5), was used in order to determinate the constants and the related complexation enthalpy (ΔH^0) for the formation of the Bovine Serum Albumin (BSA) complex with Eu(bpcd) and Eu(bisoQcd).

The instrument is composed of two cylindrical metal housings containing the measure and reference cells. The two calorimeter units (Figure 3.5) are housed in an aluminum holder block in contact with a thermostatic bath. The bath temperature is maintained constant by a series of fine thermostatic regulation systems, and the aluminum holder block ensures that temperature fluctuations. Sensitive thermocouple circuits lying on the bottom of the unit are used to detect temperature differences between reference and measure cells. The reference cell is usually filled with water, or preferably with a solution of the same ionic medium employed during the experiments, so that the reference solution has the same vapour pressure as the solution in the measure cell.

a

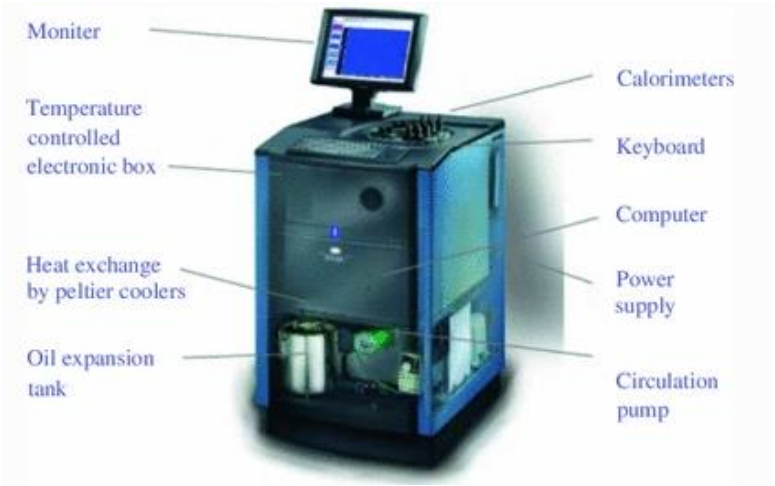

b

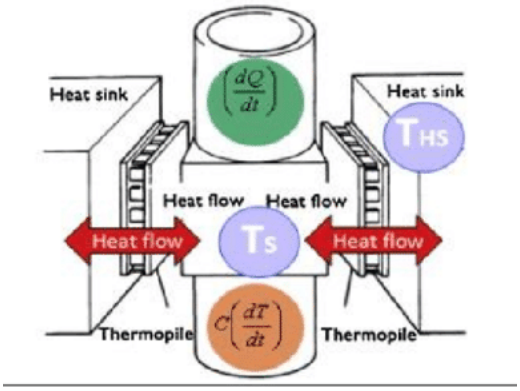

Figure 3.5 *(a) The structure of TAM (Thermal Activity Monitor) III isothermal calorimeter (b) Measurement principle of TAM III*[14]

The reference and measure cells are made of an inert Hastelloy alloy.

The measure cell is usually filled with an initial volume of the titrand solution. It is then sealed and fixed to a vertical metal tree equipped with a Hastelloy stirrer to mix the reactants. A Hamilton gastight glass syringe connected to a capillary cannula is used as a burette to add the titrant to the cell solution. A stepping motor controls the volume dispensed by the burette. In a typical experiment, successive volumes of titrant are added to the measure cell.

The well-known thermodynamic equations 3.10 and 3.11 are used in order to calculate the free Gibbs energy (ΔG^0) from *K*, and the entropy (ΔS^0), ΔH^0 and ΔG^0.

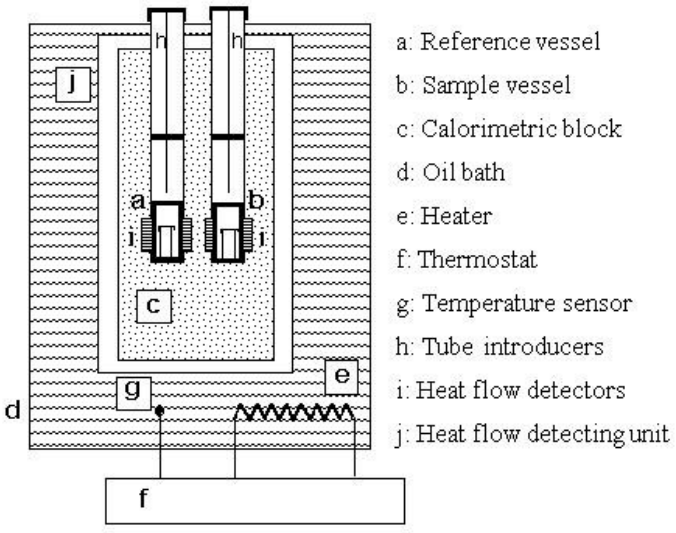

Figure 3.6 *Detail of TAM III measuring unit cylinder*[14]

Before each experiment, the system must be calibrated, for correct information about thermal variations in the measure cell during a thermal event. A precision calibration heater resistor is built into the measuring unit. The calibration resistor is integral with the measuring cup, to simulate a thermal event as closely as possible. This ensures that the output from the detector is also as near as possible identical when the same power is dissipated from both resistor and the reaction cell. During calibration, a known current is passed through the appropriate heater resistor and, because the resistor value is known, the thermal power dissipated is also known. The recorder deflection due to the thermal power dissipated gives the calibration level, which may then be used to determine quantitative experimental results.

In detail, the experiment was done at T = 298.15 K and with a stirring rate of 50 rpm. The sample cell was filled with a solution (V = 0.7 mL) of 0.25 mM of BSA in MOPS buffer (pH= 7.4). Reference cell was filled with MOPS buffer. The titration syringe contained a solution of the complex (1.5–3.0 mM) in MOPS buffer. In the case of the Eu(bisoQcd) complex, it was necessary to add 10% v/v EtOH, due to the low solubility in pure water.

From this experiment, we obtained the experimental heat (Q_{exp}). The heats of dilution (Q_{dil}) were estimated by using identical injections of buffer solution into the protein. All calorimetric data were corrected with the heat of dilution by subtracting the blank from the experiments, in order to obtain the net reaction heat, or corrected heat (Q_{corr}). At least two independent titration experiments were performed to confirm consistency. Data analysis was performed using HypDeltaH.[15]

The Q_{corr} data is correlated to the enthalpy (ΔH_n^0), as shown in Equation 3.24, where Δx_n is the change of n species moles.

$$Q_{corr,i,n} = -\sum_i (\Delta x_n) \Delta H_n^0 \qquad (3.24)$$

3.3 Luminescence

3.3.1 Luminescence and decay kinetics

Luminescence was measured at room temperature with a Fluorolog 3 spectrofluorometer (Horiba-Jobin Yvon) equipped with a single-emission monochromator (Model HR320), a Xe lamp, a double-excitation monochromator and a photomultiplier in photon counting mode for the detection of the emitted signal. All spectra were corrected for the spectral distortions of the setup.

A xenon microsecond flashlamp was used for decay kinetics measurements. The signal was recorded by a multichannel scaling method. True decay times were obtained using the convolution of the instrumental response function with an exponential function and the least-squares-sum-based fitting program (SpectraSolve software package).

The total quantum yields (Φ_{tot}) were obtained by measuring the visible emission spectrum of a fluorescence quantum yield reference sample (quinine in 1N H_2SO_4) presenting Φ_{tot} = 54.6% and using the Equation 3.25 where Φ is the quantum yield, *F* the integrated emission area across the band, *A* the absorbance at the excitation wavelength and *n* the index of refraction of the solvent. The subscript *u* refers to the unknown and *s* to the standard.

$$\Phi_u = \frac{A_s \cdot F_u \cdot n_u^2}{A_u \cdot F_s \cdot n_s^2} \cdot \Phi_s \qquad (3.25)$$

The hydration number, *q,* which is the number of water molecules bound to the metal, was determined using Horrock's equation (Equation 3.26 a). The term *A* is constant for Eu(III), with a value of 1.2. τ is the radiative lifetime (lifetime of the radiation without non-radiative deactivation processes) in water or deuterium oxide. Thus, the correcting term Q (Equation 3.26 b) is added to Horrock's equation.

$$q = A\left[\frac{1}{\tau_{H_2O}} - \frac{1}{\tau_{D_2O}} - Q\right] \qquad (3.26\ a)$$

$$Q = \sum_n (Q_1 + Q_2 + \cdots + Q_n) \qquad (3.26\ b)$$

The radiative lifetimes have been obtained either thank to an estimation using Equation 3.27 a (c = speed of light in vacuous, in cm/s; $\tilde{\upsilon}$ = frequency of the transition in cm^{-1}; n = refractive index of the medium, N_A = Avogadro's number; $\varepsilon(\upsilon)$ = absorption spectrum of the transition in $M^{-1}cm^{-1}$; g_n = degeneracy of the state (n = 0 for ground state, n = exc for the excited one) or calculation with Equation 3.27 b. ΦLn is calculated either by using Equation 3.28 b or by using a referenc6 standard. The efficiency of the sensitization (ηsens) is calculated with Equation 3.27 c.

$$\frac{1}{\tau_{rad}} = 2303 \times \frac{8\pi c n^2 \tilde{\upsilon}_{ul}^2}{N_A} \frac{g_0}{g_{exc}} \int \varepsilon(\upsilon) d\upsilon \qquad (3.27\ a)$$

$$\Phi_{Ln} = \frac{\tau_{obs}}{\tau_{rad}} \qquad (3.27\ b)$$

$$\Phi_{tot} = \eta_{sens} \Phi_{Ln} \qquad (3.27\ c)$$

3.3.2 Fluorometric titrations

In the titration of the complexes, progressive amounts of BSA (up to 180 μM for Eu(bisoQcd) and up to 24 μM for Eu(bpcd) were added to solutions containing the complexes (80 μM). Physiological solutions were prepared MOPS buffered (pH = 7.4) and as isotonic systems (0.9% w/v NaCl). After each addition of BSA, UV-Vis, fluorescence, and excitation spectra as well as the Eu(III)-$^5D_0$ excited-state lifetimes were recorded at 298 K.

Titration of BSA was carried out at 298 K. Progressive amounts of Eu(bisoQcd) or Eu(bpcd) up to 200 μM, were added to MOPS-buffered physiological solution containing 5μM of BSA.

Competitive fluorimetric titration experiments were carried out involving warfarin up to 20 μM, in the case of Eu(bpcd) and up to 100 μM in the case of Eu(bisoQcd), in a MOPS-buffered solution containing BSA-complex adducts (molar ratio Eu(bpcd) : BSA

= 4 : 1; Eu(bpcd)= 80 μM; Molar ratio Eu(bisoQcd) : BSA = 1 : 1; Eu(bisoQcd) = 80 μM). After each addition of warfarin, Eu(III) luminescence emission spectrum was recorded. Similar experiments were carried out with ibuprofen (up to 0.4 mM) and digitoxin (up to 1 mM). Emission data were analysed with as described in section 3.3.4.

3.3.3 Sensing experiments

All the luminescence measurements employed a fresh solution 0.4 mM of the Eu(III) complex previously dissolved in 1.5% v/v of MeOH and diluted in MOPS buffer (pH: 7.4, 0.9% m/v NaCl) up to 0.1 mM. All titrations were performed with the addition of the metal complex as last component of the sample.

Bicarbonate sensing in MOPS buffer 15 mM, pH=7.4, 0.9% p/v NaCl: a starting solution 50 mM of Sodium hydrogen carbonate (Merck) was diluted when required. Since the typical concentration of the analyte in extracellular fluid is between 24-27 mM, an extended range between 1.7-35 mM was examined until the complete saturation of the complex for the calculations of the binding constants.

Citrate sensing in MOPS buffer 15 mM, pH=7.4, 0.9% p/v NaCl: a mother solution of the tri-Sodium citrate dihydrate (Merck) 10 mM was opportunely diluted as well as was required. A wide range for the addition of the citrate between 0.001-5 mM including the extracellular concentration 0.3 mM27 was narrowly explored to reach the complete saturation of the complex for the calculations of the binding constants.

Citrate sensing in artificial extracellular fluid (inorganic components mostly) in MOPS buffer 15 mM, pH=7.4, 0.9% p/v NaCl: the affinity of the most promising bioanalyte for the Eu(III) complexes was pushed in a multicomponent environment. A background containing a mixture of anions and serum albumin (BSA) was fixed in all the experiment.

The investigated anions were in their typical extracellular concentrations, and the serum albumin was present at its normal concentration of 0.4 mM. Incremental additions of Sodium Citrate were done to a limit of 2 mM, in the emission intensity of the bands at 550-730 nm (red-emission of trivalent Europium). Thus, an 0.1 mM

total concentration of the Eu(III) complex was added to a background solution containing BSA (0.4 mM), Sodium hydrogen carbonate (28 mM), di-Sodium hydrogen phosphate (1.3 mM), L-lactate (2.3 mM) and Sodium Sulfate (0.6 mM) and immediately analyzed.

3.3.4 cEST and Solverstat

The Excel add-in Equilibrium speciation tool (cEST), is used for simulation of chemical equilibria in solution.[16] This software use statistical calculation to determine the concentrations of species, in non-aqueous and aqueous systems, at equilibrium. It can be used for different system such as complexation, acid-base, redox and solubility equilibria. It can also simulate, or furthermore obtain, chemical-physical parameters from experimental data. The computational methods with cEST are shown to be very consistent also when applied to homogeneous or even heterogeneous equilibrium systems.[17,18]

An important aspect of the result reliability is to validate them with a statistical analysis. SolverStat[19] is a powerful Excel add-in that performs advanced statistical tests on least squares regression data. Unlikely the Excel add-in Solver, SolverStat provides estimates of the precision of the fitted parameters and a complete and prompted analysis of fittings.

The cEST/SolverStat tools were also used in this work for luminescence data fitting to obtain the speciation model and binding constants of Eu(III) complexes with BSA, bicarbonate and citrate. The refinement of the data has been achieved by minimizing the sum of the squares differences between the experimental and the calculated data (area of the selected luminescence peaks or asymmetry ratio, more details in Section 3.3.). In order to decide the most reliable model, some statistic parameters have been taken into account; the best model for each system should present the lowest confidence interval (obtained from the standard deviation of the refined constants, 95% confidence) and Akaike Information Criteria Corrected (AICc). The AICc parameter is a correction of the AIC parameter for small populations (<10) and is based on the least-squares approach. It permits comparison between models, being the model presenting a lower AICc (or AIC) value considered better.[20,21]

3.4 Computational models

3.4.1 Density functional theory calculations

Since our efforts to obtain good crystalline samples of the Eu(III) complex for X-ray diffraction were unsuccessful, all the complexes have been studied by Density Functional Theory (DFT) calculations, in order to get the most probable structures in solution. The paramagnetic Eu(III) and Tb(III) complexes are difficult to model computationally, thus the analogues of diamagnetic Y(III) ion have been studied.[22] It has been broadly shown that Y(III) complexes may serve as suitable models for Eu(III) analogues,[1,23,24] since their ionic radii are very similar.[25]

Solvent effects were considered by using the *polarizable continuum model* (PCM). Calculations have been carried out by using either Gaussian 16.[26] All final geometries were checked in order to get the conformation with the minimal vibrational energy. Geometry optimizations were carried out at DFT level in PCM[27] water using the B3LYP[28,29] exchange–correlation functional. As previously shown, this protocol proved to provide reliable structural and energetic parameters in water and other solvents.[30–32] The 6-31+G(d) basis set was used for the ligand atoms, while Y(III) ion was described by the quasi-relativistic small core Stuttgart-Dresden pseudopotential and the relative basis set.[33] All the final structures were checked to be minima by vibrational analysis. ESP fitting charges were calculated by using the CHelpG scheme.[34]

3.4.2 Molecular simulations

The two Eu(III) complexes (EuL1 and EuL2 in Figure 3.1), were docked against BSA crystal structure (PDB code: 4F5S) using Autodock suite version 4.2.6.[35] Two docking experiments, for each complex, against two binding sites were done. These were done in order to include the two tryptophan residues of the structure. The flexible residues were selected according a cut-off of 6Å of each tryptophan residue: R194, L197, R198, S201, W213, N217, A341, V342, S343, D450, L454 and E16, E17, F126, K127, A128, D129, E130, K132, F133, W134, N158, N161, Q165 around W213

and W134, respectively. Since, Autodock suite does not include Eu(III) parameters in its force-field, those were manually added to the library. Moreover, because the lanthanide ion interacts in a non-covalent way with the molecule, it was treated as an ion. Thus, parameters of each component of the docked structured was prepared in a different way. For each Autodock run, a cluster analysis over 100 binding poses were collected.

Therefore, from each docking cluster analysis, a docked structure from the better cluster was chosen for perform small molecular dynamics simulations. All MD simulations were performed using the GROMACS program, version 2016.5.[36]

The molecule without Eu(III) was parametrized with the ANTECHAMER suite,[37] the protein was parametrized using the pdb3gmx form GROMACS with the AMBER99SB force-field, and the Eu(III), as was mentioned above, was treated as an ion. Eu(III) parameters were included manually in the force-field.[38] Water and ion molecules (0.154 M of Na^+/Cl^- to mimic physiological conditions) were added to complete the system. The system was then equilibrated through a complete workflow: steepest descents minimization of 5000 steps, NVT equilibration of 100 ps, NPT equilibration of 100 ps, and MD production under the NPT ensemble for 100 ns at room temperature. A pull code with 5000 kJ mol^{-1} nm^{-2} of force between the nitrogen, oxygen, and Eu(III) atoms was included in the MD run to keep the integrity of the complexes.

3.5 Bibliography

[1] M. Leonzio, A. Melchior, G. Faura, M. Tolazzi, F. Zinna, L. Di Bari, F. Piccinelli, *Inorg. Chem.* **2017**, *56*, 4413–4422.

[2] C. De Rosa, A. Melchior, M. Sanadar, M. Tolazzi, A. Duerkop, F. Piccinelli, *Dalt. Trans.* **2021**, *50*, 4700–4712.

[3] F. Piccinelli, C. De Rosa, A. Melchior, G. Faura, M. Tolazzi, M. Bettinelli, *Dalt. Trans.* **2019**, *48*, 1202–1216.

[4] A. E. Martell, R. J. Motekaitis, *Determination and Use of Stability Constants*, VCH Publishers, New York, **1992**.

[5] A. Vesala, *J. Chem. Educ.* **1992**, *69*, 577–578.

[6] P. Sipos, P. M. May, G. T. Hefter, *Analyst* **2000**, *125*, 955–958.

[7] G. Gran, *Analyst* **1952**, *77*, 661.

[8] M. Ronteltap, M. Maurer, W. Gujer, *Water Res.* **2007**, *41*, 977–984.

[9] P. Gans, B. O'Sullivan, *Talanta* **2000**, *51*, 33–37.

[10] H. R. F.J.C. Rossotti, *The Determination of Stability Constants*, McGraw-Hill Book Company, Inc.: New York (US), **1961**.

[11] A. I. (Arthur I. Vogel, G. H. Jeffery, A. I. Vogel, *Vogel's Textbook of Quantitative Chemical Analysis.*, Longman Scientific & Technical ;;Wiley, Harlow Essex England ;New York, **1989**.

[12] L. Alderighi, P. Gans, A. Ienco, D. Peters, A. Sabatini, A. Vacca, *Coord. Chem. Rev.* **1999**, *184*, 311–318.

[13] P. Gans, A. Sabatini, A. Vacca, *Talanta* **1996**, *43*, 1739–1753.

[14] S.-H. Liu, H.-Y. Hou, C.-M. Shu, *Thermochim. Acta* **2015**, *605*, 68–76.

[15] P. Gans, A. Sabatini, A. Vacca, *J. Solution Chem.* **2008**, *37*, 467–476.

[16] P. Polese, M. Tolazzi, A. Melchior, *J. Therm. Anal. Calorim.* **2018**, *134*, 1317–1326.

[17] H. Brandenburg, J. Krahmer, K. Fischer, B. Schwager, B. Flöser, C. Näther, F. Tuczek, *Eur. J. Inorg. Chem.* **2018**, *2018*, 576–585.

[18] S. G. Lanas, M. Valiente, E. Aneggi, A. Trovarelli, M. Tolazzi, A. Melchior, *RSC Adv.* **2016**, *6*, 42288–42296.

[19] C. Comuzzi, P. Polese, A. Melchior, R. Portanova, M. Tolazzi, *Talanta* **2003**, *59*, 67–80.

[20] D. Posada, T. R. Buckley, *Syst. Biol.* **2004**, *53*, 793–808.

[21] M. J. Brewer, A. Butler, S. L. Cooksley, *Methods Ecol. Evol.* **2016**, *7*, 679–692.

[22] M. Soulié, F. Latzko, E. Bourrier, V. Placide, S. J. Butler, R. Pal, J. W. Walton, P. L. Baldeck, B. Le guennic, C. Andraud, J. M. Zwier, L. Lamarque, D. Parker, O. Maury, *Chem. - A Eur. J.* **2014**, *20*, 8636–8646.

[23] A. C. Mendonça, A. F. Martins, A. Melchior, S. M. Marques, S. Chaves, S. Villette, S. Petoud, P. L. Zanonato, M. Tolazzi, C. S. Bonnet, É. Tóth, P. Di Bernardo, C. F. G. C. Geraldes, M. A. A. Santos, *Dalton Trans.* **2013**, *42*, 6046–57.

[24] F. Piccinelli, M. Bettinelli, A. Melchior, C. Grazioli, M. Tolazzi, **2015**, *44*, 182.

[25] S. Cotton, *Lanthanide and Actinide Chemistry*, John Wiley & Sons, Ltd, **2006**.

[26] M. J. Frisch, G. W. Trucks, H. B. Schlegel, G. E. Scuseria, M. A. Robb, J. R. Cheeseman, G. Scalmani, V. Barone, G. A. Petersson, H. Nakatsuji, et al., *Gaussian 16 Revis.* **2016**, *A 03*.

[27] J. Tomasi, B. Mennucci, R. Cammi, *Chem. Rev.* **2005**, *105*, 2999–3093.

[28] A. D. Becke, *J.Chem.Phys.* **1993**, *98*, 1372–1377.

[29] C. T. Lee, W. T. Yang, R. G. Parr, *Phys.Rev.B* **1988**, *37*, 785–789.

[30] F. Endrizzi, P. Di Bernardo, P. L. Zanonato, F. Tisato, M. Porchia, A. A. Isse, A. Melchior, M. Tolazzi, *Dalton Trans.* **2017**, *46*, 1455–1466.

[31] P. Luigi Zanonato, P. Di Bernardo, A. Melchior, M. Busato, M. Tolazzi, *Inorganica Chim. Acta* **2020**, *503*, 119392.

[32] A. Melchior, E. Peralta, M. Valiente, C. Tavagnacco, F. Endrizzi, M. Tolazzi, *Dalton Trans.* **2013**, *42*, 6074–6082.

[33] A. Weigand, X. Cao, J. Yang, M. Dolg, *Theor. Chem. Acc.* **2010**, *126*, 117–127.

[34] C. M. Breneman, K. B. Wiberg, *J. Comput. Chem.* **1990**, *11*, 361–373.
[35] G. M. Morris, H. Ruth, W. Lindstrom, M. F. Sanner, R. K. Belew, D. S. Goodsell, A. J. Olson, *J. Comput. Chem.* **2009**, *30*, 2785–2791.
[36] D. Van Der Spoel, E. Lindahl, B. Hess, G. Groenhof, A. E. Mark, H. J. C. Berendsen, *J. Comput. Chem.* **2005**, *26*, 1701–1718.
[37] J. Wang, R. M. Wolf, J. W. Caldwell, P. A. Kollman, D. A. Case, *J. Comput. Chem.* **2004**, *25*, 1157–1174.
[38] F. C. J. M. van Veggel, D. N. Reinhoudt, *Chem. – A Eur. J.* **1999**, *5*, 90–95.

Chapter 4

Protonation and complex formation

4.1 Library of ligands and complexes

When designing an efficient luminescent lanthanide complex, some factors have to be considered such as the choice of the chelating ligand and the sensitizing moiety (antenna effect, refer to Chapter 1). Furthermore, the complex has to be stable in water (biocompatible) and should present a high overall brightness, as well as leaving some space for the coordination of additional target molecules.

The overall stability of the complex is determined by the ligand structure that chelates the lanthanide ion and the choice of ligand depends on the enthalpy and entropy effects (e.g. number, charge and basicity of coordinating groups and conformational effect). In a biological medium, the complex has to compete with other chelating ligands such as protein, endogenous anions. It is critically important that the ligand chelate tightly to give thermodynamically and kinetically inert complex.

As discussed in Chapter 1, polyamino-polycarboxylate ligands are the best candidates for the formation of highly stable Ln(III) complexes, which makes them specially suitable for biomedical applications.[1–4]

Regarding the chromophore moiety (antenna group) of the ligand,[5] in literature we can find several examples of luminescent Ln(III) complexes presenting amino heteroaromatic antenna, such as pyridine,[6–8] quinoline,[9] isoquinoline[10–12] or coumarin.[13,14] What is more, a defined geometry caused by rigid and steric groups may increase the overall binding affinity.[15]

In this PhD work we propose some Eu(III) polyamino-polycarboxilate complexes presenting either pyridine and isoquinoline chromophore moieties (antenna). All the ligands present 1,2-diaminocyclohexane backbone (DACH, Figure 4.1) which confers advantages like rigidity and chirality.

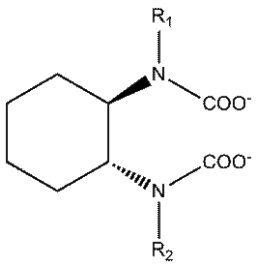

'DACH' BACKBONE

	PYRIDINE (less lipophilic)	ISOQUINOLINE (more lipophilic)
TRIACETATE (neutral)		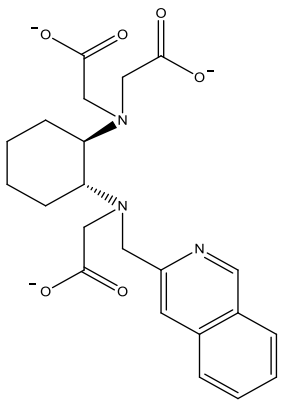 **[isoQC3A]$^{3-}$**
BIACETATE (cationic)	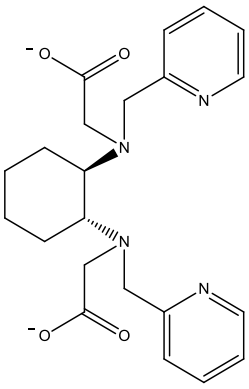 **[bpcd]$^{2-}$**	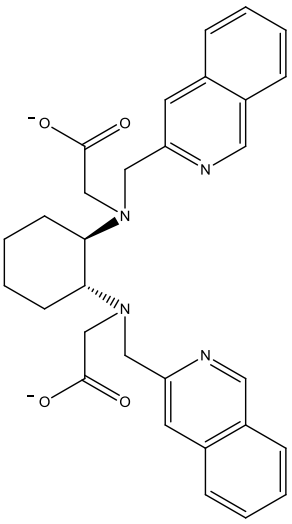 **[bisoQcd]$^{2-}$**

Figure 4.1 *Ligand discussed in this thesis*

The three presented ligands differ in charge, steric hindrance and lipophilicity. IsoQC3A is a neutral ligand, while bpcd and bisoQcd are cationic ones. Each ligand in addition have different steric hindrance on the metallic center, which is correlated to the antenna moieties. In detail, the isoquinoline-functionalization and diacetate ligands are bulkier, while the pyridine-functionalization and triacetate ligands less busy. Moreover, the complexes presenting isoquinoline moieties are more lipophilic.

The lipophilicity and the charge strongly affect the biodistribution, and *in vitro/in vivo* experiments.

The modulation of DACH backbone with varied moieties will facilitate the study towards different target bio-analytes, since we expect steric hindrance and charge to impact the stability of both the Eu(III) complexes and their adducts with target bio-analyte.

The designed Eu-complex are soluble in water, due to the presence of two carboxylate groups that also increase the stability of the complex. While the pyridine ring is capable to sensitize both Eu(III) and Tb(III) luminescence, the isoquinoline rings effectively sensitize only the Eu(III) ion. This is a crucial feature to be considered when choose the metal center for the luminescent probes purposes.

As far as the coordination number is concerned, it was usefully adopted a not saturated core scaffold with a 6-fold coordination moiety for sensing purpose. In fact, in the majority of cases, the sensing process is due to the binding of the bio-analyte to the metal center. For these reasons, not all the metal coordination sites should be occupied by the ligand but by easily displaceable solvent molecules.

4.2 Stability, speciation and structure

4.2.1 Ligand protonation constants

The protonation constants of the ligands have been determined by acid-base potentiometric titration (for experimental details, see Chapter 3). By using a four species model with Hyperquad program, it was able to obtain the best fit of experimental emf collected data for all the ligands. For bpcd ligand, the data were previously found and published by our research group.[16]

The obtained results, in term of constants, are reported in Table 4.1 with some literature data, which also presents the DACH backbone, such as QC3A and 1,2-cyclohexanediaminetetraacetic acid (CDTA). The obtained titration curve for all the ligands is showed in Figure 4.2 with its speciation, calculated with Hyss program using the experimental conditions and the founded protonation constants. It can be

observed a very similar speciation trend for all the ligands, with two clear inflection points and concurring with the maximum concentration for the species LH_2 and LH respectively.

The log*K* values reported indicate the presence of two strong acidic and two weakly basic sites in each ligand. As reported for CDTA (Figure 4.3), the first protonation constant can be assigned for all the ligands to an aliphatic amine group (log*K* ~6.9 - 10.7, depending on the substituents).

Table 4.1 *Protonation constants ($logK_i$) of all the ligands used in this work (Figure 4.1), found by potentiometry at T = 298.15 K and μ = 0.1 M NaCl. Additional protonation data from other work (μ = 0.1-0.15 M NaCl) has also been reported for comparison.*

	bisoQcd	**isoQC3A**	**bpcd**[16]	**bQcd**[17]	**QC3A**[17]	**CDTA**[18]
logK_1	9.27 ± 0.03	9.43 ± 0.03	9.72 ± 0.02	9.37 ± 0.03	10.53 ± 0.03	9.43 ± 0.02
logK_2	5.86 ± 0.07	7.37 ± 0.07	5.87 ± 0.07	5.85 ± 0.07	6.29 ± 0.09	6.01 ± 0.02
logK_3	3.43 ± 0.07	3.32 ± 0.09	2.94 ± 0.12	3.46 ± 0.10	3.60 ± 0.16	3.68 ± 0.02
logK_4	1.62 ± 0.04	2.16 ± 0.12	2.22 ± 0.17	1.79 ± 0.31	2.81 ± 0.16	2.51 ± 0.05

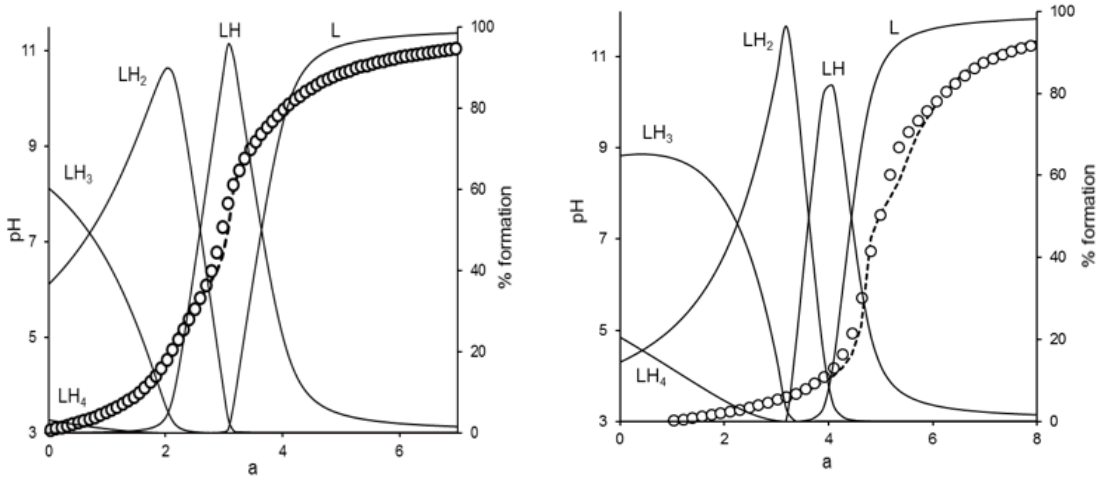

Figure 4.2 *Experimental (O) and calculated (dashed line) pH values in the potentiometric titration of: left bisoQcd (0.72mM) and right isoQC3A (0.75mM) ligand (T= 298.15 K and μ=0.1 M NaCl). a = (added mol OH^-) / (mol L).*

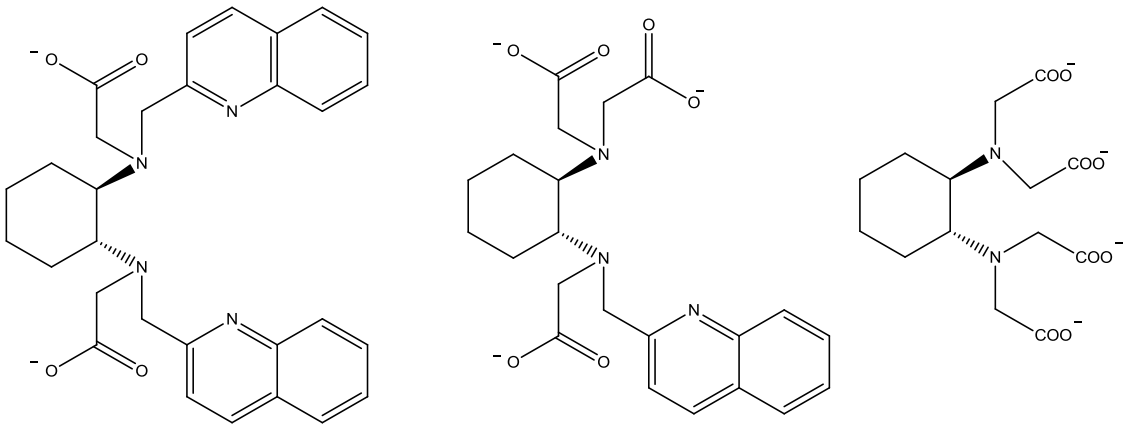

bQcd **QC3A** **CDTA**

Figure 4.3 *From left to right ligands bQcd, QC3A* and CDTA

Acid-base spectrophotometric titrations were performed in the same conditions of the protonation titrations in order to follow deprotonation of the pyridine and isoquinoline moieties during the titration. Therefore, it was able to assign other protonation constants to specific sites.

The protonation of the nitrogen present in the isoquinoline moieties of bisoQcd and isoQC3A ligands increases the molar absorbance, which permits the assignation of some protonation constants to the protonation of the heterocycle (Figure 4.4).

The molar absorbance obtained for isoquinoline-functionalized ligands (Figure 4.4) along with the speciation calculated with the Hyss program using the experimental conditions and the protonation constants found. By observing the trends of molar absorbance and speciation together, the K_3 constants can be assigned to the triacetate moiety and all K_2 constants to the protonation of the heterocyclic nitrogen. This is in agreement with the protonation constants found in literature for quinoline ($\log K = 4.97$) and picoline ($\log K = 6.06$). The remaining protonation constants may be assigned to the protonation of acetates. The protonation sequence we propose is in agreement with those already found for similar ligands.[6,17]

a

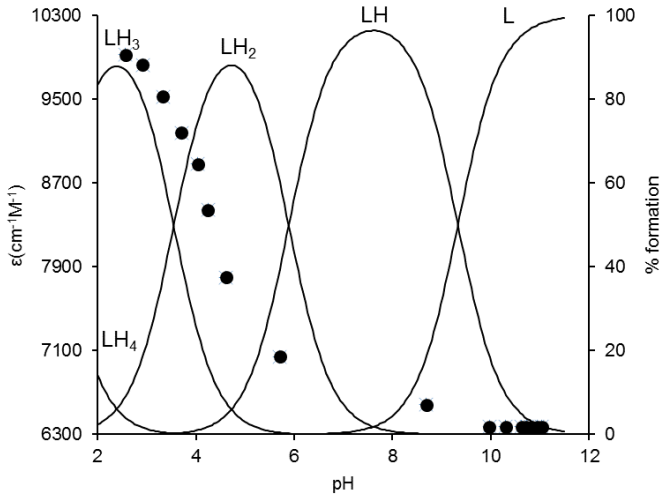

b

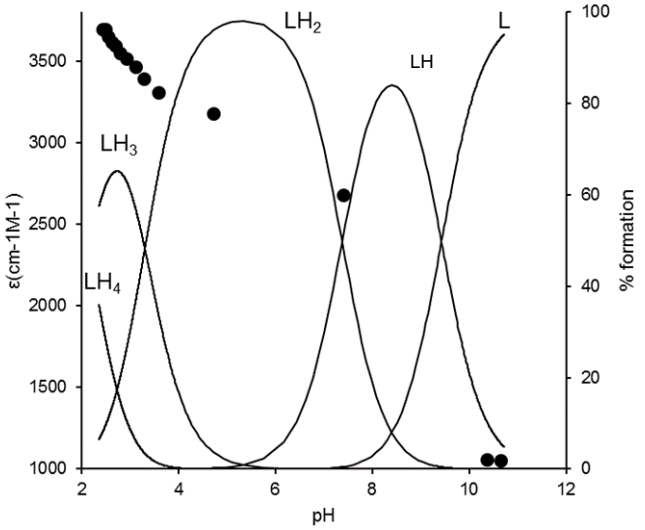

Figure 4.4 *Species distribution of (a) ligand bisoQcd (0.045 mM) and (b) isoQC3A (0.045 mM), along with the molar absorbance values (•) at λ=334 nm and λ=343 nm by acid-base spectrophotometric titration at T = 298.15 K and μ = 0.1 M NaCl. Charges omitted for clarity*

4.2.2 Stability constants

The complexation constants have been determined by acid-base spectrophotometric titrations, at T = 298.15 K and μ = 0.1 M NaCl. The best fit of the data was obtained by Hypspec program (for more experimental details, see Chapter 3).

UV-Vis titrations are shown in Figure 4.5, presenting the same chromophore and the presence of equimolar Eu(III). The stability constants obtained are reported in Table 4.2 along with additional constants from literature for similar ligands bQcd, QC3A, and CDTA (Figure 4.3).

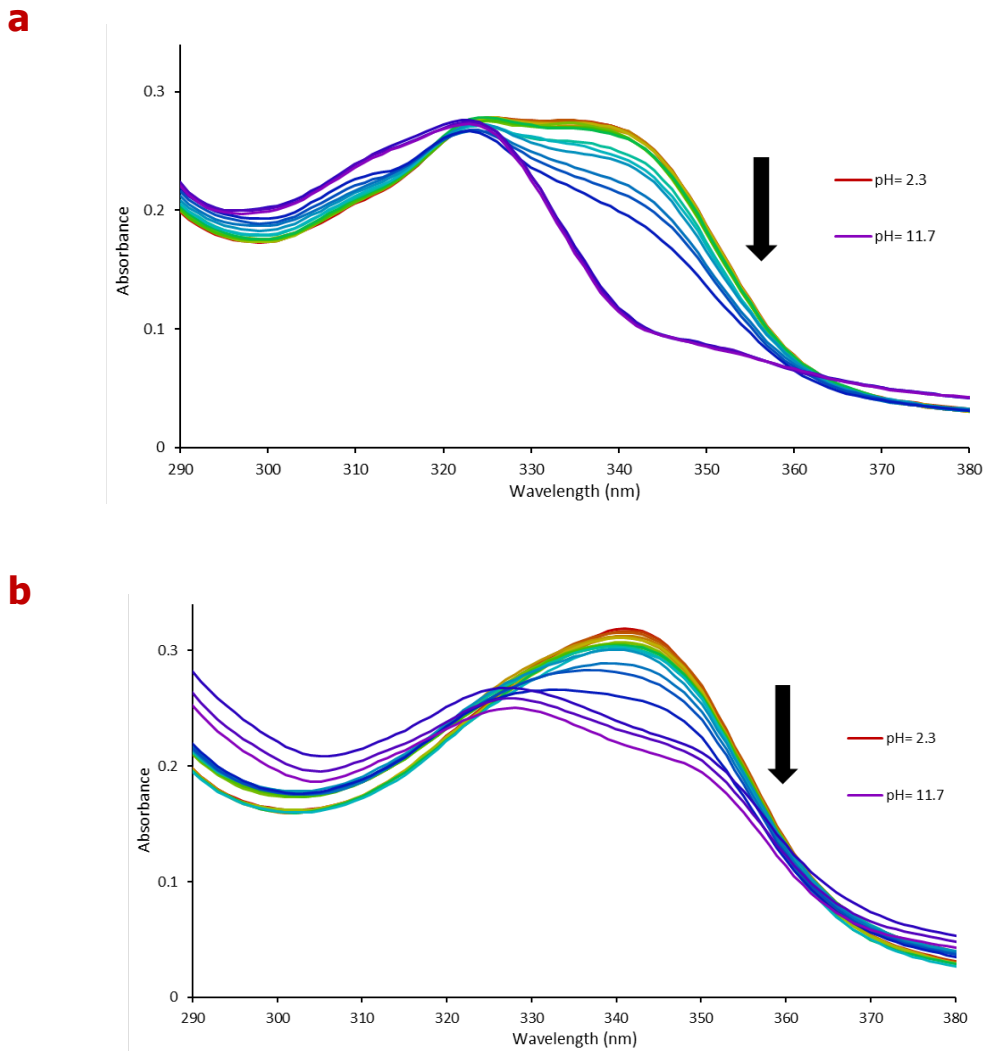

Figure 4.5 *UV-Vis absorption spectra changes during the acid-base titration for the ligands (a) bisoQcd (0.045 mM) and (b) isoQC3A (0.045 mM), in the presence of equimolar Eu(III). T = 298.15 K and μ = 0.1 M NaCl*

Table 4.2 *Stepwise formation constants (logβ) of all the complexes discussed in this work, found by spectrophotometric acid-base titration at T = 298.15 K and μ = 0.1 M NaCl. Other similar complexes have also been reported for comparison.*

	bisoQcd	**isoQC3A**	**bpcd**[16]	**bQcd**[17]	**QC3A**[17]	**CDTA**[18]
Eu(III)L	10.53 ± 0.04	14.63 ± 0.12	11.19 ± 0.32	9.97 ± 0.08	12.55 ± 0.16	19.6

Interestingly, the presented stability constants in Table 4.2, for the ligand with isoquinoline moieties (bisoQcd) present lower stability constants than their pyridine analogues (bpcd) but higher than the quinoline (bQcd) one. This behavior is not surprising, since bulkier isoquinoline-quinoline moieties cause stronger steric hindrance than pyridine ones. Moreover, the higher stability of the [Eu(bisoQcd)] complex with respect to the bQcd derivative is ascribable to the higher basicity of isoquinoline compared to quinoline.[19]

On the other hand, the triacetate complex (isoQC3A) present higher stability constants than their diacetate analogues (bisoQcd). This trend can be easily explained by the strongly noted interaction between oxygen donors and Eu(III).

a

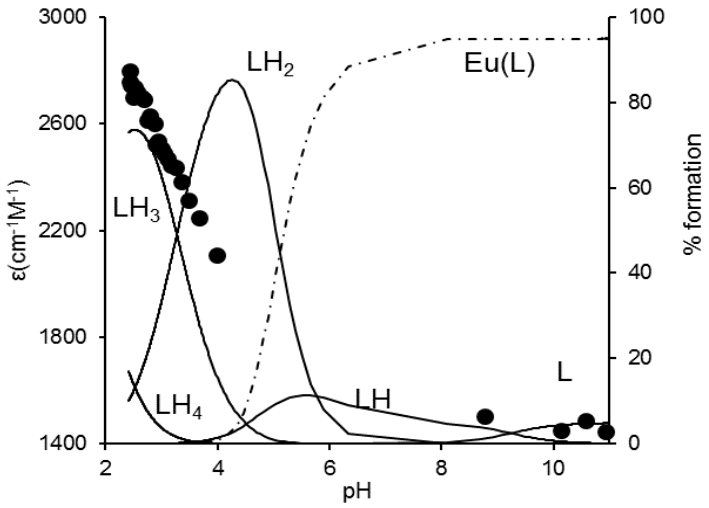

b

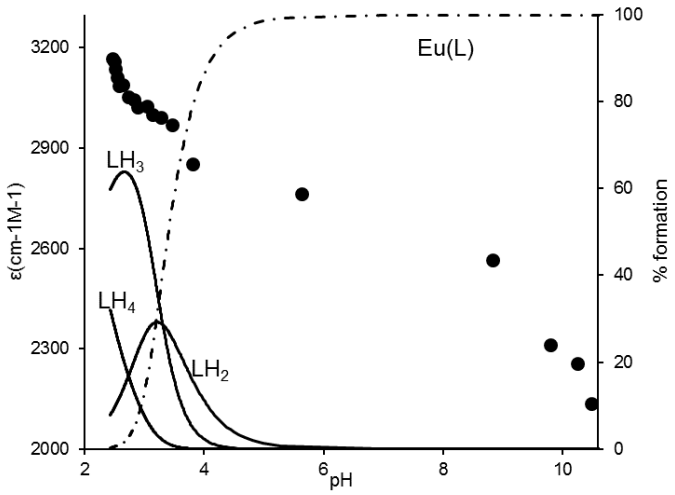

Figure 4.6 *Species distribution of the ligands (a) bisoQcd (0.045 mM) and (b) isoQC3A (0.045 mM) in the presence of Eu(III), ratio 1:1 M:L, with a little excess of metal. Also the molar absorbance values (•) at λ=334nm (bisoQcd) and λ=343 nm (isoQC3A) obtained by acid-base spectrophotometric titration at T = 298.15 K and μ = 0.1 M are reported. Charges are omitted for clarity*

Using Hyperquad simulation and speciation (HySS) utility program, with the found protonation and stability constants, it was possible to obtain the species distribution of the ligands bisoQcd and isoQC3A in water in presence of Eu(III) at 298.15 K. The speciations are reported in Figure 4.6, along with the molar absorbances from pH 2 to 11.5. We can notice that, in both cases, the luminescent lanthanide complex is the most abundant species at physiological pH around 7.4, representing near the 100% of the total L species at that pH. We can also observe that the molar absorbance decreases with the formation of the Eu(III) complex. Since molar absorbance is higher for the protonated heteroaromatic antenna, we may assume the coordination of Eu(III) with the heterocyclic nitrogen/s.

4.2.3 Structure

Since single crystals suitable for X-ray diffraction experiments were not obtained, all the complexes under investigation (Figure 4.1) have been studied by DFT calculations, in order to get the most probable structures in solution. As discussed in Chapter 3, this computational method has been previously successfully used to obtain structural and thermochemical data for f-block metal complexes.[20–22] As Eu(III) is paramagnetic, it is very difficult to fit in the model. Thus, Y(III) analogue can be used instead as a suitable substitute, as the ionic radii of Eu(III) and are quite similar (differs by only 0.05 Å) due to the lanthanide contraction.[6] Data for bpcd and bQcd are also reported, for comparison.

Each complex structure shows an 8-fold coordination at the metal centre due to the presence of a 6-fold coordinating ligand and two water molecules. An equilibrium between two isomers in solution was found in both cases, with *trans-N,N* and *trans-O,O* structures for the cationic diacetate complex ([Ln-bisoQcd]$^+$) and *trans-O,O* and *trans-N,O* structures for the neutral triacetate ones (Ln-isoQC3A).

Comparable data have been previously published in literature for analogous complexes, such as Gd(III)-bpcd,[23] Ga(III)-bped (M = Ga, In).[24,25] Unfortunately, it was not possible to confirm these structures via nuclear magnetic resonance (NMR), as the spectra of the complexes present hardly-assignable broad resonances.

Besides, the number of water molecules obtained by DFT calculation are in partial agreement with those calculated by luminescence spectroscopy (around 2.5).

The higher stability of the Eu(bisoQcd) complex to the bQcd derivative, can be deduced from the comparison of the energies of the Yttrium counterparts. The possible isomers [Y(bisoQcd)(H_2O)$_2$]$^+$ and [Y(bQcd)(H_2O)$_2$]$^+$ shown in Figure 4.7.

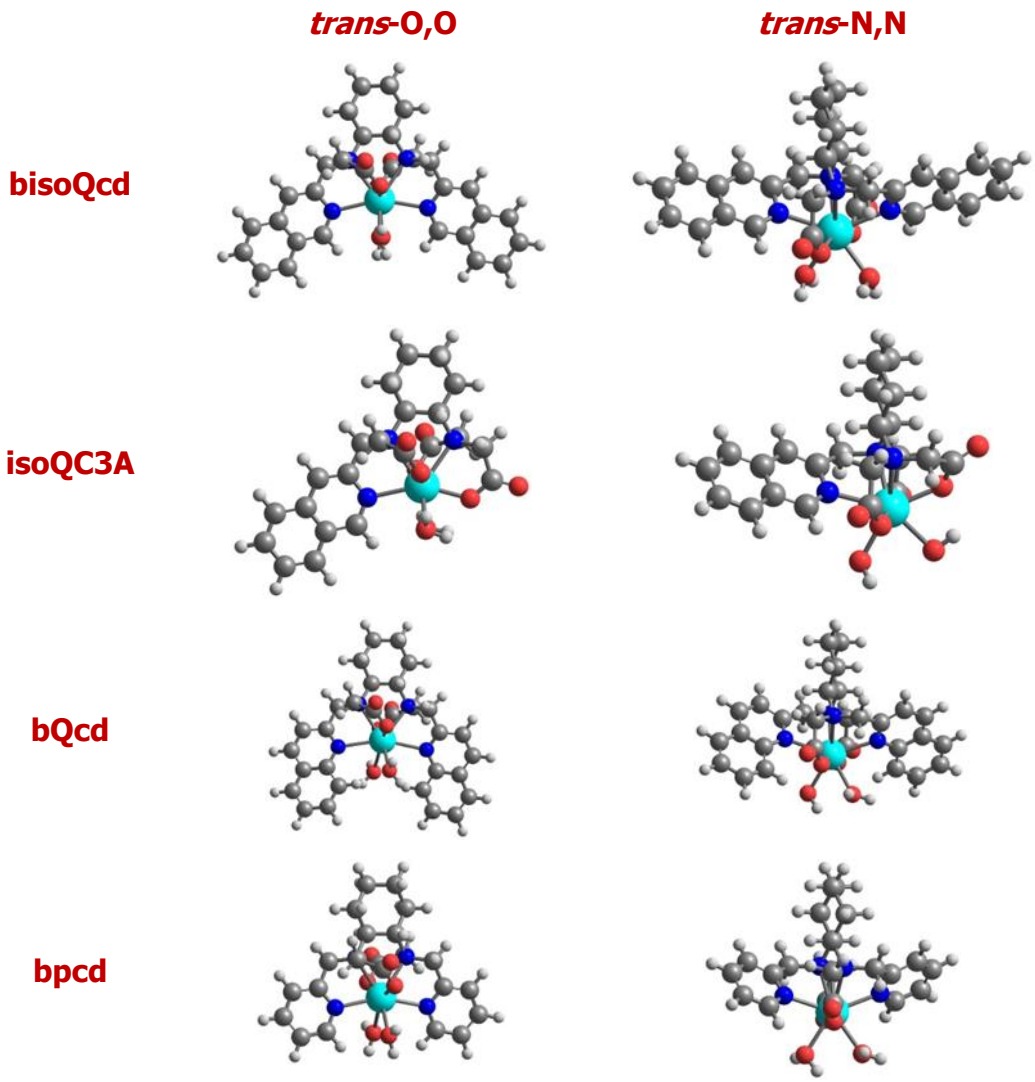

Figure 4.7 *Minimum energy structures of the $[Y(L)(H_2O)_2]^+$ complexes (L = bisoQcd, isoQC3A, bQcd, bpcd)*

The isomers with bisoQcd are more stable than the bQcd ligand by 6.8 and 8.9 kcal mol^{-1}, respectively. This difference seems related with the metal-N_{hetero} bonds which are clearly shorter in $[Y(bisoQcd)(H_2O)_2]^+$ (0.14 and 0.08 Å for the trans-O,O and trans-N,N isomers, respectively) and similar to those found in the (somewhat more stable) complex with bpcd. Also, in both cases, the *trans*-O,O isomer is the most stable (ΔG(*trans*-O,O-*trans*-N,N) = −3.0 and −5.1 kcal mol^{-1} for the complex with bisoQcd and bQcd, respectively), suggesting it as the prevalent form in solution.

From the obtained bond distances (Table 4.3) it is clearly evident that the substitution of pyridine by quinoline or isoquinoline has nearly no effect on the Y(III)-$O_{acetate}$ bonds and Y(III)-N_{amine} distances. The Y(III)-O_{water} bonds in the quinoline and isoquinoline complexes are slightly affected.

The steric hyndrance at the metal ion in the case of bulky quinoline ring could be responsible for the lengthening of the Y(III)-$N_{heterocycle}$ bond, which increases significantly when pyridine is replaced by quinoline ($\Delta Py \rightarrow Q \sim +0.11$ Å). This indicates the weaker interaction of the quinoline with respect to pyridine ligands with the metal ion.

This evidence should contribute to the loss of stability of the quinoline complexes respect to the pyridine analogues (an average difference of ~1.4 and 3.4 log units for the di and tri-acetate ligands). The isoquinoline complexes possess a stability, which is in the middle between the one of pyridine and quinoline complexes. It is expected that quinoline has also a notable impact on the solvation properties of the complex, which often have a strong influence on the stability.

Table 4.3 *Representative bond distances (Å) found by DFT calculations for the complexes represented in Figure 4.7*

Complex	Y-$O_{acetate}$	Y-N_{amine}	Y-$N_{heterocycle}$	Y-O_{water}
[Y(*trans*-O,O bisoQcd)$(H_2O)_2$]$^+$	2.262	2.577	2.526	2.451
[Y(*trans*-N,N bisoQcd)$(H_2O)_2$]$^+$	2.283	2.565	2.614	2.463
[Y(*trans*-O,O isoQC3A)$(H_2O)_2$]	2.259	2.554	2.525	2.505
[Y(*trans*-N,O isoQC3A)$(H_2O)_2$]	2.262	2.578	2.548	2.508
[Y(*trans*-O,O bQcd)$(H_2O)_2$]$^+$	2.268	2.557	2.661	2.464
[Y(*trans*-N,N bQcd)$(H_2O)_2$]$^+$	2.284	2.567	2.594	2.482
[Y(*trans*-O,O bpcd)$(H_2O)_2$]$^+$	2.262	2.550	2.525	2.448
[Y(*trans*-N,N bpcd)$(H_2O)_2$]$^+$	2.292	2.610	2.503	2.492

4.2.4 Luminescence

In our case, upon ligand complexation with Eu(III) we can observe an *hyperchromic effect*, with evident enhancements of the molar extinction coefficient (ε), and/or a *bathochromic or red shift*, of 3-4 nm respect to the ligand, towards upper values of maximum absorption wavelength.

The UV-Vis electronic absorption spectra in aqueous solution for complexes Eu(bisoQcd) and Eu(isoQC3A) are depicted in Figure 4.8. Even if the complexes contain the same heteroaromatic antenna, the complex Eu(bisoQcd) is are red shifted respect to the complex Eu(isoQC3A). This is due to the different number of chromophoric units, where the values of the molar extinction coefficient (ε) are also different.

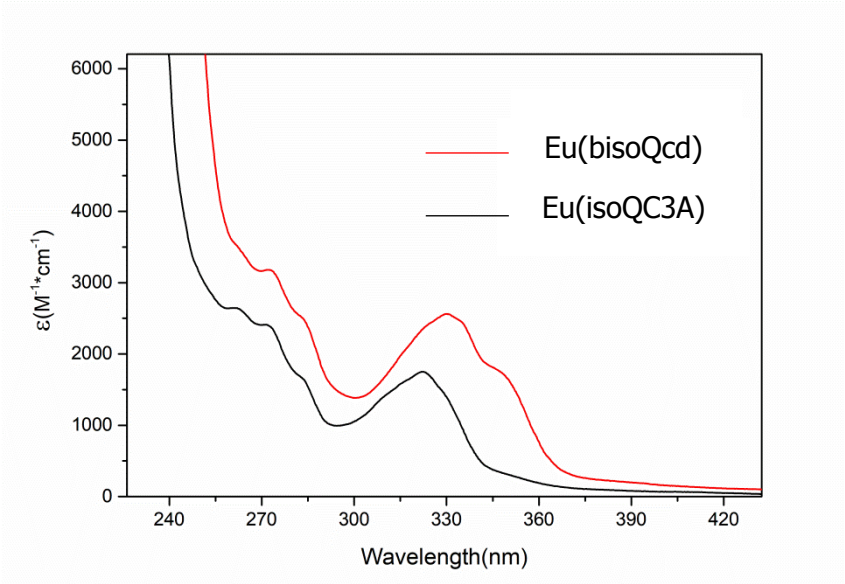

Figure 4.8 *UV-Vis absorption spectra for bisoQcd and isoQC3A Eu(III) complexes*

Excitation spectra of the complexes Eu(bisoQcd) and Eu(isoQC3A) dissolved in water upon monitoring the $^5D_0 \rightarrow {}^7F_2$ transition of Eu(III) (λ_{em} = 612-615 nm) are shown in the Figure 4.9. All the spectra are superimposable with the corresponding absorption ones, an efficient ligand to metal energy transfer mechanism works in all the complexes under investigation. While the pyridine ring is capable to sensitize both Eu(III) and Tb(III) luminescence, the quinoline and isoquinoline rings efficiently sensitize only Eu(III) ion.

a

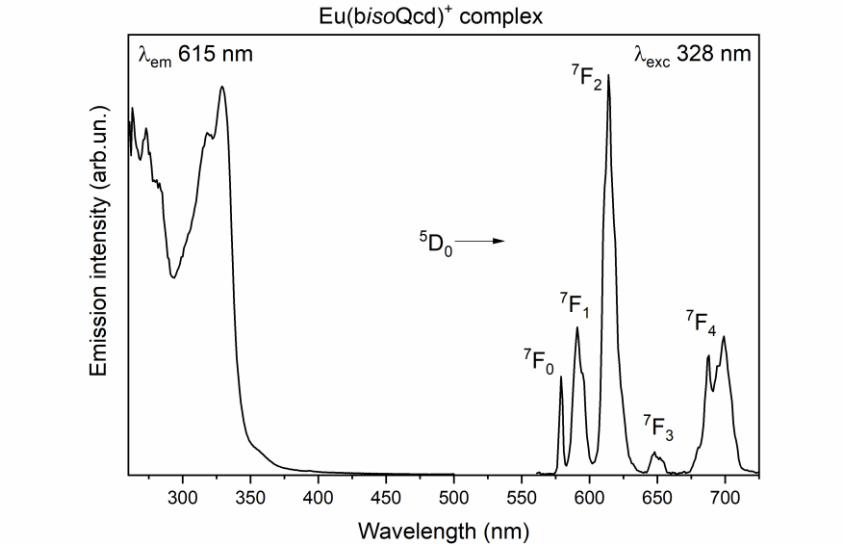

b

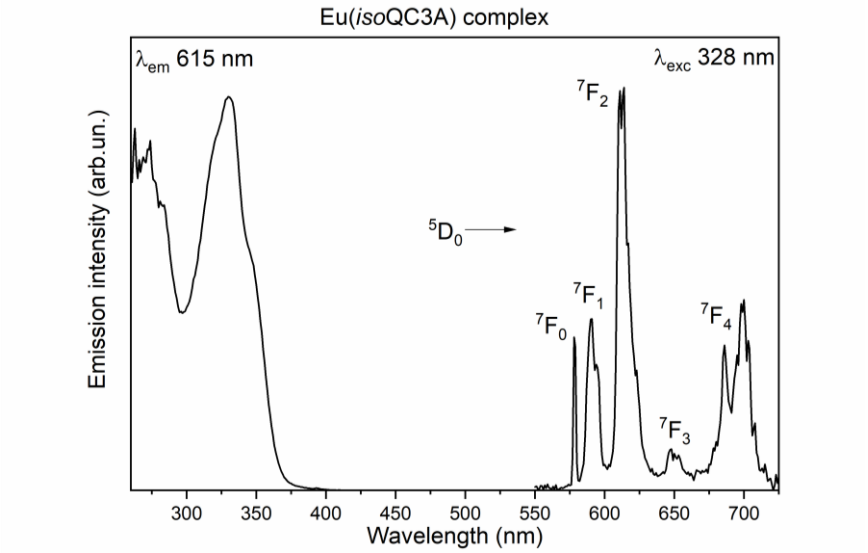

Figure 4.9 *Luminescence excitation spectra (left) and emission spectra (right) of (a) Eu(bisoQcd) complex and (b) Eu(isoQC3A), in water solution (10^{-4} M) at 298 K*

The luminescence emission spectra shown on the right of Figure 4.9 show the presence of the typical *f-f* transitions of the Eu(III) ion.

The antenna effect is efficient for both complexes, as upon excitation around 330 nm (main absorption bands of the ligands) the typical Eu(III) luminescence in the visible red spectra region can be seen. The emission bands corresponding to the $^5D_0 \rightarrow {}^7F_2$ transition can be easily detected in the spectra.

Moreover, the luminescent decay curves in aqueous solution for Eu(III) ($^5D_0$ excited state) were recorded for both the complexes studied. As evidently observed (see

Chapter 5, Figure 5.30), the curves are well fitted by a single exponential function, which confirm the presence of a main emitting species in solution.

The observed lifetimes (τ_{obs}), in water and deuterium oxide, are reported in Table 4.4, along with the values of hydration number (*q*), radiative lifetime (τ_{rad}) and intrinsic (Φ_{Ln}) quantum yields.

Table 4.4 *Observed and radiative lifetimes, hydration number (q) and intrinsic quantum yield for Eu(bisoQcd) and Eu(isoQC3A) complexes*

Complex	$\tau_{obs(ms)}$ H_2O	D_2O	$\tau_{rad(ms)}$*	*q* ǂ	Φ_{Ln}(%)¶
Eu(biQcd)OTf	0.26(1)	1.30(1)	5.20	2.8(1)	5.0
Eu(iQC3A)	0.29(1)	1.87(1)	5.37	2.8(1)	5.4

* estimated from the analysis of the Eu(III) emission spectra by using the formula reported by Werts *et al.* ǂ calculated by means of the Horrocks equation, based on the values of τ_{obs} in H_2O and D_2O. ¶ calculated by τ_{obs}/τ_{rad}

The apparently low total quantum yields (Φ_{Tot}) have to be reassessed in the light of the following statements: i) the quantum yield of many lanthanide and d-block compounds used for cellular imaging is around 4-10% range;[26,27] ii) the total quantum yield of our complexes, is expected to grow upon interaction with a target molecule, thanks to the simultaneous displacement of water molecules from the metal ion. For these reasons, we believe that the class of complexes under investigation can be considered a promising family of optical probes for sensing application.

4.2.5 Conclusions

The proposed ligands are stable in water at the studied pH range (from 2 to 11), temperature (298.15 K) and ionic strength (0.1 M NaCl). The found protonation constants are in accordance with values found in literature for similar ligands and conditions. They all have four dissociable protons assigned to either acetate, heteroaromatic nitrogen or ternary nitrogen positions.

The Eu(III) and Tb(III) complexes studied are stable at the proposed pH range (from 2 to 11), temperature (298.15 K) and ionic strength (0.1 M NaCl). The calculated overall stability constants are high and in accordance with values found in literature for similar complexes and conditions. The tri-acetate ligands form more stable lanthanide complexes than the di-acetate ones due to the higher negative charge of the former ones and the oxophilicity of lanthanide cations. The predominant species, with prevalence around 100%, in solution at pH 7.4 is in all cases the luminescent lanthanide complex. All complexes are octacoordinated, with two waters in the first coordination sphere. The presence of these coordinated waters, which quench the luminescent signal, can be replaced by a target bio-analyte, which cause a rising in the luminescence.

Eu(III) is efficiently sensitized by all the ligands in study and the stoichiometry (1:1 ligand-Eu(III)) is confirmed by the fitting of the luminescent decay curves in single exponential functions. Total quantum yields are in the range of values commonly found in literature for cell imaging with either lanthanide or d-block complexes.

4.3 Bibliography

[1] R. Janicki, A. Mondry, P. Starynowicz, *Coord. Chem. Rev.* **2017**, *340*, 98–133.
[2] F. Caillé, C. S. Bonnet, F. Buron, S. Villette, L. Helm, S. Petoud, F. Suzenet, É. Tóth, *Inorg. Chem.* **2012**, *51*, 2522–2532.
[3] E. N. Zapolotsky, Y. Qu, S. P. Babailov, *J. Incl. Phenom. Macrocycl. Chem. 2021* **2021**, *1*, 1–33.
[4] M. Briganti, G. F. Garcia, J. Jung, R. Sessoli, B. Le Guennic, F. Totti, *Chem. Sci.* **2019**, *10*, 7233–7245.
[5] M. J. Beltrán-Leiva, E. Solis-Céspedes, D. Páez-Hernández, *Dalt. Trans.* **2020**, *49*, 7444–7450.
[6] M. Leonzio, A. Melchior, G. Faura, M. Tolazzi, M. Bettinelli, F. Zinna, L. Arrico, L. Di Bari, F. Piccinelli, *New J. Chem* **2018**, *42*, 7931.
[7] J. Florián, C. C. McLauchlan, D. S. Kissel, C. C. Eichman, A. W. Herlinger, *Inorg. Chem.* **2015**, *54*, 10361–10370.
[8] C. C. McLauchlan, J. Florián, D. S. Kissel, A. W. Herlinger, *Inorg. Chem.* **2017**, *56*, 3556–3567.
[9] C. M. G. dos Santos, A. J. Harte, S. J. Quinn, T. Gunnlaugsson, *Coord. Chem. Rev.* **2008**, *252*, 2512–2527.
[10] Z. Cai, C. Wei, B. Sun, H. Wei, Z. Liu, Z. Bian, C. Huang, *Inorg. Chem. Front.* **2021**, *8*, 41–47.
[11] S. Di Pietro, D. Iacopini, B. Storti, R. Nifosì, V. Di Bussolo, M. Pineschi, A. Moscardini, G. Signore, R. Bizzarri, *Mol. 2021* **2020**, *26*, 58.
[12] F. Caillé, C. S. Bonnet, F. Buron, S. Villette, L. Helm, S. Petoud, F. Suzenet, É. Tóth, *Inorg. Chem.* **2012**, *51*, 2522–2532.
[13] A. Arauzo, L. Gasque, S. Fuertes, C. Tenorio, S. Bernès, E. Bartolomé, *Dalt. Trans.* **2020**, *49*, 13671–13684.
[14] D. Kovacs, X. Lu, L. S. Mészáros, M. Ott, J. Andres, K. E. Borbas, *J. Am. Chem. Soc.* **2017**, *139*, 5756–5767.
[15] D. Häussinger, J. R. Huang, S. Grzesiek, *J. Am. Chem. Soc.* **2009**, *131*, 14761–14767.
[16] M. Leonzio, A. Melchior, G. Faura, M. Tolazzi, F. Zinna, L. Di Bari, F. Piccinelli, *Inorg. Chem.* **2017**, *56*, 4413–4422.
[17] F. Piccinelli, C. De Rosa, A. Melchior, G. Faura, M. Tolazzi, M. Bettinelli, *Dalt. Trans.* **2019**, *48*, 1202–1216.
[18] E. M. Gale, S. Mukherjee, C. Liu, G. S. Loving, P. Caravan, *Inorg. Chem.* **2014**, *53*, 10748–10761.
[19] R. S. Hosmane, J. F. Liebman, *Struct. Chem.* **2009**, *20*, 693–697.
[20] A. C. Mendonça, A. F. Martins, A. Melchior, S. M. Marques, S. Chaves, S. Villette, S. Petoud, P. L. Zanonato, M. Tolazzi, C. S. Bonnet, et al., *Dalton Trans.* **2013**, *42*, 6046–57.
[21] F. Endrizzi, A. Melchior, M. Tolazzi, L. Rao, *Dalton Trans.* **2015**, *44*, 13835–13844.
[22] M. Soulié, F. Latzko, E. Bourrier, V. Placide, S. J. Butler, R. Pal, J. W. Walton, P. L. Baldeck, B. Le Guennic, C. Andraud, et al., *Chem. – A Eur. J.* **2014**, *20*, 8636–8646.
[23] J. Florián, C. C. McLauchlan, D. S. Kissel, C. C. Eichman, A. W. Herlinger, *Inorg. Chem.* **2015**, *54*, 10361–10370.
[24] P. Caravan, S. J. Rettig, C. Orvig, *Inorg. Chem.* **1997**, *36*, 1306–1315.
[25] G. Tircsó, M. Regueiro-Figueroa, V. Nagy, Z. Garda, T. Garai, F. K. Kálmán, D. Esteban-Gómez, É. Tóth, C. Platas-Iglesias, *Chem. – A Eur. J.* **2016**, *22*, 896–901.
[26] D. Parker, P. K. Senanayake, J. A. G. Williams, *J. Chem. Soc. Perkin Trans. 2* **1998**, *0*, 2129–2140.
[27] K. L. Peterson, J. V. Dang, E. A. Weitz, C. Lewandowski, V. C. Pierre, *Inorg. Chem.* **2014**, *53*, 6013–6021.

Chapter 5

Luminescent sensing of bio-analytes

5.1 Introduction: sensing of bio-analytes

The current Chapter is devoted to the interaction study between our luminescent probes and selected bio-analytes. We will discuss their affinity with the target bio-analyte, the structure of the adducts and their luminescent response. The main biological target bio-analytes are components of the extracellular fluid (EF): bicarbonate (HCO_3^-), citrate and the human serum albumin (HSA) protein (see Table 5.1).

Table 5.1 *Typical concentrations (mM) of selected anions in humans* [1]

Anion	Extracellular fluid	Intracellular fluid*	Cerebrospinal fluid
Bicarbonate	24-27	10-12	20-23
Lactate	0.6-2.3	3-22	0.5-2.2
Citrate	0.1-0.3	2-4	0.05-0.25
Phosphate	1.2-1.3	0.8-1.2	0.15
Chloride	104-115	3-15	115-130
Sulfate	0.4-0.6	0.3-04	0.06-0.2

* Concentrations may vary considerably depending on the cell type.

Fluorimetric sensors are especially convenient as they facilitate the development of non-invasive and miniaturized sensors, which may permit the commercialization of biocompatible devices with the capability of constantly checking the concentration of relevant bio-analytes.

5.2 Sensing of Serum Albumin: effect of the heteroaromatic antenna on the binding

5.2.1 Introduction

In biological fluids, one of the most important proteins belong to the family of SA, which represent 52% of the total composition in the circulatory system. Human

Serum Albumin (HSA) and Bovine Serum Albumin (BSA) are the most extensively studied serum proteins, and they are classified as homologous proteins.[2] They have many physiological and pharmacological functions.[3,4] SA, the primary transport and reservoir protein in the human circulatory system, interacts with plentiful endogenous and exogenous ligands of varying structural characteristics such as fatty acids, bilirubin, drugs, steroids and several dyes.[5–7]

They have a limited number of binding sites with high specificity which confers an important role in the transport and deposition of a variety of endogenous and exogenous substances in the blood.[8,9]

Changes of the SA levels in blood could be induced by several disorders, including liver disease, neoplasia, nephrotic syndrome, severe dehydration and more.[10]

It is thus crucial in clinical diagnosis to design an analytical method for the quantification of these proteins. It has previously been shown that SA binds to lanthanide complexes and often, as a consequence of the interaction, significant changes of the Eu(III) and Tb(III) luminescence emission features as well as protein fluorescence, have been observed.[11–13]

In this work, after the synthesis and physicochemical characterization of two cationic water-soluble Eu(III) luminescent complexes, the BSA interaction was studied by several complementary experimental techniques (emission spectroscopy, isothermal titration calorimetry) and biomolecular simulations, to obtain informations on the affinity, specificity, and structural details of the complex/protein adduct. The investigated complexes (Figure 5.1) differ in the nature of the heteroaromatic antenna (pyridine vs isoquinoline), thus being labelled as [Eu(bpcd)(H_2O)$_2$]Cl and [Eu(bisoQcd)(H_2O)$_2$]OTf, respectively.

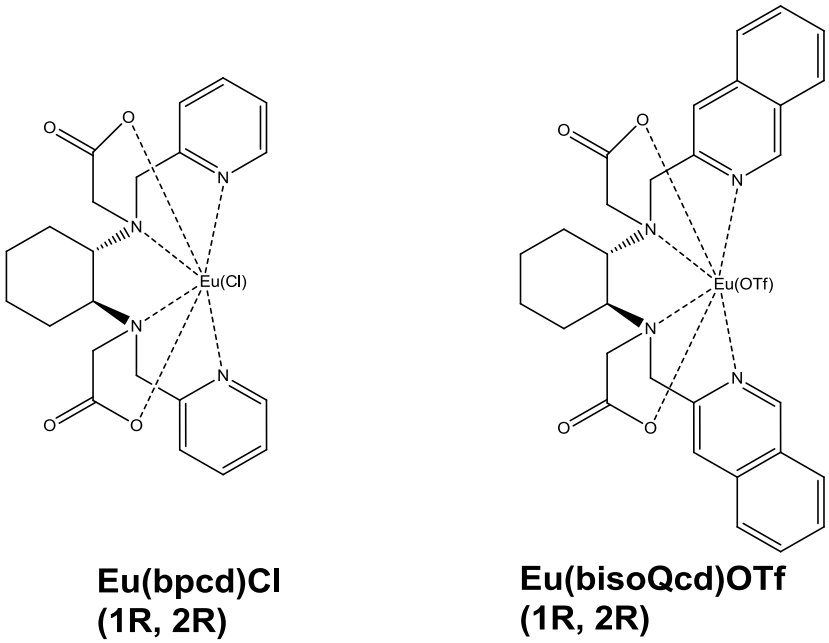

Figure 5.1 *Molecular structure of the Eu(III) complexes for BSA detection*

For sensing purposes, the coordinated water molecules can be easily displaced by the target bio-analyte. Since the chirality plays an important role in the interaction with biomolecules, the configuration of the two stereogenic carbon atoms of the ligands was fixed (R,R stereochemistry), in order to study enantiopure complexes.

5.2.2 Luminescence

Upon titration of the two Eu(III) complexes with BSA, two opposite trends have been observed. In the case of Eu(bpcd) complex, a gradual decrease of the Eu(III) luminescence intensity was detected; oppositely, a noticeable enhancement of the lanthanide emission was observed for Eu(bisoQcd) (Figure 5.2).

a

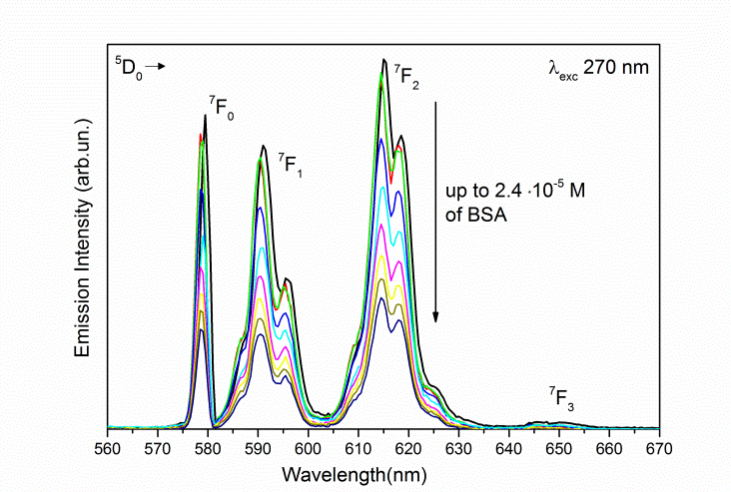

b

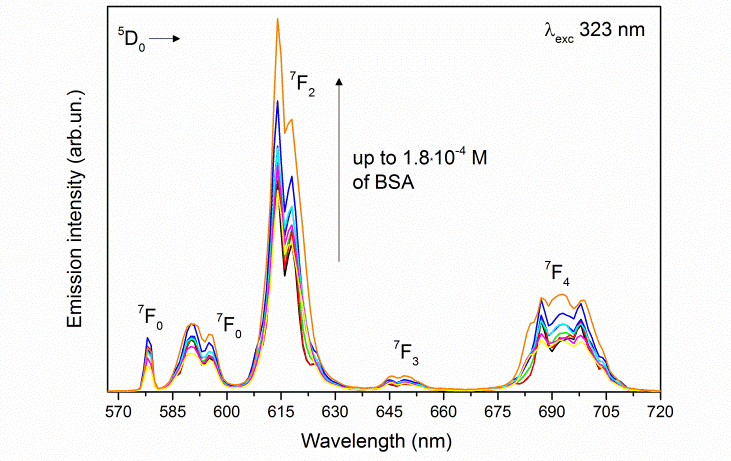

Figure 5.2 *Evolution of the Eu(III) luminescence emission of (a) Eu(bpcd) complex (80 μM) in MOPS-buffered solution (pH 7.4) upon addition of BSA in the 0-2.4·10^{-5} M concentration range and (b) Eu(bisoQcd) complex (80 μM) upon addition of BSA in the 0-1.8·10^{-4} M concentration range, at 298 K*

The spectral fingerprint of the hypersensitive $^5D_0 \rightarrow {}^7F_4$ transition is clearly affected by the BSA addition. This behaviour is due to a change in the nature of the primary donors to the Eu(III) center,[14] since the oxygen atom of a water molecule can be displaced by a functional group of the protein.

In the case of Eu(bpcd), the overlap in the UV spectral region between the BSA (280 nm) and the complex (270 nm) has limited the addition of the protein up to 2.4·10^{-5} M concentration, whose absorbance value is within the Lambert-Beer law. On the contrary, the BSA concentration limit can be extended to 1.8·10^{-4} M in the case of Eu(bisoQcd) complex, whose excitation wavelength is relatively red-shifted (328 nm).

In order to further study, the BSA-Eu(III)complexes interaction, the luminescence decay of $^5D_0$ excited state have been measured. The Eu(bpcd) complex has not indicated any significant change in the observed lifetime (fixed around 0.30 ms) during the titration with the protein, differently for the Eu(bisoQcd) complex which the lifetime increased considerable (Figure 5.3).

a

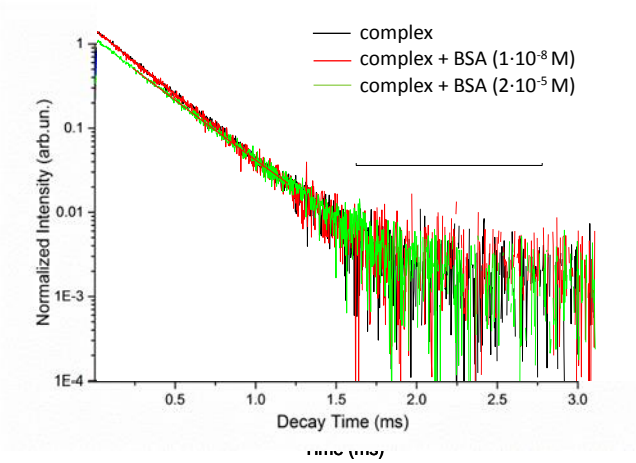

b

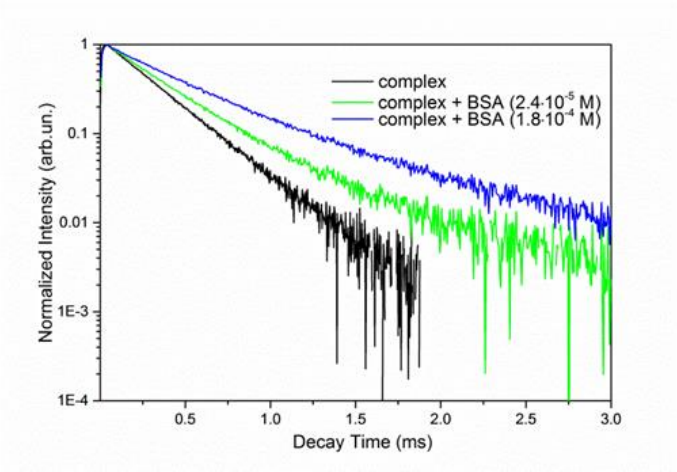

Figure 5.3 *Luminescence decay curves of the $^5D_0$ excited state of Eu(III) for (a) Eu(bpcd) complex (80 μM) and (b) Eu(bisoQcd) complex (80 μM), upon addition of BSA*

When BSA and the complex are present at the same time in solution, the decay curves cannot be simply fitted by a single exponential function since more than one emitting species (complex/protein adducts) is present. Upon addition of the protein to the Eu(bisoQcd) complex, the increase of the $^5D_0$ excited state lifetime [0.28 ms

for only the complex, 0.34 ms and 0.50 ms after BSA addition ($2.4 \cdot 10^{-5}$ M and $1.8 \cdot 10^{-4}$ M, respectively)] can be due to a lower efficiency of the multiphonon relaxation process (a process able to quench the excited state of the lanthanide ion in a non-radiative way). Some protein functional groups may replace water molecules in the inner coordination sphere of the metal ion.[15] In this regard, literature data confirm that Ln(III) complexes wherein the metal center is coordinated by two water molecules (as in our case) are susceptible to ligand displacement by competitive binding to endogenous serum anions, such as carbonate, or protein carboxylic acid residues.[16]

In addition, an increase of the luminescence quantum yield was observed, with consequently increase of the Eu(III) luminescence intensity. On the other hand, after Eu(bpcd)-protein complex interaction, the number of water molecules bound to the metal ion is not affected. Moreover, the decrease of the Eu(III) emission intensity could be related to the less efficiency of the ligand to metal energy transfer. In literature there are such cases of the decrease in sensitization of Eu(III) in complexes upon interaction with BSA, where the tryptophan residues in the protein found in domain I and II (Trp-134 and Trp-213, Figure 5.4) are involved.[17]

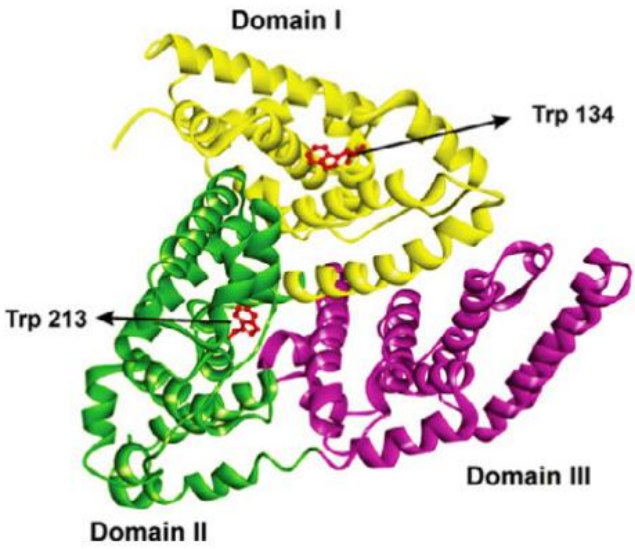

Figure 5.4 *Secondary structure of BSA. From* [4]

After protein addition, the excitation spectrum of Eu(bpcd) showed a progressive decrease of the peak around 265 nm, which is indicative of a decreased sensitization of Eu(III) luminescence by the pyridine rings. Nevertheless, the absence of peaks around 280 nm ruled out the involvement of the tryptophan rings in the sensitization mechanism (Figure 5.5 a).

a

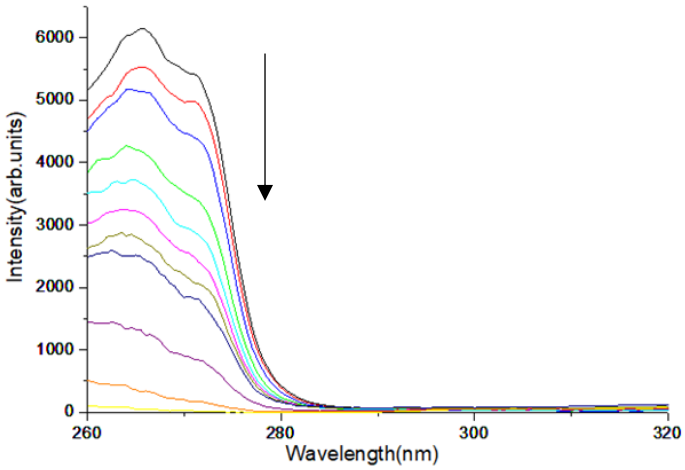

b

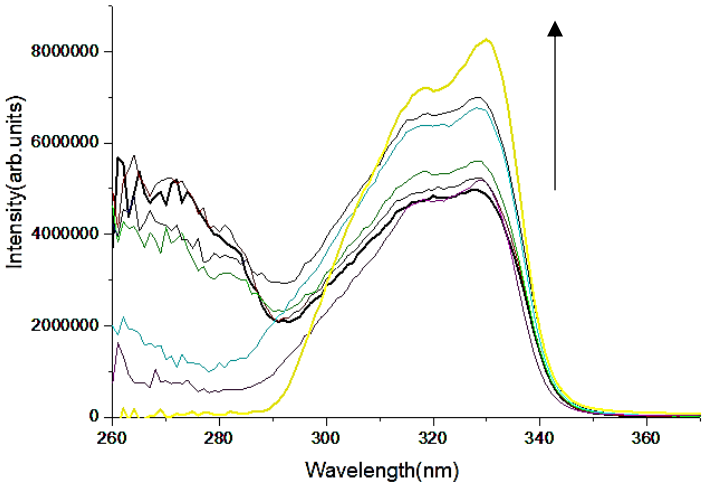

Figure 5.5 *Eu(III) excitation spectra for (a) Eu(bpcd) complex (80 μM) in MOPS-buffered solution (pH 7.4) upon addition of BSA in the 0-2.4·10^{-5} M concentration range (λem = 614 nm); and (b) Eu(bisoQcd) complex (80 μM) upon addition of BSA in the 0-1.8·10^{-4} M concentration range at 298 K (λem = 611 nm)*

The unusual behaviour of the Eu(bpcd) complex revealed a different nature of the protein-complex interaction. The Trp-134 and 213 are not significantly involved in the bond with Eu(III), and therefore the coordination sphere of the metal ion is preserved. On the other hand, the excitation spectra of the Eu(bisoQcd) complex showed an opposite trend with an increase of the emission intensity for the peak around 330 nm (Figure 5.5 b).

Moreover, the asymmetry ratio R increased upon addition of the protein in the case of Eu(bisoQcd) complex, indicative of the direct involvement of the metal center coordination sphere interaction with the protein. On the contrary, the R values do not change during the titration with the Eu(bpcd) complex.

As well known, the intrinsic fluorescence of BSA is mainly due to tryptophan residues, Trp-134 and Trp-213, and to a much lesser extent to tyrosine and phenylalanine residues. Trp-134 is located on the protein surface, in domain I, while Trp-213 is located inside the protein in domain II.

In order to get more insights into the interaction mechanism, the evolution of the protein fluorescence upon addition of the Eu(III) complex has been also investigated. Lambert–Beer law validity cover both a wider complex concentration range (up to 200 μM) and a larger complex/protein molar ratio, in a fixed background solution of the protein (5 μM). The titrations with the two Eu-complexes evidenced a decrease of the fluorescence intensity, which was particularly marked in the case of Eu(bisoQcd) complex and almost negligible for Eu(bpcd) (figure 5.6 a and b).

a

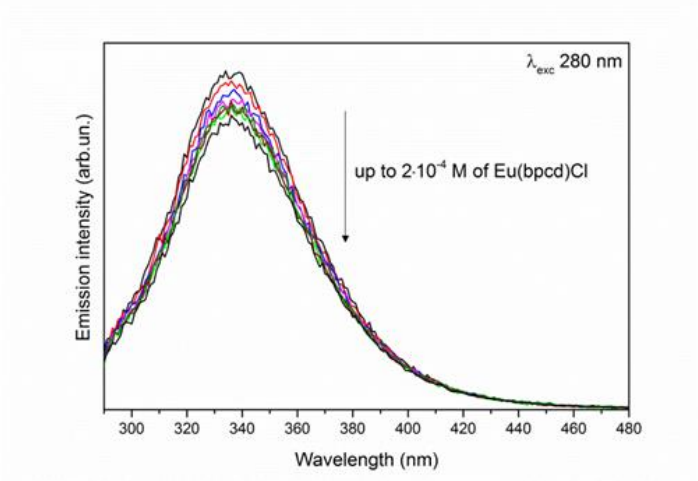

b

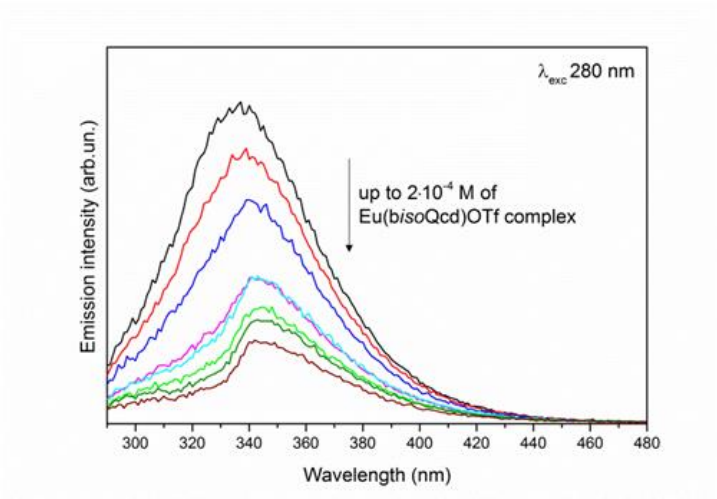

Figure 5.6 *Evolution of BSA fluorescence spectrum (5μM solution) upon increasing addition of (a) Eu(bpcd) and (b) Eu(bisoQcd) complexes. MOPS buffer (pH 7.4)*

The maximum of the protein emission peak, remained generally unchanged for the Eu(bpcd) complex, while a red shift of ≈10 nm has been detected for the Eu(bisoQcd) complex (up to 340 nm). In accordance with the literature, the red shift of the emission wavelength is probably due to conformational changes in protein structure upon binding with the Eu(bisoQcd) complex, with connected increase of polarity and hydrophilicity around the tryptophan residues.[18] This finding is in agreement with a direct interaction between Trp fragments and the complex.

The quenching of protein fluorescence done by the complexes, can be due to phenomena like molecular interactions such as collisional (or dynamic) quenching and static quenching.[19]

As a result of the collisional quenching, the fluorophore excited-state is deactivated upon contact with some other molecules in solution (in our case: Eu(III) complex). Otherwise, fluorophore can form at the ground-state, non-fluorescent adducts with the complex. This process is known as static quenching. In order to distinguish between static or dynamic quenching, one should measure the protein excited state lifetime. The fluorescence decay of BSA was best fitted to a biexponential function, and the corresponding averaged lifetimes, τ_{av}, remained unaltered upon addition of both complexes (around 7.5 ns). This indicated that the quenching of the fluorescence follows a static mechanism and a ground-state complex between BSA and each Eu(III) complex should be present in solution.[19]

5.2.3 Binding constants

The stability constants for the adduct between Eu(bpcd) and Eu(bisoQcd) with BSA has been determined via two independent experiments: fluorescent titration (Figure 5.6) and isothermal titration calorimetry (Figure 5.8). For experimental and calculation details, see Chapter 3. The fluorescence data were analyzed by means of the program MSExcel cEST macro.[20] The analysis provided best-fitting models (Figure 5.7) which correspond to the formation of a 1:1 adduct for the Eu(bpcd) complex (Figure 5.7 a) and of 1:1 + 1:2 species for Eu(bisoQcd) complex (Figure 5.7 b). The obtained formation constants (logK) are reported in Table 5.1. The data from ITC experiments was processed with the HypΔH program (Section 3.2.6).[21]

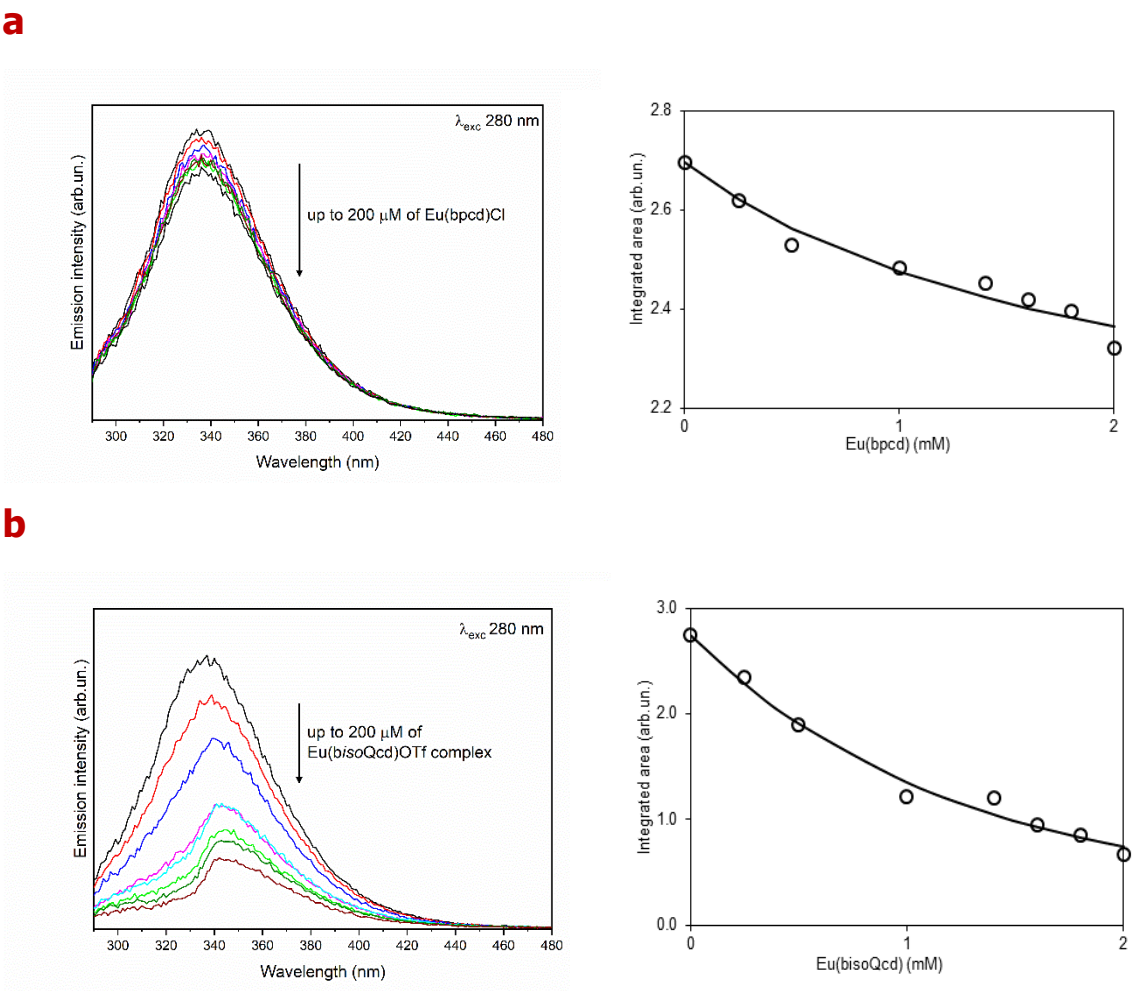

Figure 5.7 *Evolution of BSA fluorescence spectrum (5 μM solution) upon addition of (a) Eu(bpcd) and (b) Eu(bisoQcd). On the right, the integrated area of each spectrum (○) vs total complex concentration together with the fit (line) obtained with the formation constants in Table 5.1*

Different models provided a reasonable fluorimetric data fit and could potentially be affected by the inner filter effect (IFE), therefore the BSA-complexes interaction was also studied by a different experimental technique such as isothermal titration calorimetry (ITC). For the Eu(bpcd) (Figure 5.8 a) a 1:1 model well fited the heat data, resulting in logK = 3.61 and a negative formation enthalpy (ΔH) (Table 5.1). This value of logK agrees with the constant obtained from luminescence data (Figure 5.6 a), where a small change in the intensity of the protein fluorescence was observed upon titration with the complex. This result suggests that IFE does not affect dramatically the protein fluorescence in the presence of Eu(bpcd).

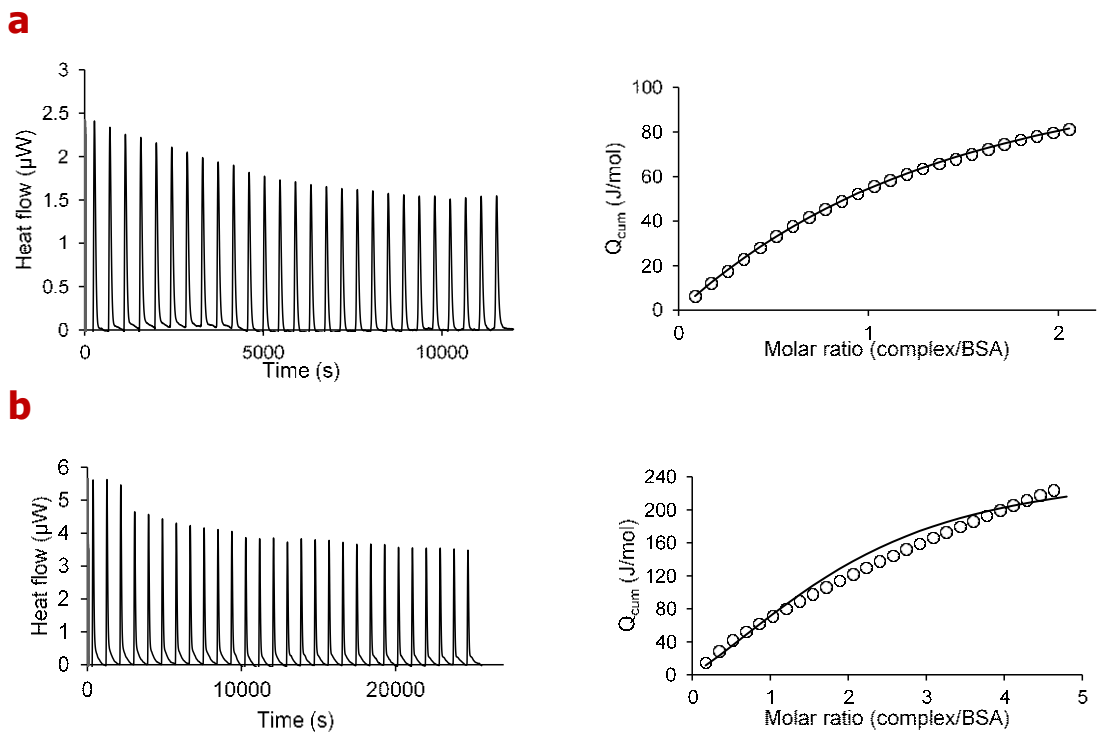

Figure 5.8 *Calorimetric titrations of (a) BSA (0.25 mM) with Eu(bpcd) (1.5 mM). Solvent: aqueous solution of MOPS, 13 mM; pH = 7.4. Final Eu/BSA molar ratio = 2.14. (b) BSA (0.25 mM) with Eu(bisoQcd) (3 mM). Solvent: aqueous solution of MOPS 13 mM with EtOH 10% v/v; pH = 7.4. Final Eu/BSA molar ratio: 4.8. On the right, the experimental (○) and calculated (line) Q_{cum} (cumulative heat exchanged / total moles of added reactant) vs complex /BSA molar ratio*

For Eu(bisoQcd) complex, ITC data (Figure 5.8 b) supported the presence of 1:1 + 1:2 protein-complex adducts, with a stronger interaction compared to the other derivative. When both logK and ΔH were set as free parameters in ITC data fitting, very large errors were obtained, hence the values are not reported in Table 5.2.

Table 5.2 *Formation constants for the complex/BSA adducts obtained from fluorimetric and ITC titrations*

L =	Reaction	log*K* Fluorimetry	log*K* ITC	ΔG (kJ mol^{-1})	ΔH (kJ mol^{-1})	TΔS (kJ mol^{-1})
bpcd	BSA + EuL ⇋ BSA[EuL]	3.7 ± 0.6	3.61± 0.23	-20.6	-13.1 ± 0.1	7.5
bisoQcd	BSA + EuL ⇋ BSA[EuL]	3.9 ± 0.2	-	-21.7	-16 ± 3	5.7
	BSA[EuL] + EuL ⇋ BSA[EuL]$_2$	3.6 ± 0.4	-	-26.3	-32 ± 4	-5.7

In order to identify the BSA sites involved in the interaction with the Eu(III) complexes, fluorimetric titrations using site-selective competitive ligands (the clinically-established drugs ibuprofen, warfarin and digitoxin) were done.[22–24] Warfarin is well known to be selective for an external site (domain I), where Trp-134 residue is present, while ibuprofen for the domain II, associated with the inner Trp-213 residue (Figure 5.4). While, digitoxin displays a selective interaction with the domain III, which is not fluorescent and which seemingly our complexes not interact.[23,25]

When warfarin was added to the solution containing BSA/Eu(bpcd) adduct, a decrease of the Eu(III) luminescence intensity within the experimental error was observed. Since the BSA-warfarin adduct have a logK_1 = 5.07,[26] higher than the one calculated for the BSA/Eu(bpcd), there is no competition for domain I. Moreover, the Eu(bpcd) complex does not interact with the domain II, as the Eu(III) luminescence intensity does not change upon addition of ibuprofen to the BSA/complex adduct. On the other hand, the addition of warfarin to the BSA adduct(s) with Eu(bisoQcd)

gave rise to a significant decrease (around 85%) of the Eu(III) luminescence intensity (Figure 5.9).

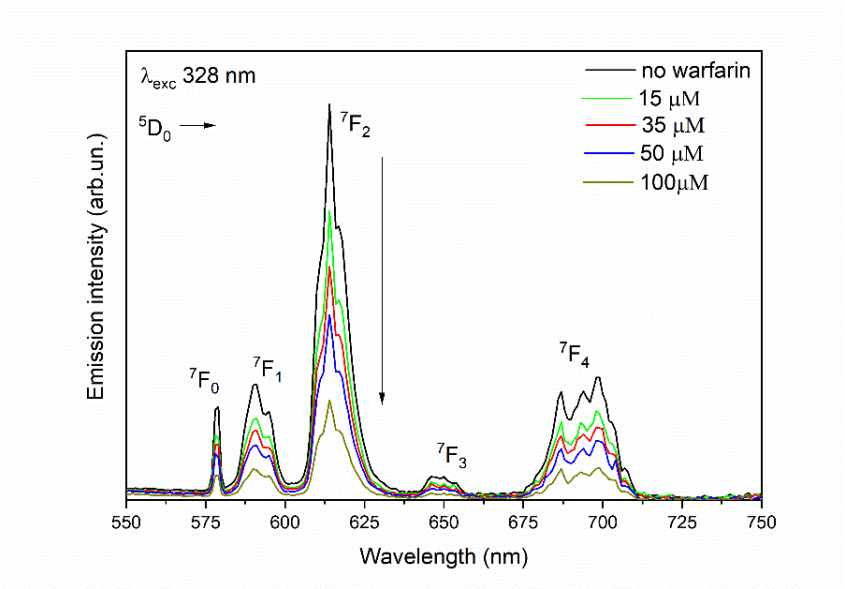

Figure 5.9 *Luminescence of the complex Eu(bisoQcd) (80 μM) interacting with BSA (80 μM) upon titration with warfarin (up to 100 μM); room temperature; solvent: aqueous solution of MOPS 13 mM (pH = 7.4)*

This behavior, opposite to the one depicted in Figure 5.2 b, showed that the Eu(III) complex is replaced by warfarin at the site I (Trp 134). However, both fluorimetric and calorimetric titrations suggest that Eu(bisoQcd) can interact with BSA in an additional position. Since the Eu(III) luminescence intensity does not change for this compound upon addition of both ibuprofen and digitoxin, the second interaction site is different from those of the two here studied drugs.

For warfarin and ibuprofen, it was checked that each drug interacts with the protein by monitoring, upon titration, the BSA fluorescence stemming from the adduct with the complexes. The addition of these drugs results in a significant decrease of the protein fluorescence intensity. In order to better understand the nature of the protein/complex interactions, molecular docking and molecular dynamics simulations were performed.

5.2.4 Structural characterization

The interaction between BSA and Y(bpcd) complex, for which the structure was previously obtained by DFT calculations (Fig. 4.3), was studied by means of molecular docking and molecular dynamics calculations.

When the Y(bpcd) complex was docked close to the sites I and II (with Trp134 and Trp213, respectively), it did not remain in these binding sites. As the interaction was not so strong at the starting configuration, the complex started to explore all the protein's surface until it found a superficial cavity where it spent half the simulation time (Figure 5.10 and 5.11).

a

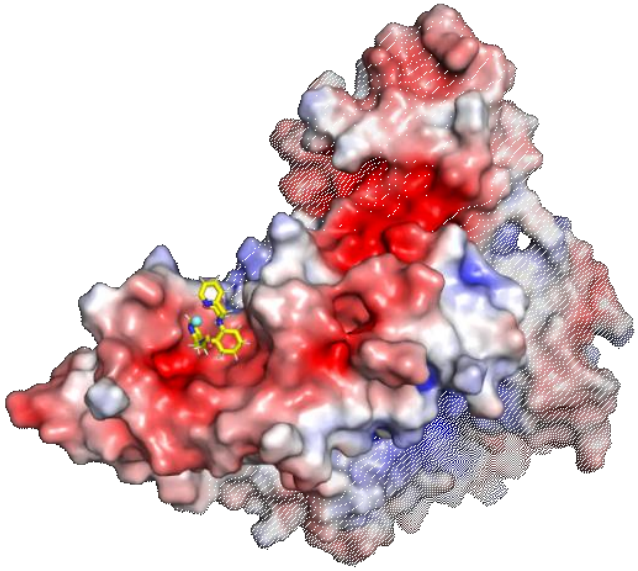

b

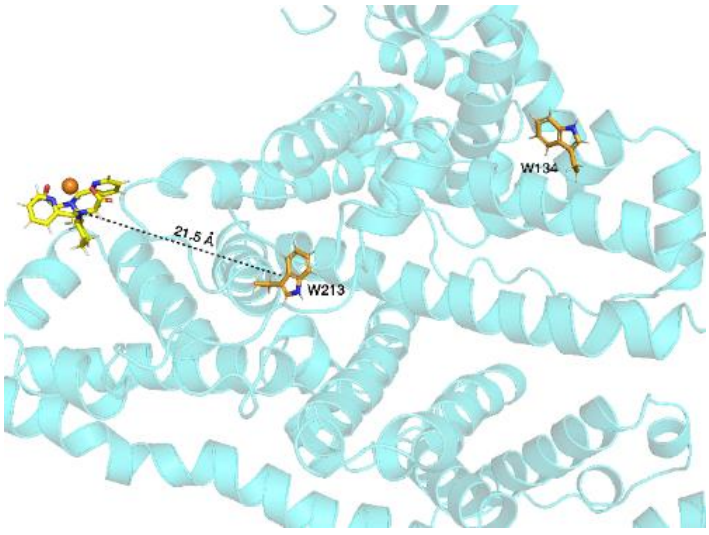

c

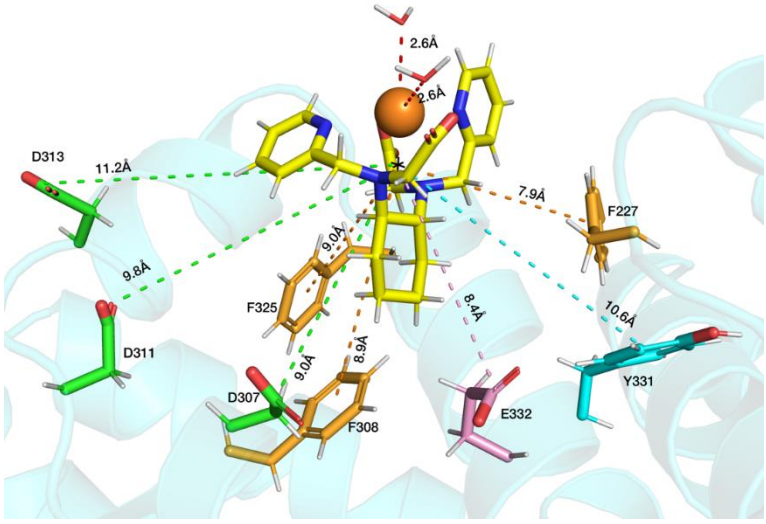

Figure 5.10 *(a) BSA superficial interaction site with the Y(bpcd) complex. The electrostatic potential is represented (electronegative cavities are red coloured). (b) The distance between the interacting complex and the buried Trp 213. (c) Close-up on the Y(bpcd) that lies on the superficial cavity and representation of the aminoacidic residues surrounding the complex (distances averaged along the simulation)*

It was interesting to note a "non-conventional" hydrogen bond that involves the aromatic ring of Trp 134 as H-bond acceptor and a C-H bond of the isoquinoline ring as donor (Figure 5.11). The phenomenon of the "CH/π interaction" in organic and biological chemistry has been explored and reviewed in literature.

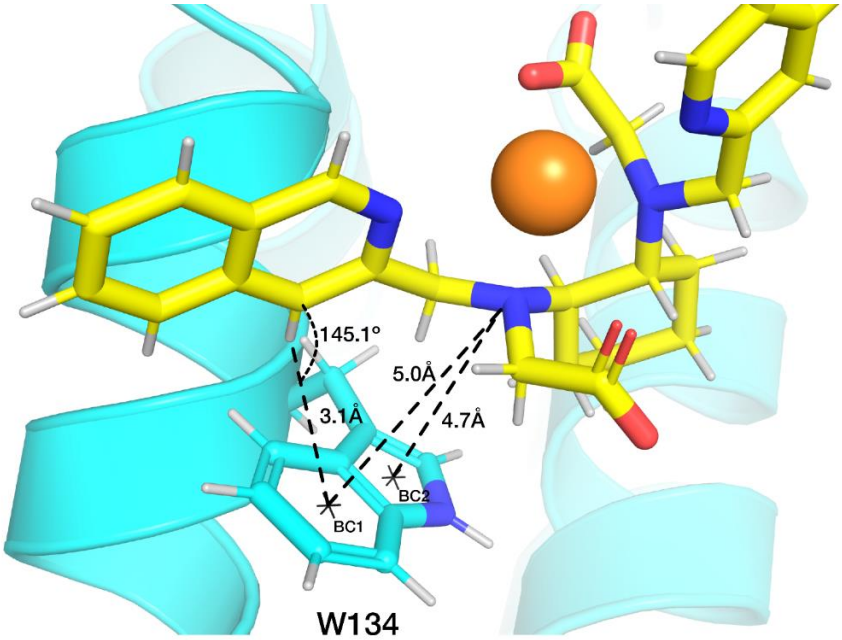

Figure 5.11 *Structural detail of the "CH/π interaction" involving Trp134 of BSA and one isoquinoline ring of Y(bisoQcd) complex*

These results are in perfect agreement with the outcomes associated with the analysis of the BSA fluorescence upon interaction with the complex and the competitive titration experiments with the drug warfarin. In addition, one coordinated water molecule is displaced by one monodentate carboxylic group of the glutamic acid residue 17 (E17) (Figure 5.12).

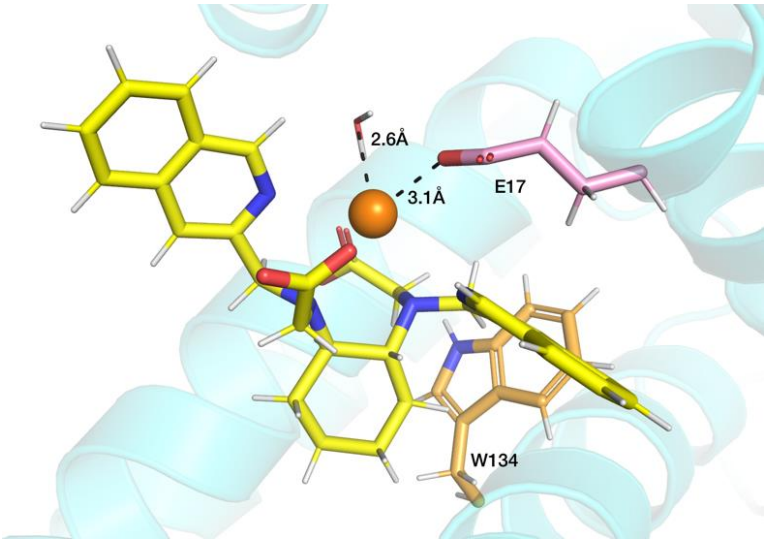

Figure 5.12 *Snapshot of the interaction site of BSA with the Y(bisoQcd) complex*

Also this finding is in agreement with the increase of the observed luminescence lifetime of Eu(III) during the titration of Eu(bisoQcd) complex with the protein (Figure 5.3). In fact, the removal of one water molecule from the inner coordination sphere of Eu(III) reduces the multiphonon relaxation process.

5.2.5 Conclusions

The luminescence changes observed upon Eu(bisoQcd) complex-BSA interaction involved the displacement of one water molecule from the metal centre by protein coordinating groups (carboxylic group of GLU17 residue). With consequently enhance of Eu(III) emission intensity and lifetimes. The interaction occurred close to the indole ring of the TRP-134 unit (distance Y-TRP134 ~6.8 Å). Upon interaction, the structural changes of the protein decreased the efficiency of the fluorescence emission, as clearly reported in Figure 5.6 b.

On the other hand, the luminescence changes in the case of the Eu(bpcd) complex have been explained by a protein/complex interaction on the surface of the protein, far from the Tryptophan units, without a direct involvement of the Eu(III) inner coordination sphere. These remarks have been also confirmed in the quite low evolution of the protein fluorescence during titration with the Eu(bpcd) complex (Figure 5.6 a).

The overall hydration state remained constant, resulting in unchanged emission lifetime of Eu(bpcd). As far as the decrease of the lanthanide luminescence is concerned, two main effects could occur: i) the interaction of the pyridine fragments with the external residue of the protein cavities that influences the antenna-metal centre distance, and ii) a change in the excited state energy of the ligand by resulting in a lower efficiency of the energy transfer to the metal centre.

5.3 Isoquinoline-based luminescent probes

5.3.1 Introduction

One of the main biosensing challenges is the overlap between the absorption wavelengths of the probe and the biomolecules, in the biological fluid under investigation.

As already mentioned, an efficient luminescent bioprobe should be excited at least above 300 nm. Below this excitation wavelength, the majority of the biochromophores absorbs light. Moreover, the irradiation in the far UV spectral region have harmful effects on cells, an additional reason to prefer bio-probes with longer excitation wavelength.

Among several Eu(III)-complexes described in Chapter 4, the most promising bioprobes are certainly the Isoquinoline di- and tri-acidic derivatives (Figure 5.13), whose excitation wavelength around 325 nm is quite red-shifted respect to the analogous Quinoline (318 nm), and even more to the Pyridine derivatives (265 nm).

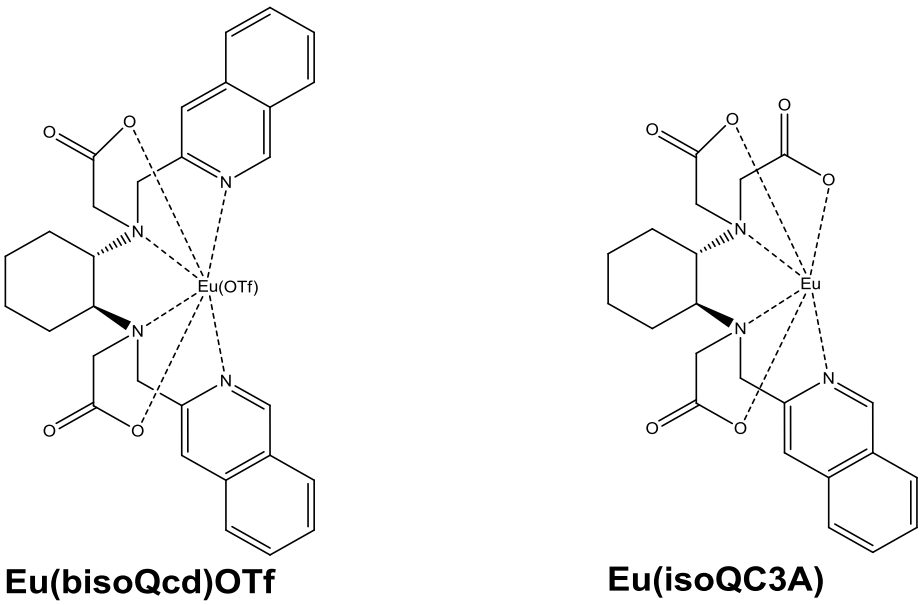

Figure 5.13 *Molecular structure of the Eu(III) isoquinoline based complexes*

The main components the EF have been already listed in Table 5.1 of Chapter 5, but for sake of clarity, their typical extracellular concentration ranges are reported again:

- Bicarbonate ion (24-27 mM)
- Citrate ion (0.1-0.3 mM)

- Serum albumins (≈0.4 mM)
- L-lactate ion (0.6-2.3 mM)
- Sulphate ion (0.4-0.6 mM)
- Phosphate ion (1.2-1.3 mM)

Under extracellular matrix, it is denoted all the body fluid outside of cells, which consists of plasma, interstitial, and transcellular fluid.

The above-mentioned biological composition is referred to a simplified composition of the interstitial and transcellular fluids, which it is mainly composed by cations and anions. Contrary, the plasma contains mostly water but also, hormones, clotting factors, glucose and different proteins. Regarding the protein contribution, only the major albumins have been considered, in their typical extracellular concentration range of 0.4 mM. Some other electrolytes, like NaCl are in their typical EF (concentration ~ 100 mM). We take into account its contribution, since NaCl is present in the working buffer solution.

As already discussed in Chapter 1, all the trivalent lanthanide ions are classified as Hard acids and according to the "hard and soft (Lewis) acids and bases" theory they should preferentially interact with oxophilic ions like HCO_3^-, citrate, lactate.

We explored the potential of both europium complexes as probes for the luminescence determination of important bio-analytes that are present in various biological environments. Therefore, the change of the luminescence emission spectra of Eu(bisoQcd) and of Eu(isoQC3A) upon titration with each of the main bio-analytes contained in a typical extracellular interstitial fluid was monitored. The complexes show a notable increase of the luminescence intensity in response to the presence of typical concentrations of citrate, hydrogen carbonate (HCO_3^-) and albumin protein (Figure 5.14).
Very small or no change in the luminescence spectra are detected when both complexes were titrated with lactate, hydrogen phosphate, sulfate anions, at their typical extra cellular concentrations [L-lactate (2.3 mM), di-Sodium hydrogen phosphate (1.3 mM) and Sodium sulfate (0.6 mM)]. Hence, we conclude that our

optical probes are selective towards citrate, hydrogen carbonate and the albumin protein. We wanted to further deeply investigate such behavior.

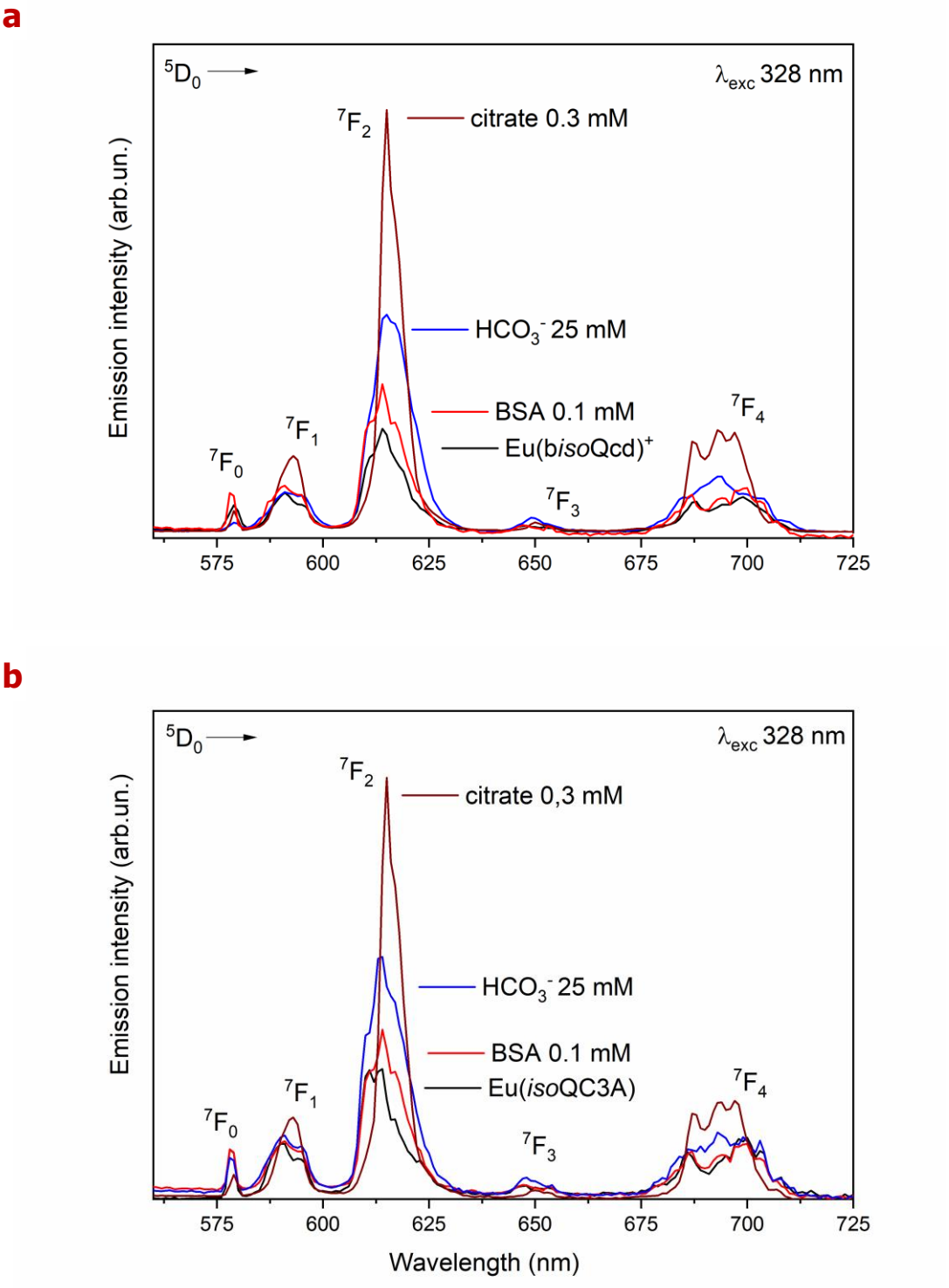

Figure 5.14 *Eu(III) luminescence emission spectra upon addition of HCO_3^-, BSA and citrate around their typical extracellular concentrations (reported in the picture) for (a) Eu(bisoQcd) and (b) Eu(isoQC3A) complexes. The concentration of the complexes was 80 μM*

5.3.2 Bicarbonate: luminescence and binding constants

The bicarbonate presents the protonation constants pK_{a1} = 9.87 and pK_{a2} = 6.11 at 298.15 K, and pK_{a1} = 9.67 and a pK_{a2} = 6.04 at 323 K, both with μ = 0.1 M (Equations 5.1 a and b).[27]

$$pK_{a1} = \frac{[HCO_3^-]}{[CO_3^{2-}][H^+]} \qquad (5.1\ a)$$

$$pK_{a2} = \frac{[H_2CO_3]}{[HCO_3^-][H^+]} \qquad (5.1\ b)$$

Using Henderson-Hasselbalch equation (Equation 5.2):

$$pH = pKa + \log([A^-]/[HA]) \qquad (5.2)$$

one can easily calculate the approximated ratios of carbonate/bicarbonate and bicarbonate/carbonic acid expected under physiological pH (Equations 5.3 a and b) and critically low pH (Equations 5.3 c and d) at 298.15 K (calculations at 323 K omitted, since constants for both temperatures are comparable).

7.4 = 6.11 + log ([bicarbonate] / [carbonic acid]) → 20:1 *(5.3 a)*

7.4 = 9.87 + log ([carbonate] / [bicarbonate]) → 1:295 *(5.3 b)*

6.8 = 6.11 + log ([bicarbonate] / [carbonic acid]) → 5:1 *(5.3 c)*

6.8 = 9.87 + log ([carbonate] / [bicarbonate]) → 1:1174 *(5.3 d)*

One may affirm that carbonate will be usually in the form of bicarbonate in physiological conditions. Thus, in carbonate/bicarbonate/carbonic acid studies for biomedical applications, the bicarbonate form will be considered (Figure 5.15).

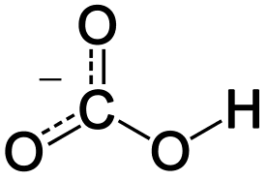

Figure 5.15 *Bicarbonate (hydrogen carbonate) anion*

Changes in the HCO_3^- concentrations may be related to irregular pH homeostasis and, thus, to many diseases. Metabolic acidosis (unusually high hydrogen ion concentration) may indicate the presence of solid tumors or cause chronic kidney disease.[28–30]

Regarding physiological processes, apart from pH homeostasis and kidney function, many of them depends on this equilibrium, such as sperm maturation and blood flow.[1,31,32] Moreover, HCO_3^- is 10 times more concentrated than other anions present in human body's fluids and tissues (except within cells, where lactate could compete with HCO_3^- in specific cell types) (Table 5.1).

In literature many examples of Eu(III) and Tb(III) complexes can be find, which can successfully detect HCO_3^- in physiological conditions.[1] Bretonniere *et al.*[33,34] reported some Eu(III) complexes, bearing acridone as chromophore moieties (Figure 5.16), with a good luminescent response between 5-25 mM HCO_3^- concentration. Besides, a selectivity towards HCO_3^- ($\log K$ = 0.8-2.3, depending on the ligand) in the presence of chloride, phosphate, lactate, citrate and protein was observed.

Murray *et al.*[35] reported a non-toxic (to several cell types, with an IC_{50} > 200 μM) Eu(III) complex selective for HCO_3^- ($\log K$ = 3.50) and citrate ($\log K$ = 6.02), for local changes monitoring of this anions within the mitochondrial region. This same complex and two analogues have also been reported by Smith *et al.*;[36,37] they monitored *in vivo* for the first time the concentration of HCO_3^- in cell mitochondria. Imperio *et al.*[38] reported an Eu(III) luminescent complex that selectively binds HCO_3^- in the presence of competing anions, such as lactate and citrate. However, the stability of the adduct does not accomplish the conditions required for actual applications. In 2013, Butler *et al.*[39] reported Eu(III) complexes capable of

selectively binding HCO_3^- in a complex medium when found in a concentration >10 mM (log*K* between 3 and 4, 295 K, 50% MeOH / 0.1 M NaCl).

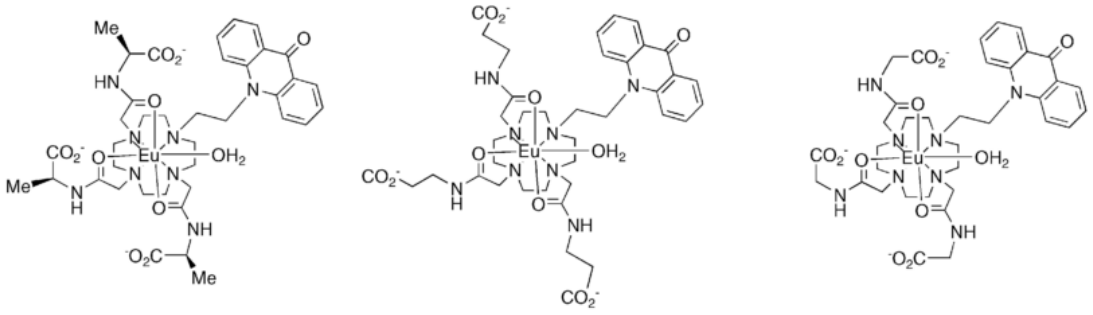

Figure 5.16 *Three representative Eu(III) complexes presenting acridone chromophore moieties*[33,34]

As already described in Chapter 4, the complexes we present in this work differ in charge, steric hindrance and lipophilicity. It is expected that these differences will confer them different affinity towards diverse bio-analytes (selectivity towards diverse target bio-analyte), and lipophilicity strongly affect the mobility of the complexes in the organism, which is a very important fact to take into account for medical sensors. Moreover, the complexes proposed present a 6-fold coordination (ignoring water molecules) in comparison to that commonly found in literature (7-fold coordination, ignoring water molecules, strongly pre-oriented) which may allow them the reversible binding of more than one target bio-analyte at the same time (higher affinity) when the target molecule is small enough, such as in the case of HCO_3^-.

We will start our sensing studies with the small, relevant bio-analyte HCO_3^- with the library of Eu complexes introduced in Chapter 4, in order to not just study their viability as sensors, but also to begin a broader study about the selectivity of these complexes towards diverse bio-analytes and interferings.

Increasing addition of the bio-analyte to our Eu(bisoQcd) complex, lead to a considerably modification of the geometric environment around the metal center (change of R value from the initial value of 2.88 to 5.05 in the presence of 28 mM of

HCO_3^-). This is related to a consistent enhancement of the $^5D_0 \rightarrow {}^7F_2$ luminescence intensity (Figure 5.17). The HCO_3^- anion after the coordination with the Eu(III) ion, displace the water molecules from the inner coordination sphere, reducing therefore the undesiderable multiphonon relaxation process. A decrease of the emission intensity of the $^5D_0 \rightarrow {}^7F_0$ transition has been also detected, resulting in a minor axial geometry of the Eu(III) environment.

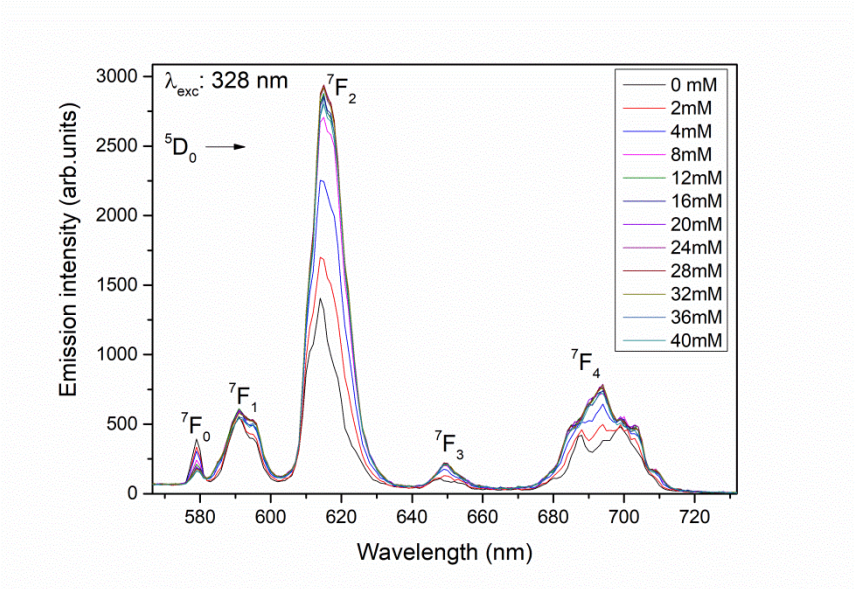

Figure 5.17 *Eu(III) luminescence emission spectra of the Eu(bisoQcd) complex [0.1 mM] in MOPS buffer 15 mM, pH≈7.4, NaCl 0.15 mM. The concentration of the anion is reported*

It is important to evidence the trend of the average maximum intensity as a function of the target anion concentration. For both bisoQcd and isoQC3A complexes, we observe an increase of this intensity, even if some differences are noted (Figure 5.18). In particular, i) a different relationship between intensities values and target ion concentration. A rapid parabolic enhancement has been obtained for the Eu(bisoQcd) complex, whereas a linear increase has been observed for the Eu(isoQC3A) complex. ii) differences in the absolute emission intensity related to the number of chromophoric units in the complex. In fact, upon the same experimental conditions, the bisoQcd complex shows higher maximum luminescence intensity than the isoQC3A complex. Another feature that is worth evidencing iii) the different sensitivity of the two complexes in the working ion concentration range. The bisoQcd complex showed the best sensitivity in the concentration range of HCO_3^- connected

with a metabolic acidosis disease (2-10 mM). In fact, we detect an intensity increase of the luminescence around 120% (≈10 mM HCO_3^-), whilst for isoQC3A complex only around 30% (≈10 mM HCO_3^-).

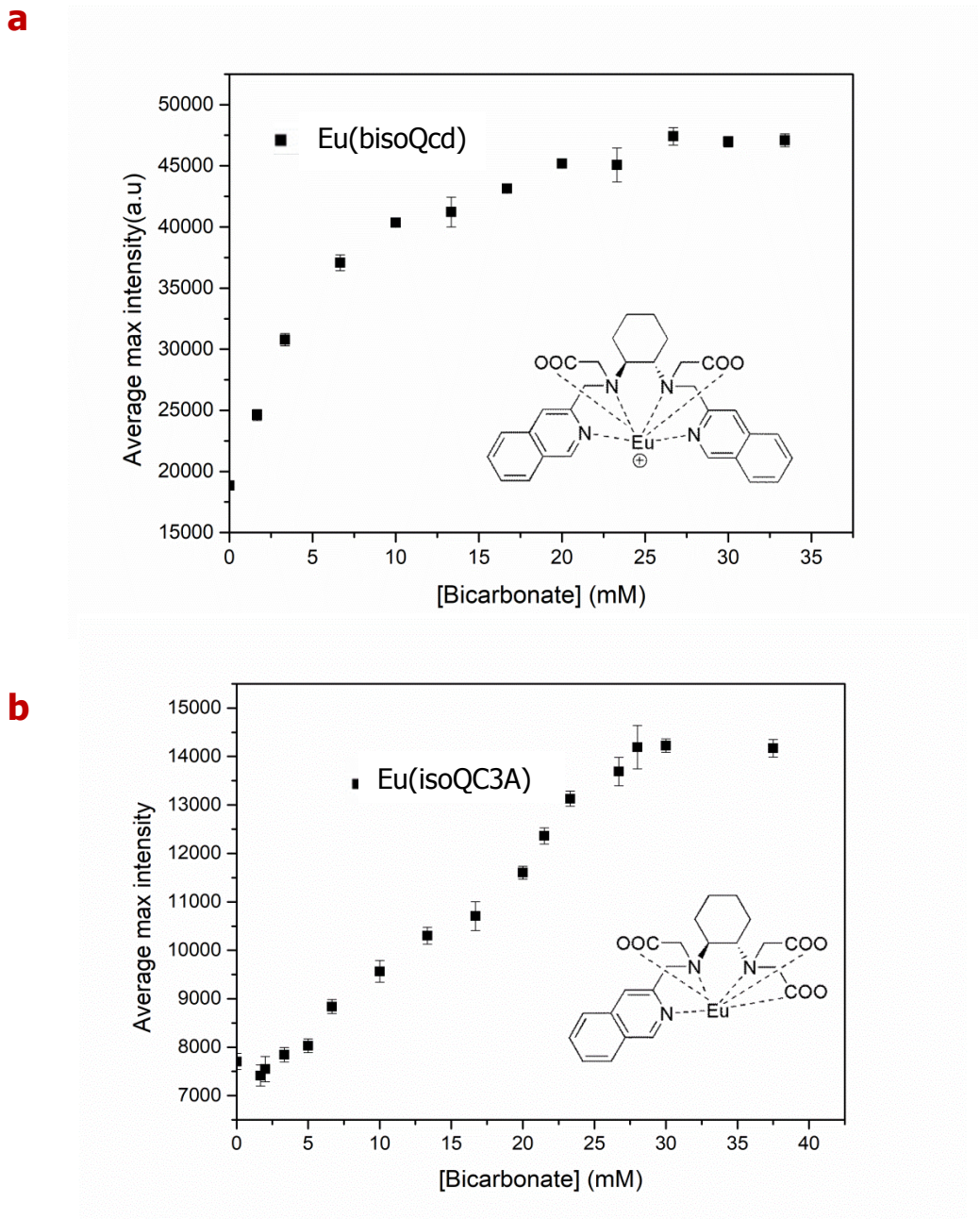

Figure 5.18 *Average maximum intensity* vs. [HCO_3^-] concentration plots for (a) Eu(bisoQcd), I_{max}≈1.47 fold increase, LOD=0.123 mM and (b) Eu(isoQC3A), I_{max}≈0.85 fold increase, LOD=2.32 mM. * It is referred to an average of luminescence intensity upon 6 replicas*

The affinity constants of the adduct between HCO_3^- and the two Eu(III) complexes with where obtained by means of cEST/Solverstat software using data from Figure 5.18.

Table 5.3 *Binding constants (logK) of the bio-analytes to Eu(III) complexes referred to the reaction: EuL + nA ⇋ EuL(A)n*

Complex-HCO_3^-	***n***	**Log(*K*)**
Eu(bisoQcd)	2	4.6 ± 0.2
Eu(isoQC3A)	1	3.4 ± 0.1

The cationic complexes can bind two HCO_3^- anions at the metal centre resulting in a higher affinity constant.

5.3.3 Citrate: luminescence and binding constants

Citrate has p*K*a values of 3.13, 4.76 and 6.40 at T = 298.15 K. Thus, we expect to find it as a trianion at a physiological pH around 7.4 (Figure 5.19).

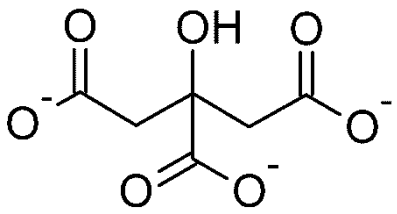

Figure 5.19 *Citrate trianion*

This anion has a key role as intermediates in anaerobic cells Krebs cycle and in glycolysis.[1,40] It is not difficult to deduce that it may be a good bio-analyte for some organism anomalies. Low levels of urine citrate (usually around 10 - 12 µmol/g) may

indicate diverse kidney dysfunctions and even prostate cancer (1 - 3 µmol/g).[40] This fact alone would already be a good pretext for the development and study of potential citrate probes but, furthermore, the assessment of the affinity for citrate of probes initially developed for the sensing of other bio-analyte is also interesting in order to study the possible competence between potentially interfering molecules currently found in the fluids of interest.

In literature we may find several examples studying citrate as either just a mere potential interfering[33,34,38,41–43] or by actually quantifying its affinity towards the studied probe.[1,35,44–46] In Table 5.4 some affinity constants found in literature, for luminescent lanthanide complexes towards citrate. The charges of binary complexes are reported, since coulombic interactions between complex and citrate strongly affect the stability. It can be appreciated that the affinity constants are higher for positively-charged Ln(III) complexes, which makes sense, since the interaction of the positively-charged Ln(III) complexes with citrate (with three negative charges) would be favoured by coulombic attraction.

Table 5.4 *Apparent affinity constants of some luminescent Ln(III) complexes towards citrate, T = 298.15 K, µ = 0.1 M NaCl, pH = 7.4. The highest value found in each reference is reported. Also the total charge of the adducts is reported * T = 295 K, ** 0.1 M NaCl, 4 mM KCl, 0.1 M HEPES and 0.9 mM NaH_2PO_4, *** 10 mM $ZnCl_2$*

REF.	Murray 2008[35]	Pal 2009[46]	Smith 2011[36]	Smith 2012[44]	Butler 2013[39]	Mc Mahon 2014[47]
log *K*	6.02	5.26**	5.21	4.80*	3.65	3.95***
Q binary complex	+3	+3	+3	+3	-1	+1

Regarding the luminescence trends, both Eu(III) bisoQcd and isoQC3A complexes showed a significant enhancement of the average maximum intensity, due to the already discussed displacement of the water molecules bound to the metal centre (Figure 5.20). The increase of the luminescence emission intensity for Eu(bisoQcd)

complex upon titration with citrate is around 1.44 fold; nearly the same observed for the HCO_3^-.

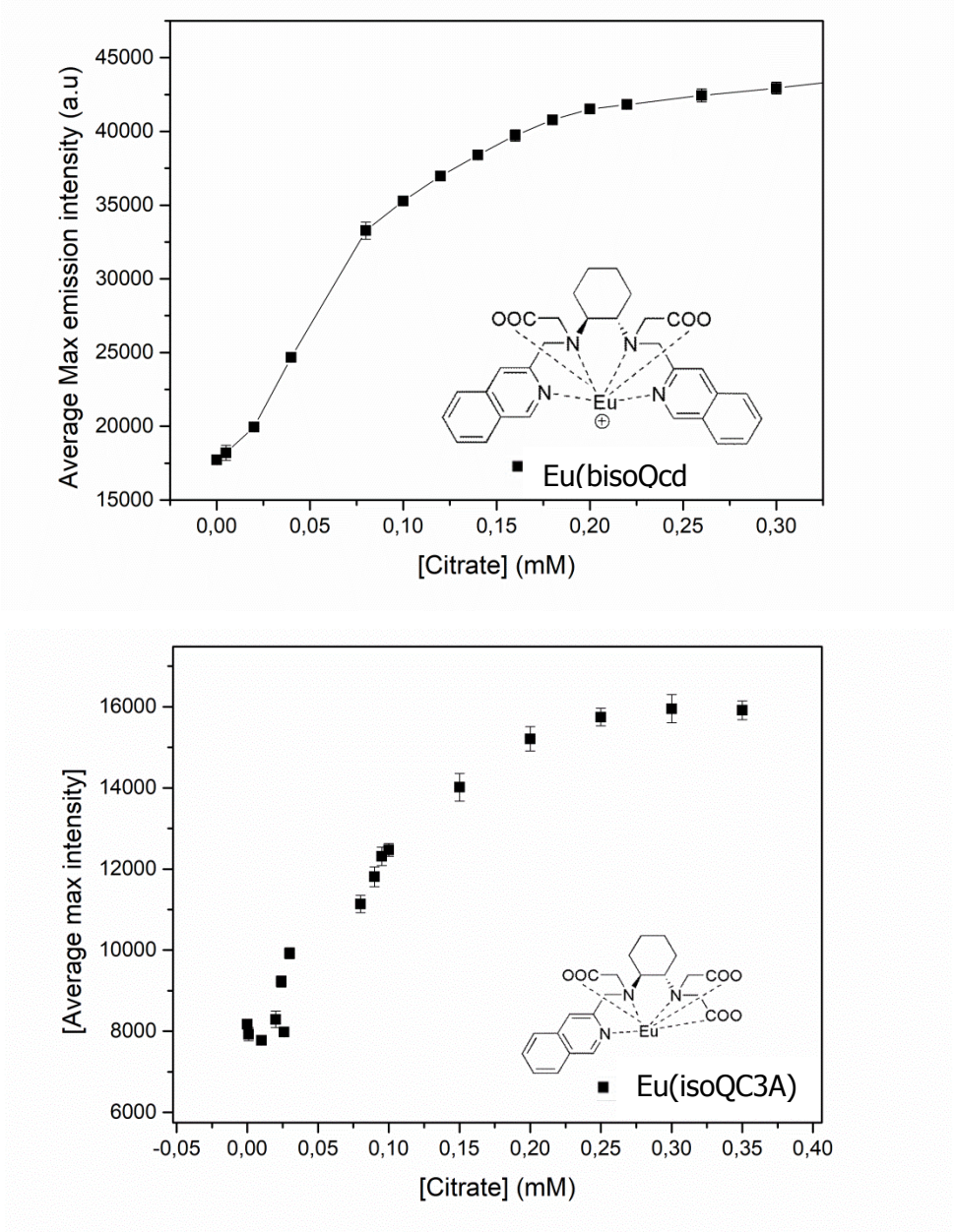

Figure 5.20 *Average maximum intensity* vs. [citrate] concentration plots for the complexes (a) bisoQcd, 0.1 mM, I_{max}≈1.44 fold increase, LOD=0.028 mM and (b) isoQC3A, 0.1 mM, I_{max}≈0.95 fold increase, LOD=0.011 mM. * It is referred to an average of luminescence intensity upon 6 replicas*

From the evolution of the luminescence emission spectra during the titrations it was possible to define the stoichiometry formed adducts between the optical probes and the bio-analytes and to calculate the binding constants (Table 5.5).

The affinity constants of the adduct between HCO_3^- and the two Eu(III) complexes with where obtained by means of cEST/Solverstat software using data from Figure 5.20.

Table 5.5 *Binding constants (logK) of the bio-analytes to Eu(III) complexes referred to the reaction: EuL + nA ⇋ EuL(A)n*

Complex-Citrate	*n*	Log(*K*)
Eu(bisoQcd)	1	4.1 ± 0.3
Eu(isoQC3A)	1	4.1 ± 0.2

5.3.4 Interaction with Serum albumin

The interaction study on SA, in our case represented by more accessible and cheaper BSA that has been above described in Chapter 5.2.1.

As the protein is chiral, the interaction of the enantiopure bisoQcd and isoQC3A complexes would generate two different diastereoisomeric adducts. Therefore, both enantiomer forms (1R, 2R / 1S, 2S) of the complexes have been investigated. In the end, similar increases of the luminescence response were observed. Upon progressive addition of the protein, to its extracellular concentration range (0.4 mM), upon excitation at 328 nm, an overall enhancement of the signal around 25-30% (Figure 5.21 a-d) has been detected for both enantiomers of the complexes.

a

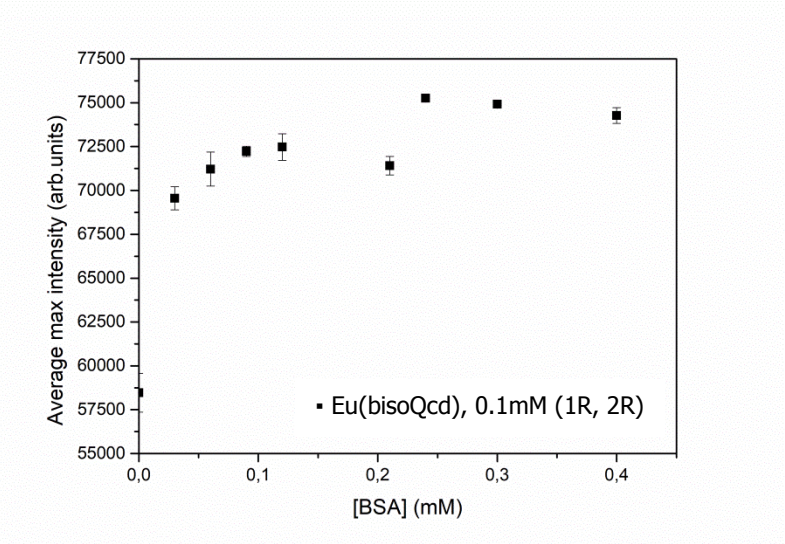
Average max intensity (arb.units)
77500
75000
72500
70000
67500
65000
62500
60000
57500
55000
0,0
0,1
0,2
0,3
0,4
[BSA] (mM)
▪ Eu(bisoQcd), 0.1mM (1R, 2R)

b

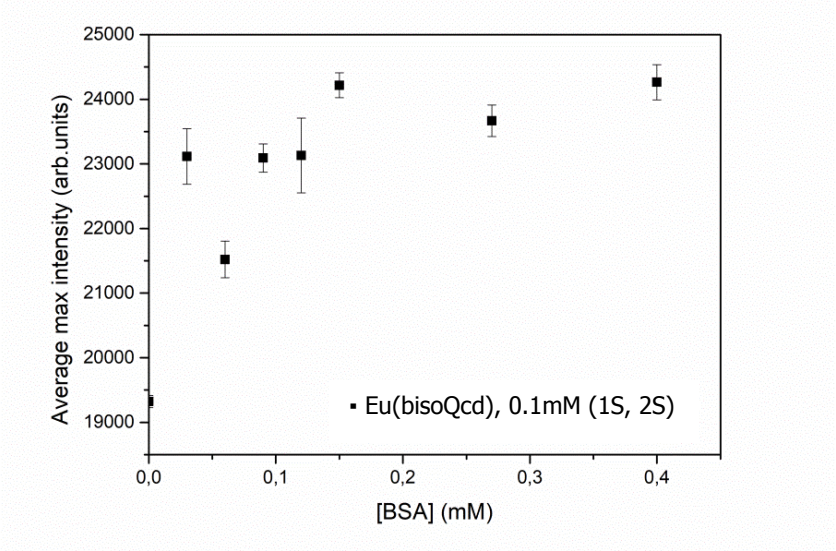
Average max intensity (arb.units)
25000
24000
23000
22000
21000
20000
19000
0,0
0,1
0,2
0,3
0,4
[BSA] (mM)
▪ Eu(bisoQcd), 0.1mM (1S, 2S)

c

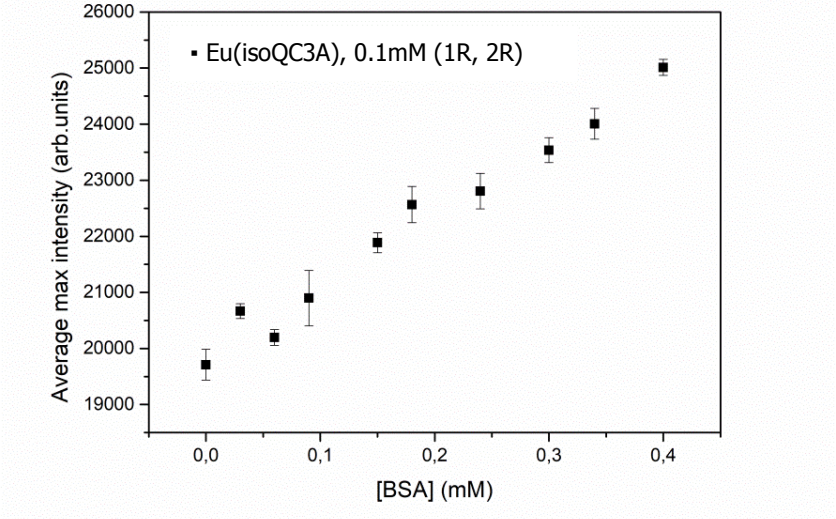
Average max intensity (arb.units)
26000
25000
24000
23000
22000
21000
20000
19000
0,0
0,1
0,2
0,3
0,4
[BSA] (mM)
▪ Eu(isoQC3A), 0.1mM (1R, 2R)

d

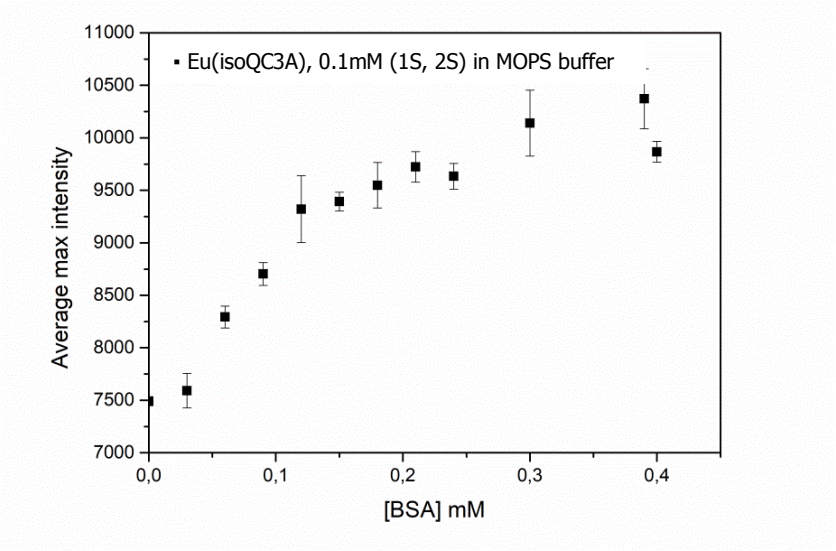

Figure 5.21 *Average maximum intensity* vs. [BSA] concentration plots for the Eu(III) complexes (a) bisoQcd (1R, 2R), Luminescence increase ≈27%; (b) bisoQcd (1S, 2S), Luminescence increase ≈25%; (c) isoQC3A (1R, 2R), Luminescence increase ≈27%; (d) isoQC3A (1S, 2S), Luminescence increase ≈31%. * It is referred to an average of luminescence intensity upon 6 replicas*

As observed for the two adducts of Eu(bisoQcd) with HCO_3^- or citrate, it is not possible to correlate a major affinity constant with a most selective and sensitive probe. Even if the affinity constants of the isoquinoline complexes (bisoQcd and isoQC3A) with SA (Table 5.6) are similar to the corresponding adducts with the citrate ion (Table 5.5), the sensitivity was still high for the citrate.

Table 5.6 *Binding constants (logK) of the bio-analytes to Eu(III) complexes referred to the reaction: EuL + nA ⇋ EuL(A)n*

Complex-BSA	*n*	Log(*K*)
Eu(bisoQcd)	1	3.9 ± 0.2
	2	3.6 ± 0.4
Eu(isoQC3A)	1	4.2 ± 0.6

An additional key experiment has been reported (Figure 5.22 a-b), where the final emission intensity of the bisoQcd complex in a background solution of the protein (0.4 mM) and increasing citrate (up to 0.3 mM) is 0.68 fold increased. On the other hand, when the protein concentration is increasing in a background solution of citrate (0.3 mM), the final emission intensity is just 0.28 fold increased, by evidencing the major affinity for the anion.

a

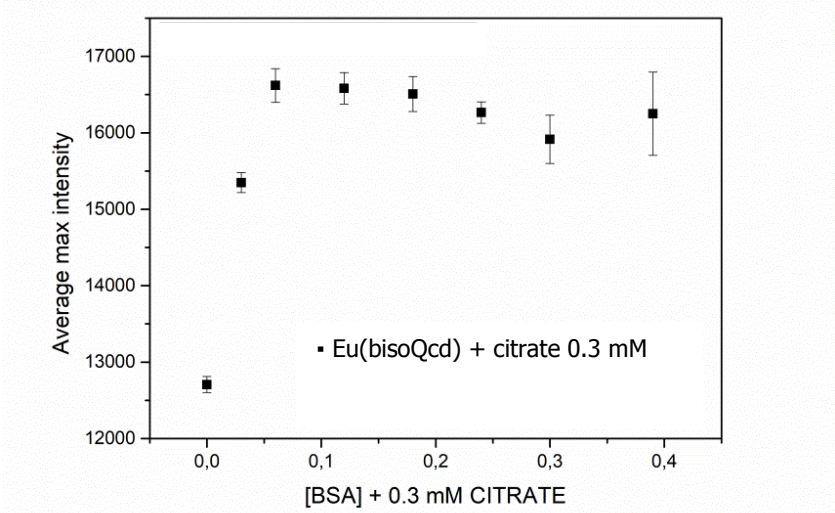

b

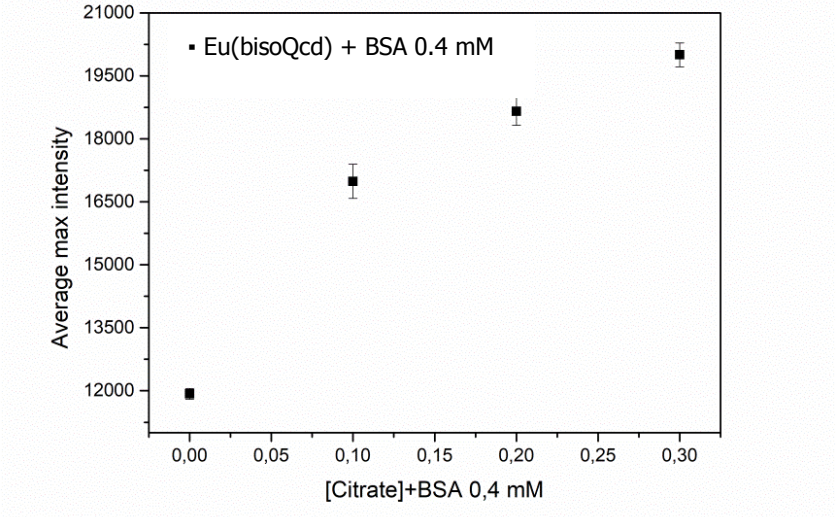

Figure 5.22 *Average maximum intensity* vs. [BSA] or [citrate] concentration plots for the complexes (a) bisoQcd (1S, 2S) 0.1 mM, Luminescence increase ≈68%, in a fixed background of BSA: 0.4 mM; (b) bisoQcd (1S, 2S) 0.1 mM, Luminescence increase ≈28%, in a fixed background of citrate: 0.3 mM; * It is referred to an average of luminescence intensity upon 6 replicas*

Interestingly, bisoQcd adducts with HCO_3^- and citrate, shows similar emission intensity (Figure 5.23). The difference can be seen in the curve slope, as in the same concentration range (i.e. 0-2 mM) the optical response towards citrate is more sensitive. Indeed, the final emission intensities are the same, but with very different slopes in the working range of the target bio-analytes, where the citrate concentration is almost ten times lower than the one of HCO_3^-. The bisoQcd complex in presence of BSA gave surprizing results, revealing the lowest sensitivity, even if its affinity constant is similar to citrate one. (Figure 5.23, orange line). In fact, the sensitivity of the optical response towards a particular bio-analyte is related not only to the probe-analyte affinity but also to the overall luminosity of the adduct. In fact, the adducts with citrate and HCO_3^- showed higher overall luminosity than the BSA adduct.

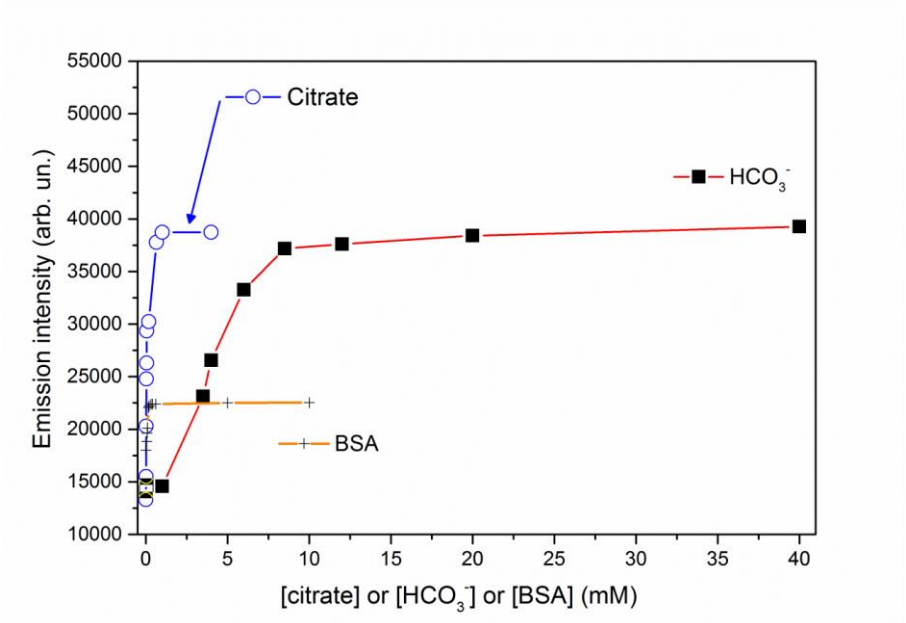

Figure 5.23 *Emission intensity of bisoQcd complex (0.1 mM) vs. [citrate] (blue curve), [HCO_3^-] (red curve) or [BSA] (orange curve), pH=7.4 in MOPS, 298.15 K, NaCl 0.15 M*

5.3.5 The detection of citrate in extracellular fluid

As already discussed, the isoquinoline complexes showed a notable increase of the luminescence intensity in response to the presence of typical concentrations of citrate, hydrogen carbonate and albumin protein (Figure 5.24).

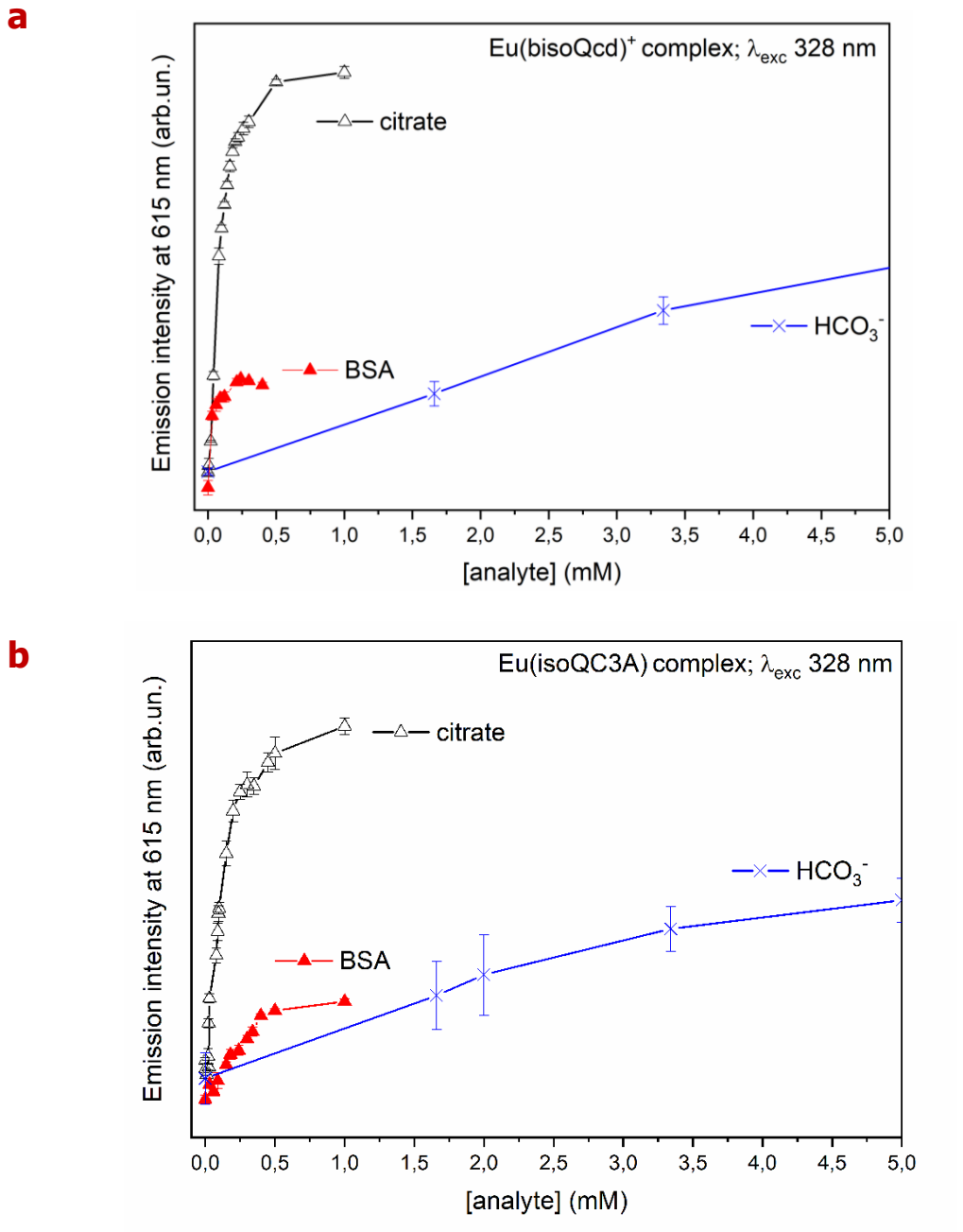

Figure 5.24 *Evolution of the Eu(III) luminescence emission intensity at 615 nm upon addition of HCO_3^-, BSA and citrate for (a) Eu(bisoQcd) and (b) Eu(isoQC3A) complexes. The concentration of the complexes was 80 μM. 0-5 mM concentration range for hydrogen carbonate and 0-1 mM for citrate and BSA are reported*

The respectively anion binding constants were previously reported separately. For but for sake of clarity are summarized again in Table 5.7. The values are relatively high and similar for both Eu(III)-complexes and a clear selectivity towards a particular bio-analyte was not observed.

In addition, using the observed excited state lifetimes (τ_{obs}) from the Eu(III) $^5D_0$ state (achievable from the decay curves depicted in Figure 5.25) and the estimation of the τ_{rad} by means of the Werts equation,[48] we could derive the intrinsic quantum yield of each Eu(III) adduct at its saturation concentration (Table 5.8).

Table 5.7 *Binding constants (logK) of the bio-analytes to Eu(III) complexes referred to the reaction: EuL + nA ⇋ EuL(A)n*

		L=		
	n	**citrate**	**HCO_3^-**	**BSA**
Eu(bisoQcd)	1	4.1 ± 0.3	-	3.9 ± 0.2
	2	-	4.6 ± 0.2*	3.6 ± 0.4‡
Eu(isoQC3A)	1	4.1 ± 0.2	3.4 ± 0.1	4.2±0.6

*[Eu(bisoQcd)]·$(HCO_3^-)_2$ adduct has been detected. ‡[Eu(bisoQcd)]·BSA and $[Eu(bisoQcd)]_2$·BSA adducts have been detected

a

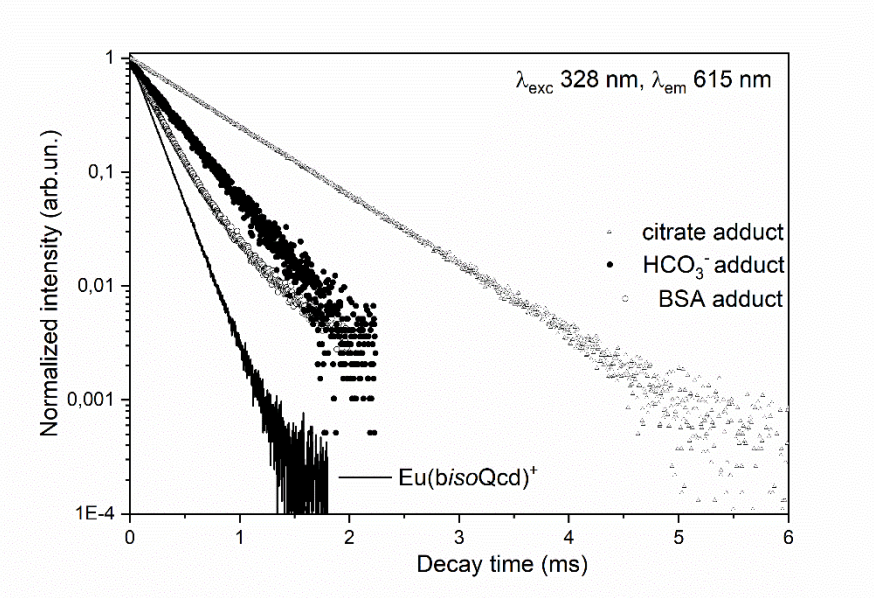

b

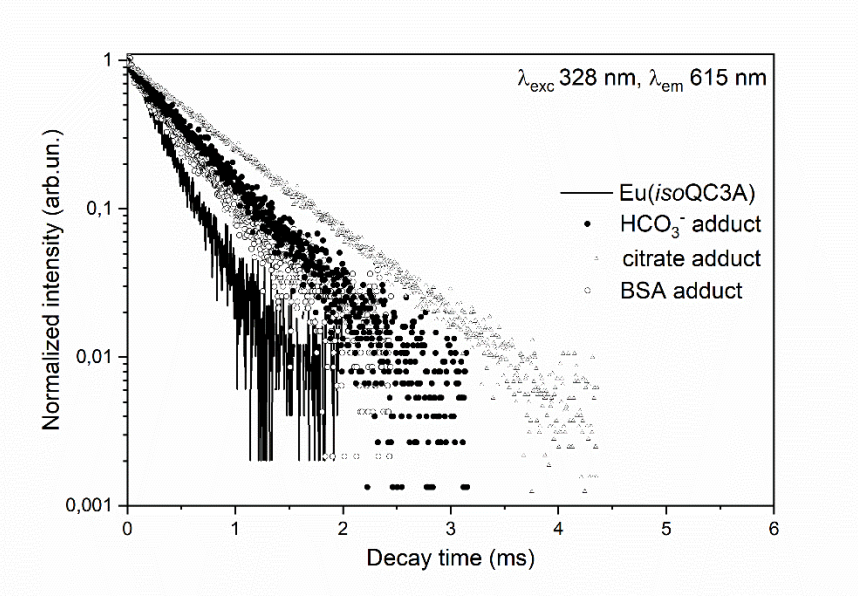

Figure 5.25 *Luminescence decay curves from $^5D_0$ level of Eu(III) in case of aqueous solution of (a) Eu(bisoQcd) and its adducts and (b) Eu(isoQC3A) and its adducts. All the decay curves can be well fitted by a single exponential function, except in the case of the BSA adduct with Eu(bisoQcd) complex: in this case, the 1/e folding time is used as τ_{obs}*

Table 5.8 *Observed and radiative lifetimes, and intrinsic quantum yield [ϕLn(%)] for the luminescent adducts under investigation*

Adduct	τ_{obs} (ms)	τ_{rad}(ms)	ϕ_{Ln}(%)
Eu(bisoQcd):BSA*	0.35(1)	5.38	6.5
Eu(bisoQcd):$(HCO_3^-)_2$	0.46(1)	3.70	12.4
Eu(bisoQcd):citrate	0.83(1)	3.77	22.0
Eu(isoQC3A):BSA	0.33(1)	5.16	6.4
Eu(isoQC3A):HCO_3^-	0.43(1)	3.71	11.6
Eu(isoQC3A):citrate	0.72(1)	3.47	21.0

*The presence of [Eu(b*iso*Qcd)]$_2$·BSA adduct is negligible at the working concentration

Is curious to note that both Eu(III) complex-adducts show higher luminescence efficiency, respect to the related starting complexes. However, among these adducts the ones with citrate exhibits the highest luminescence efficiency, while the adducts with the protein emit light with lowest efficiency. As reported previously both HCO_3^-

anion and BSA are capable to displace at least one water molecule from the inner coordination sphere of Eu(III) which increases the luminescence quantum yield by reducing the efficiency of the non-radiative multiphonon relaxation process. It is proposed that upon interaction with citrate, the inner, and maybe the outer spheres of the metal ion are better shielded from water molecules than in the case of the two other bio-analytes. Furthermore, there is a good agreement between the calculated Eu(III) luminescence efficiency [Φ_{Ln} (%)] and the total Eu(III) emission intensity of the complexes and their adducts under investigation (see for comparison data in Chapter 4 Table 4.4, Chapter 5 Table 5.8 and Figure 5.17).

To understand the reasons on the basis of such a different Eu(III) luminescence efficiency of the adducts, the hydration number *q* once the bio-analyte is coordinated to Eu(III) is determined. In the case of BSA, one water molecule is still present when Eu(bisoQcd) interacts with the protein, so that the protein is capable to remove around 1.8 water molecules from the vicinity of Eu(III) upon interaction with the complex [calculated as a difference from value of *q* in the starting complex (Chapter 4, Table 4.4)]. In the case of hydrogen carbonate, we measured the decay curves of the $^5D_0$ Eu(III) excited state in D_2O (Figure 5.26 a) and by including the values of the observed lifetime in water and deuterium oxide in the Horrock's equation, we estimated a hydration number around 0.8 (Table 5.9). A similar behavior has been observed in the case of the adduct with Eu(isoQC3A) complex (Table 5.9 and Figure 5.27 a).

a

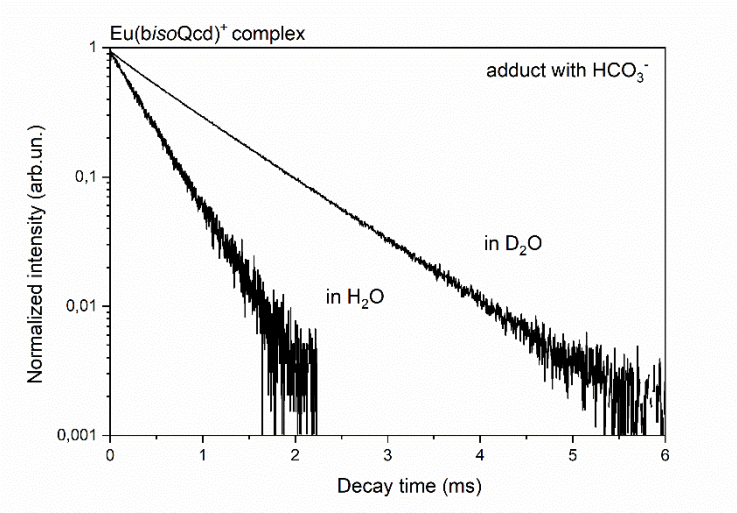

b

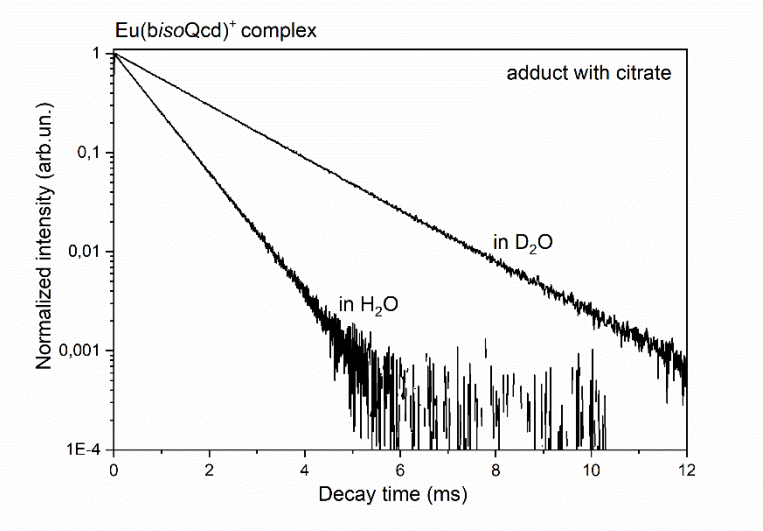

Figure 5.26 *Decay curves of the luminescence from $^5D_0$ level of Eu(III) in H_2O and D_2O, in the case of the adducts of Eu(bisoQcd) complex with HCO_3^- (a) and citrate (b). λ_{exc} was 328 nm, λ_{em} was 615 nm. All the decay curves can be well fitted by a single exponential function*

a

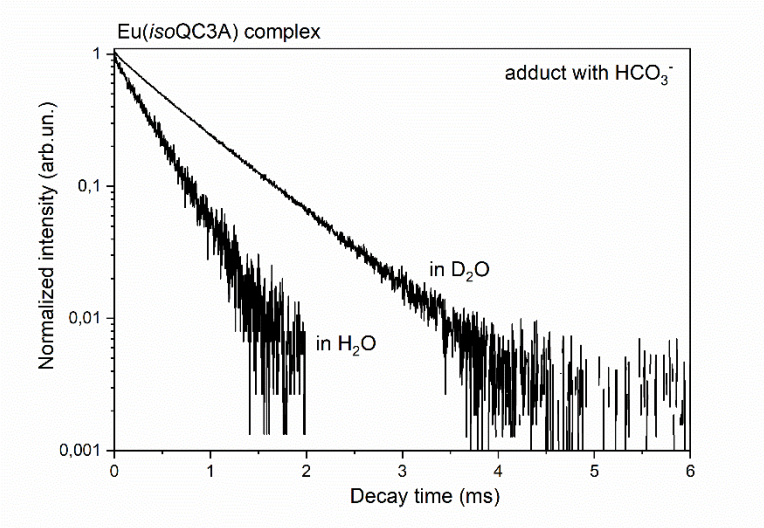

b

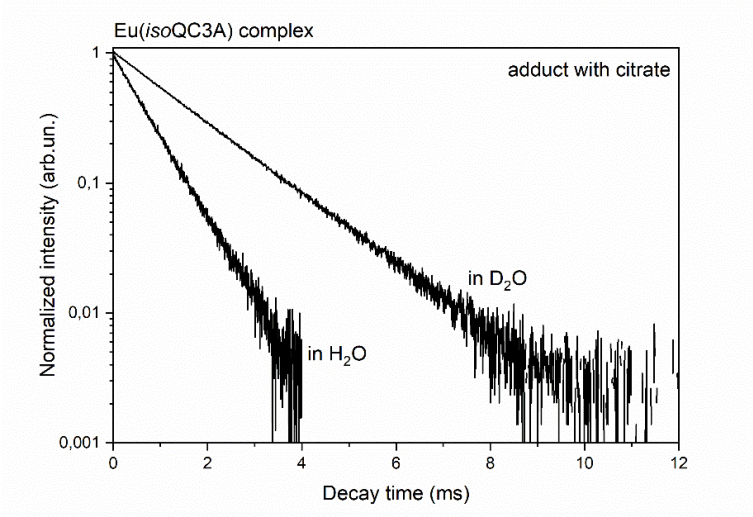

Figure 5.27 *Decay curves of the luminescence from $^5D_0$ level of Eu(III) in H_2O and D_2O, the case of the adducts of Eu(isoQC3A) complex with HCO_3^- (a) and citrate (b). λ_{exc} was 328 nm, λ_{em} was 615 nm. All the decay curves can be well fitted by a single exponential function*

Table 5.9 *Observed lifetimes in H_2O (τH_2O) and D_2O (τD_2O) of the adducts, hydration number of the starting complex (qi, Chapter 4 Table 4.4), hydration number of the adduct (qf), number of removed water molecules close to the metal ion upon interaction with the bio-analyte (Δq =qi - qf) and Eu(III) intrinsic quantum yield [ϕLn (%)] of the adduct*

Adduct	τ_{H2O} (ms)	τ_{D2O} (ms)	q_i	q_f	Δq	Φ_{Ln} (%)
Eu(bisoQcd):BSA	0.35(1)	–¶	2.8(1)	1*	1.8	6.5
Eu(bisoQcd):$(HCO_3^-)_2$	0.46(1)	0.88(1)	2.8(1)	0.8(1)	2.0	12.4
Eu(bisoQcd):citrate	0.83(1)	1.98(1)	2.8(1)	≈ 0	2.8	22.0
Eu(isoQC3A):BSA	0.33(1)	–¶	2.8(1)	–	–	6.4
Eu(isoQC3A):HCO_3^-	0.43(1)	0.72(1)	2.8(1)	0.7(1)	2.1	11.6
Eu(isoQC3A):citrate	0.72(1)	1.82(1)	2.8(1)	0.1(1)	2.7	21.0

*determined by a computational study

¶not determined: too large amount of D_2O are required to prepare MOPS buffered solution of BSA.

The flexible citrate anion is able to coordinate to the metal ion in different ways involving the α-hydoxyl and α/β-carboxylate groups and can therefore remove water molecules from the coordination spheres most efficiently. Based on the luminescence lifetimes and increase of intensity it is reasonable that only water molecules are removed from the first coordination sphere of the metal ion.

DFT calculations can be useful to clarify this point: the minimum energy structures of the *trans*-O,O isomers of $[Y(isoQC3A)cit]^{3-}$ and $[Y(bisoQcd)cit]^{2-}$ with the citrate in all possible coordination modes have been calculated and are shown in Figure 5.28.

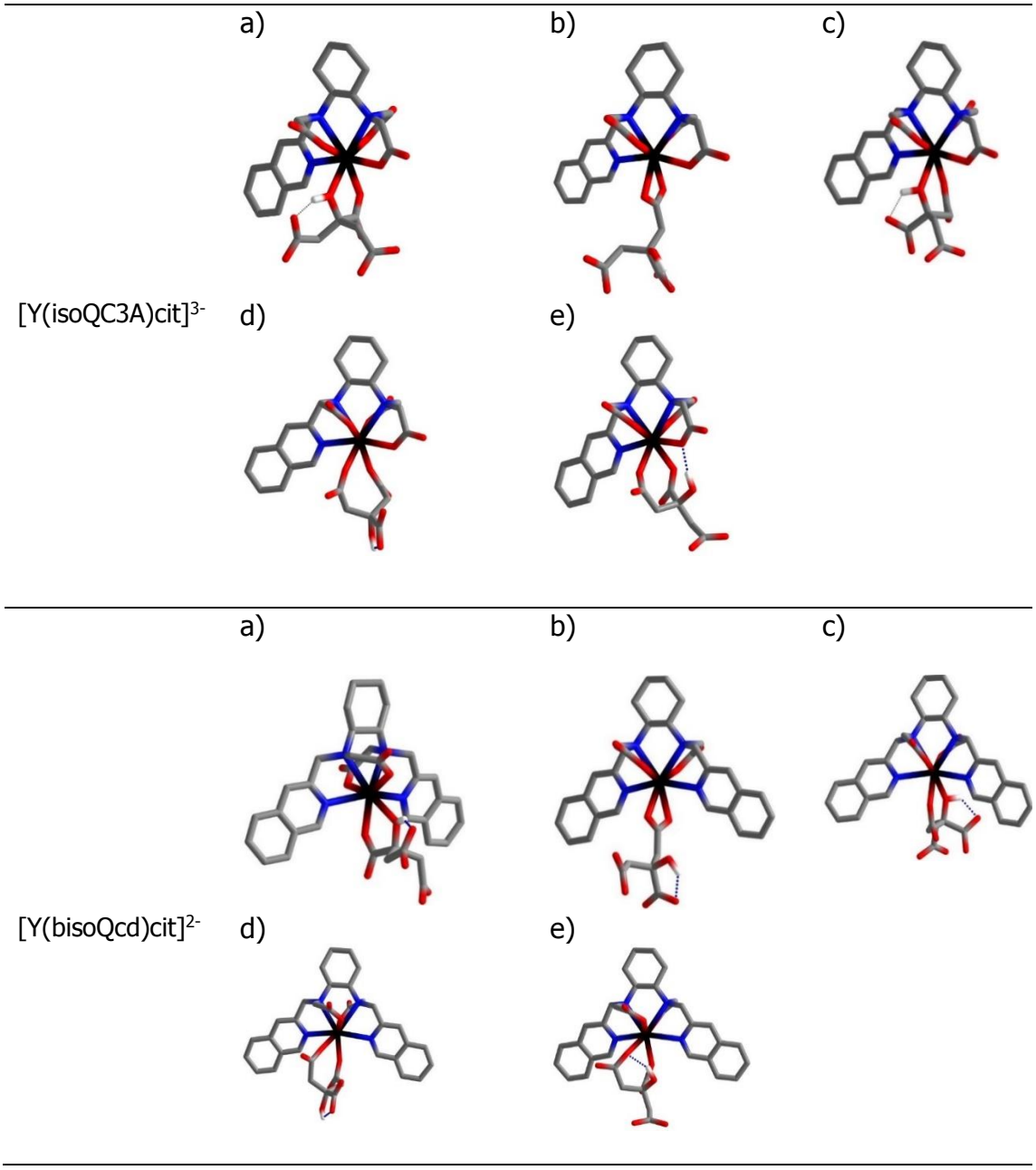

Figure 5.28 *Minimum energy structures of [Y(isoQC3A)cit]$^{3-}$ and [Y(bisoQcd)cit]$^{2-}$ differing by the coordination mode of the citrate anion. Non polarizable hydrogens are removed for clarity*

In Table 5.10 the energy differences between the isomers evidence that in both cases the isomers a), where the α-hydoxyl and α-carboxylate groups of citrate are coordinated, are energetically most favored as found in the only reported structure of a citrate adduct of a Eu(III) complex.[49]

Table 5.10 *Energy differences (ΔE =E – E(a)) between the isomers in Figure 5.33*

Isomer	ΔE (kcal mol^{-1})	
	[Y(isoQC3A)cit]$^{3-}$	[Y(isobQcd)cit]$^{2-}$
a)	0.0	0.0
b)	4.1	6.8
c)	6.1	8.5
d)	3.7	4.5
e)	1.2	5.9

In the case of [Y(isoQC3A)cit]$^{3-}$ the isomer e) is only ~1 kcal mol^{-1} less stable suggesting the presence of a mixture of these isomers. Therefore, in the most stable species, the OH group is coordinated to the metal ion.

On the basis of the DFT results, we used the modified Horrock's equation,[50] in which B = 0.30 + 0.44·*n*OH (*n*OH is the number of OH oscillators in the first coordination sphere; in the case of citrate *n*OH = 1). Interestingly, in both complexes no water molecules are present in the close environment of Eu(III) any more, once citrate is coordinated to the metal center (*q* is close to 0 in both cases, table 5.9). Taking into account the detrimental effect of the OH vibrations in the close proximity of Eu(III) on its luminescence efficiency, we can establish a relationship between the decreasing *q* values along the BSA-HCO_3^--citrate series and the increase of the Eu(III) luminescence efficiency of the related adduct. In other words, the higher the number of removed water molecules by the bio-analyte, the higher is the quantum yield of the related adduct.

Sensing experiments were done with simulated real extracellular conditions of all the major bio-analytes present in EF. It is worth noting that in the following experiments it is assumed that, the total luminescence efficiency of the solution can be assumed to be the sum of the single luminescence efficiency of each adduct weighed by its relative molar fraction (Xi). By expressing this relationship in terms of Eu(III) intrinsic quantum yield [Φ_{Eu} (%)] in solution), we can write the linear combination as Equation 5.4:

$$\Phi_{tot}\mathrm{Eu}(\%) = \sum_i \Phi_i Eu(\%) \cdot X_i \qquad (5.4)$$

Although the similar affinity of both Eu(III) complexes towards the three bio-analytes (hydrogen carbonate, BSA and citrate), one could expect a higher sensitivity towards the bio-analyte (citrate) which causes the larger increase of the quantum yield once it interacts with the complex. Driven by this conviction, we performed four titration experiments in a complex matrix, simulating a real interstitial EF with respect to its main constituents.

1

The citrate ion has been added to a matrix containing HCO_3^- and BSA at their typical extracellular concentration (Figure 5.29). It should be pointed out that for each point of the titration plot, where the citrate is added in a fixed background of HCO_3^- (25 mM) and protein (0.4 mM), the luminescence should be considered as the total contribution of all luminescent adducts ($EuLbic_2$, EuLBSA, EuL and progressive EuLcit) each weighed for their relative amount. The speciation plot (Figure 5.30) has been obtained using Hyss program.[20]

The obtained luminescence increase is around 30% (Figure 5.29), and is explained with the marked increase of the EuL-citrate adduct concentration (red line, Figure 5.30), whose final formation (around 10%, red line in Figure 5.30) foresaw a slight decrease of the EuL-BSA adduct (≈3%) and $EuLbic_2$ adduct (≈4%).

Furthermore, since the final emission intensities of citrate (0.3 mM) and HCO_3^- (25 mM) adducts are quite comparable (Figure 5.23) the effective luminescence change is mainly attributed the displacement of the BSA by citrate from the complex that produces a luminescence increase around 30%.

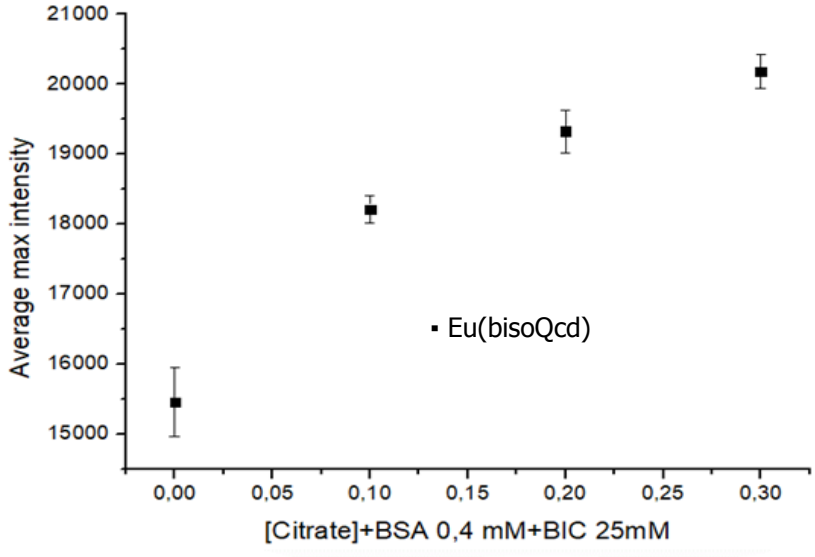

Figure 5.29 *Plot of average maximum intensity* vs. [citrate] in a fixed background of BSA (0.4 mM) and HCO_3^- 25 (mM) for the complex bisoQcd (1S, 2S), where the appreciated luminescence increase has been around 30%. * It is referred to an average of luminescence intensity upon 6 replicas*

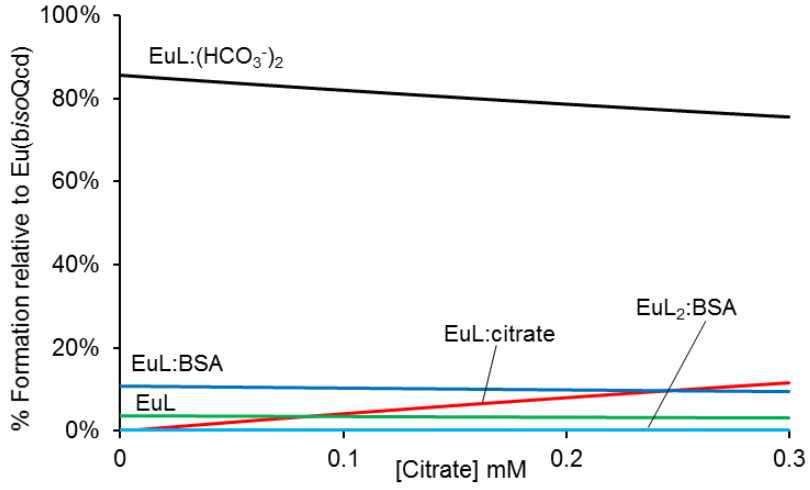

Figure 5.30 *Species distribution in the titration of Eu(bisoQcd) [EuL = 0.1 mM] (green line) with HCO_3^- (black line), BSA (blue line) and citrate (red line) during citrate addition [HCO_3^- = 25 mM, BSA = 0.4mM, citrate = 0 - 0.3 mM]. Percentages are relative to total EuL concentration [EuL = 0.1 mM]*

The obtained results can be compared with the total luminescence theoretical plot (Figure 5.31), calculated using equation 5.4, with three different citrate concentrations (0, 0.15 and 0.3 mM). As stated before, the percentage of each

species has been estimated by Hyss program,[20] while the luminescence intensity for each adducts has been showed from Figure 5.28.

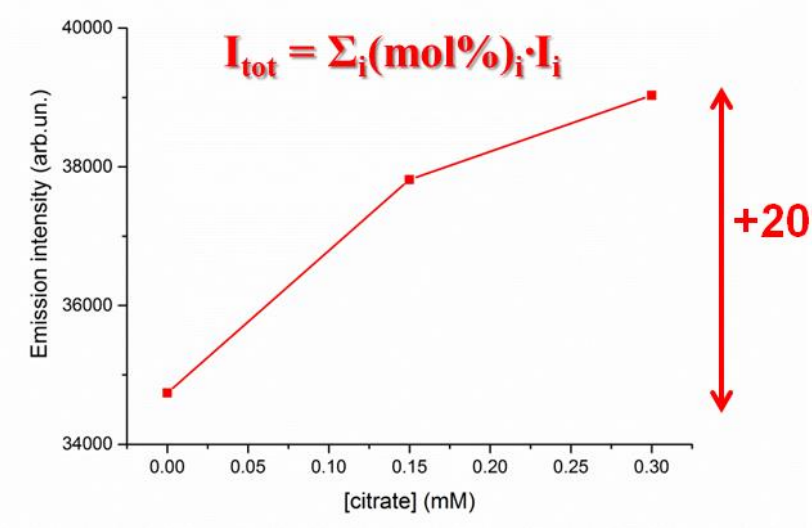

Figure 5.31 *Theoretical plot obtained by Equation 5.4*

The theoretical luminescence enhancement of around 20% is comparable with the experimental luminescence variation depicted in Figure 5.29. The minor discordance between the observed values could be ascribed to matrix effects.

2

The HCO_3^- was added up to the physiological range (25 mM), in a matrix with fixed concentration of BSA (0.4 mM) and citrate (0.3 mM) (Figure 5.32). In this experiment, through the progressive addition of HCO_3^-, the $EuLbic_2$ adduct concentration increase (black line, Figure 5.32) is correlated to a diminishing amount of EuL-BSA, EuL-citrate adducts and EuL (Figure 5.32), giving rise to a compensation in the total emission intensity.

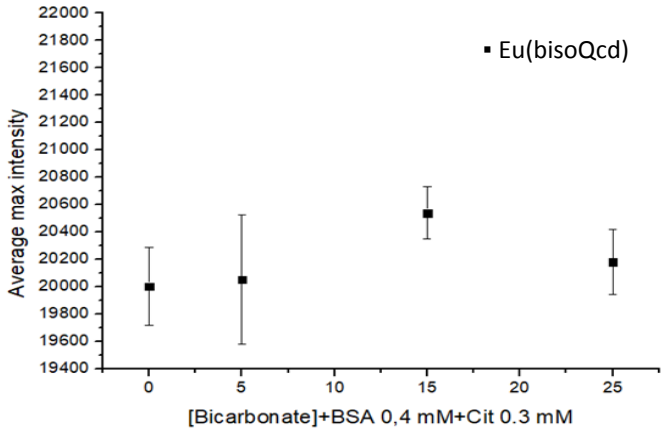

Figure 5.32 *Plot of average maximum intensity* vs. [HCO_3^-] in a fixed background of BSA 0.4 mM and citrate 0.3 mM for the bisoQcd complex (1S, 2S); luminescence response mostly unchanged. * It is referred to an average of luminescence intensity upon 6 replicas*

To sum up, the overall luminescence intensity does not change during the titration, since the main initial contribution to the luminescence is related to EuL-citrate, whose decrease during the titration (red curve, Figure 5.33) is compensated by the EuL-HCO_3^- adduct formation. The increase of this adduct compensates also the loss of luminescence intensity due to the decreasing amount of EuLBSA adduct (Figure 5.33). This is also in agreement with the theoretical plot obtained by equation 5.4 (Figure 5.34).

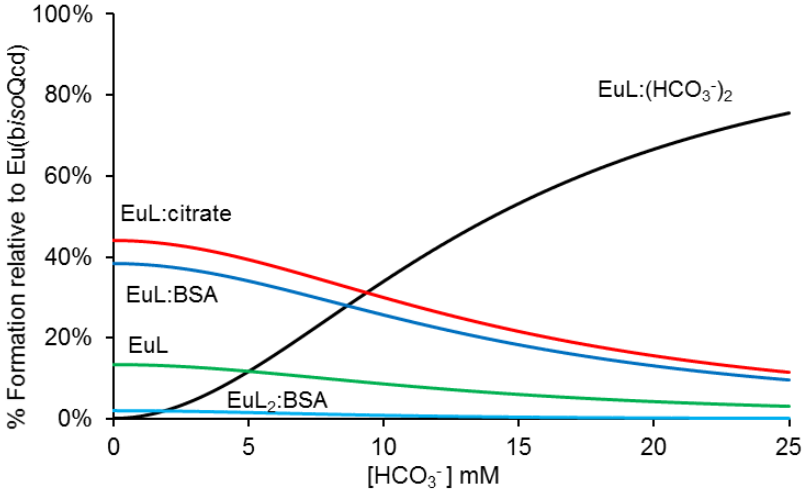

Figure 5.33 *Species distribution in the titration of Eu(bisoQcd) [EuL = 0.1 mM] (green line) with HCO_3^- (black line), BSA (blue line) and citrate (red line) during a) hydrogen carbonate addition [BSA = 0.4 mM, citrate = 0.3mM, HCO_3^- = 0 - 25 mM]. Percentages are relative to total EuL concentration [EuL = 0.1 mM]*

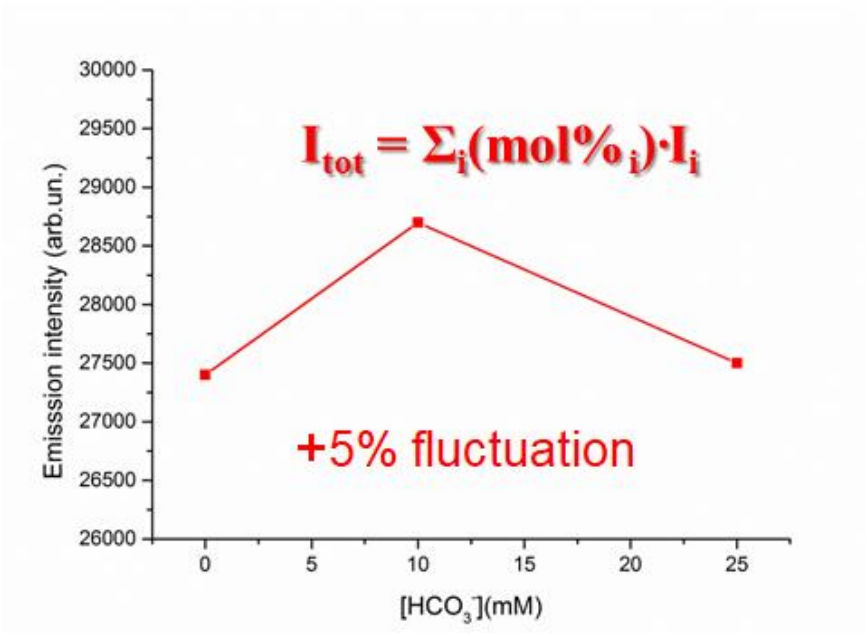

Figure 5.34 *Theoretical plot obtained by equation 5.4*

3

The BSA (up to 0.5 mM) was added in a fixed background of citrate (0.3 mM) and HCO_3^- (25 mM). A small decrease (≈10% at 0.4 mM BSA) of the luminescence intensity has been observed (Figure 5.35).

This can be explained by an increase of the EuL-BSA adduct concentration (≈13%) accompanied by a concomitant decrease of the EuL-HCO_3^- (≈7%) and EuL-citrate (≈3%) adducts (Figure 5.36).

Since the overall luminosity of the EuL-BSA adduct is the lowest one compared to the adducts with citrate and HCO_3^- in extracellular range, a slight loss in luminescence intensity is noticed. This is also in partial agreement with the theoretical plot obtained by equation 5.4 (Figure 5.37).

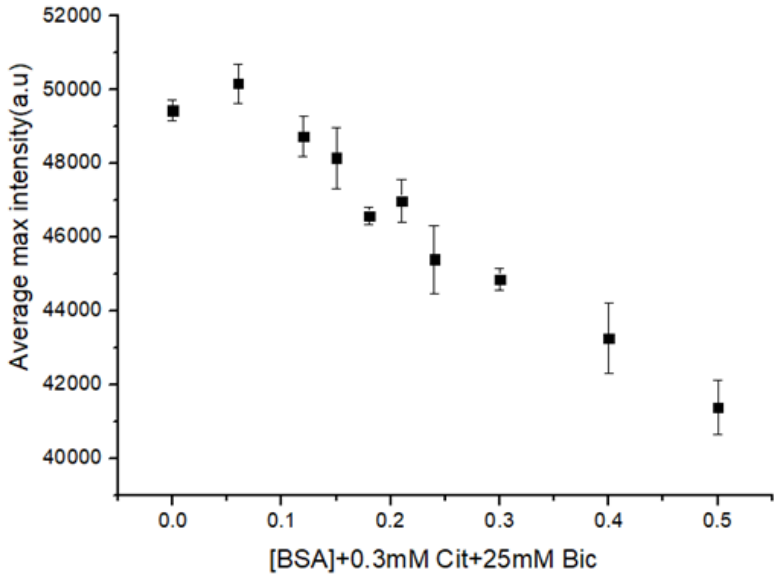

Figure 5.35 *Average maximum intensity* vs. [BSA] mM in a fixed background of HCO_3^- 25 mM and citrate 0.3 mM for bisoQcd (1S, 2S), with a luminescence decrease of around 12%. * It is referred to an average of luminescence intensity upon 6 replicas*

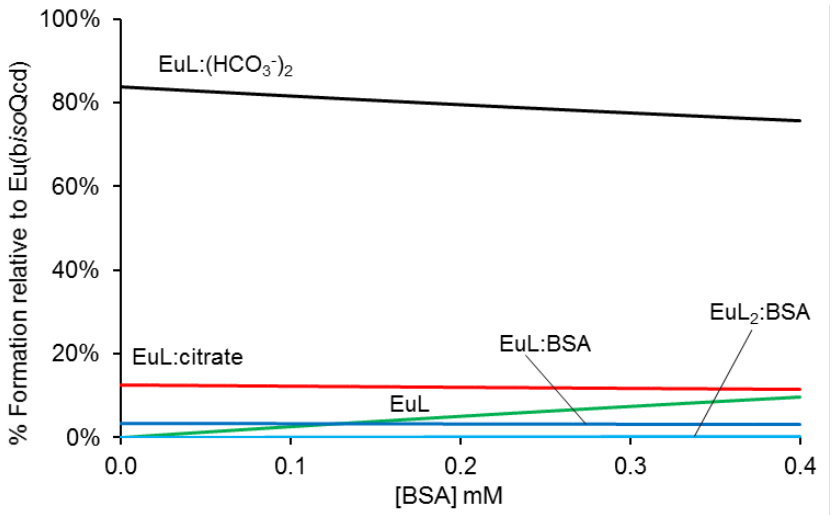

Figure 5.36 *Species distribution in the titration of Eu(bisoQcd) [EuL = 0.1 mM] (green line) with HCO_3^- (black line), BSA (blue line) and citrate (red line) during BSA addition [HCO_3^- = 25 mM, citrate = 0.3 mM, BSA = 0 - 0.4 mM]. Percentages are relative to total EuL concentration [EuL = 0.1 mM]*

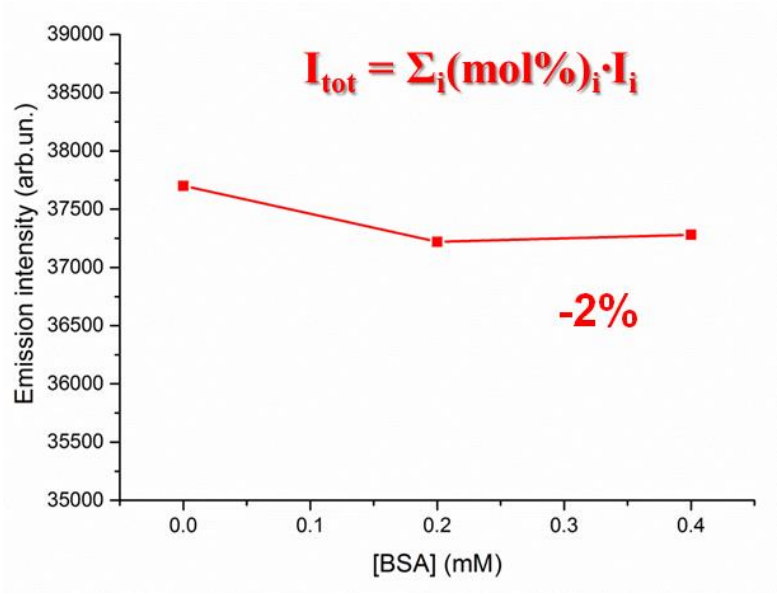

Figure 5.37 *Theoretical plot obtained by equation 5.4*

In the case of the Eu(bisoQcd) complex, the theoretical plots for experiments 1, 2 and 3 are reported in Figure 5.38, by applying Equation 5.4, at the begin, in the middle and at the end of the titrations. The molar fractions (X_i) of each luminescent species obtained under these conditions are reported in Table 5.11.

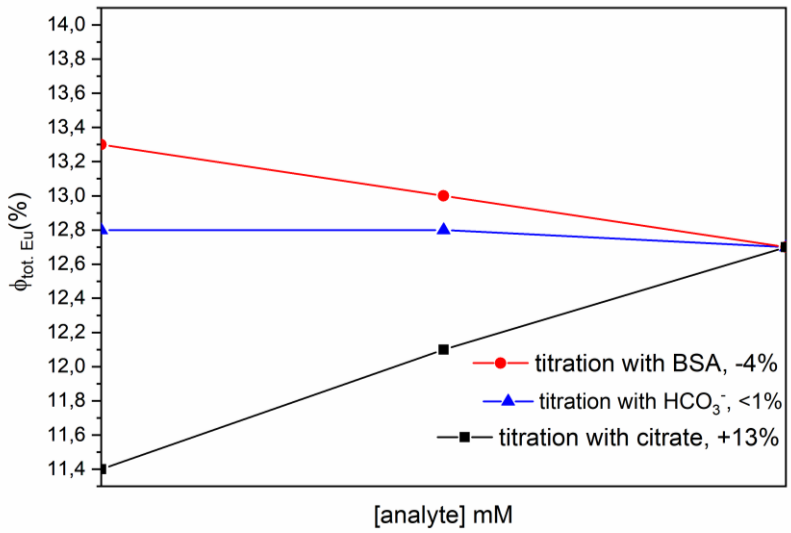

Figure 5.38 *Theoretical plot of $\Phi_{tot}Eu(\%)$ vs mM concentration of the bio-analyte during the titration. Bio-analyte = HCO_3^- (exp. 1, red line, triangle, 0 - 25 mM concentration range); BSA (exp.2, green line, circle, 0 - 0.4 mM concentration range) and citrate (exp. 3, blue line, square, 0 - 0.3 mM concentration range). In all cases, the contribution to $\Phi_{tot}Eu(\%)$ of the [Eu(bisoQcd)]$_2$BSA adduct was neglected due to its very low concentration in solution*

It is interesting to note that, upon addition of citrate at its typical extracellular concentration range a significant increase of the Eu(III) luminescence quantum yield is predicted the theoretical model. Additionally, a small decrease of the quantum yield was calculated in the case of BSA, whereas for hydrogen carbonate the luminescence quantum yield remained unchanged. Hence, from a qualitative point of view, all these findings well agree with the experimental results shown Figure 5.24. This, in turn, also demonstrates the validity of the lifetime data obtained by the decay time measurements, as well as those of the speciation analysis.

Table 5.11 *Concentrations (mmol L^{-1}) and the relative formation percent (Xi) of each luminescence species upon titration of Eu(bisoQcd) with HCO_3^-, BSA and citrate, at the beginning, in the middle and at the end of the titrations, referred to total EuL concentration. The total concentration of the Eu(III) is 0.1 mM. The total concentration of the interfering bio-analytes is the typical extracellular one (25 mM for HCO_3^-, 0.4 mM for BSA and 0.3 mM for citrate). In all solutions, the concentration of the $[Eu(bisoQcd)]_2$·BSA adduct is negligible*

$[HCO_3^-]_{TOT}$	[free complex]	[BSA adduct]	$[HCO_3^-$ adduct]	[citrate adduct]	$\%HCO_3^-$ adduct	%BSA adduct	%citrate adduct	% free complex
0	0.0134	0.0383	0	0.0442	**0**	**38.3**	**44.2**	**13.4**
12.5	0.00723	0.0217	0.0443	0.0255	**44.3**	**21.7**	**25.5**	**7.23**
25	0.00308	0.00954	0.0756	0.0114	**75.6**	**9.54**	**11.4**	**3.08**
$[BSA]_{TOT}$	[free complex]	[BSA adduct]	$[HCO_3^-$ adduct]	[citrate adduct]	$\%HCO_3^-$ adduct	%BSA adduct	%citrate adduct	% free complex
0	0.00342	0	0.0839	0.0127	**83.9**	**0**	**12.7**	**3.42**
0.2	0.00324	0.00502	0.0795	0.0120	**79.6**	**5.02**	**12.0**	**3.24**
0.4	0.00308	0.00954	0.0756	0.0114	**75.6**	**9.54**	**11.4**	**3.08**
$[citrate]_{TOT}$	[free complex]	[BSA adduct]	$[HCO_3^-$ adduct]	[citrate adduct]	$\%HCO_3^-$ adduct	%BSA adduct	%citrate adduct	% free complex
0	0.00348	0.0108	0.0855	0	**85.5**	**10.8**	**0**	**3.48**
0.15	0.00327	0.0101	0.0802	0.00606	**80.2**	**10.1**	**6.06**	**3.27**
0.3	0.00308	0.00954	0.0756	0.0114	**75.6**	**9.54**	**11.4**	**3.08**

4

In last experiment, we employed an even more complex matrix to further highlight the capabilities of our Eu(III) probes for citrate determination. Citrate (0-3.5 mM) was added to a simulated serum fluid containing BSA (0.4 mM), Sodium hydrogen carbonate (28 mM), di-Sodium hydrogen phosphate (1.3 mM), L-lactate (2.3 mM) and Sodium sulfate (0.6 mM). After progressive addition of citrate, the final emission reached a moderate increase of 23% and 16% respectively for Eu(bisoQcd) and Eu(isoQC3A) complex (Figure 5.39).

It is obvious from the obtained data that, citrate can be determined quantitatively with both complexes in complex matrices up to concentrations of 500 μM, due to the considerable luminescence increase induced by the coordination of citrate. This makes both Eu(bisoQcd) and Eu(isoQC3A) viable probes for citrate analysis in complex biological fluids.

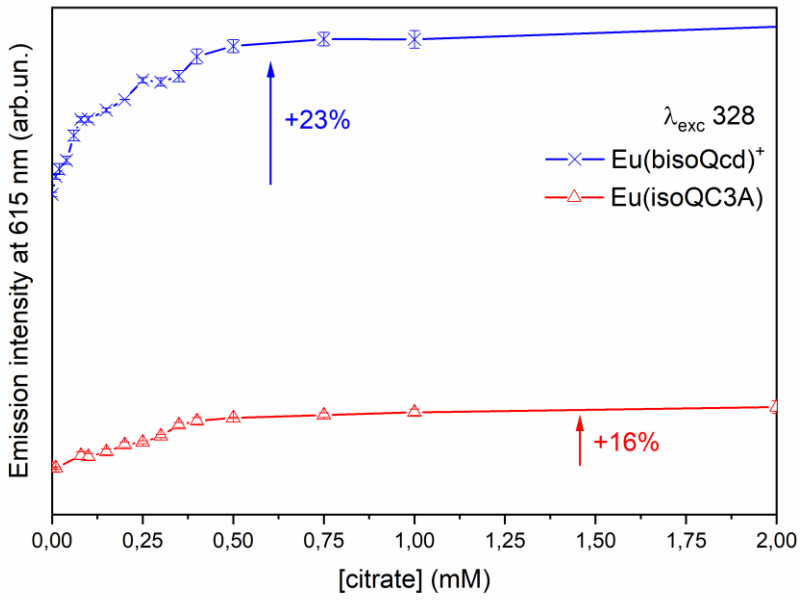

Figure 5.39 *Evolution of Eu(III) emission intensity upon titration (in simulated EF) of Eu(bisoQcd) and Eu(isoQC3A), both 0.1 mM, with citrate. Fixed background: BSA (0.4 mM), HCO_3^- (28 mM), Na_2HPO_4 (1.3 mM), L-lactate (2.3 mM) and Na_2SO_4 (0.6 mM)*

5.3.6 Conclusions

The isoquinoline-based complexes Eu(bisoQcd) and Eu(isoQC3A) have revealed to be valid probes for the optical detection of citrate anions in complex matrix, like for instance interstitial EF. Moreover, they exhibit good thermodynamic stability in water, an efficient sensitization of the Eu(III) luminescence upon excitation of the organic ligands in the near-UV spectral region (330 nm) and a high selectivity concerning the citrate anion.

In the case of the Eu(bisoQcd) complex, a total Eu(III) luminescence intensity increase of 30% at 615 nm was detected when the extracellular concentration of citrate is reached in a complex matrix containing hydrogen carbonate and BSA, as main interfering bio-analytes. In addition, when all major constituents of interstitial extracellular fluid are considered (hydrogen carbonate, BSA, L-lactate, hydrogen phosphate and sulphate) this increase is still high at 23%.

Even though a similar affinity of both Eu(III) complexes towards hydrogen carbonate, BSA and citrate was observed, the selectivity towards the latter bio-analyte can be explained by considering the highest Eu(III) luminescence quantum yield of the corresponding adduct. Nevertheless, the absorption intensity of the excitation light is lower in the case of the Eu(isoQC3A) complex, since only one chromophoric unit is present. This is in accordance with its lower optical sensitivity towards citrate concentration changes. In conclusion, Eu(bisoQcd) can be considered a better optical probe for citrate detection in various kinds of biological fluids.

A further application can foresee the development of an analytical method to measure the citrate level in interstitial EF both in normal condition (0.1 - 0.3 mM of citrate) and in samples where the citrate concentration is altered (above 0.3 mM).

5.4 Bibliography

[1] S. J. Butler, D. Parker, *Chem. Soc. Rev.* **2013**, *42*, 1652–1666.
[2] X.-L. Han, F.-F. Tian, Y.-S. Ge, F.-L. Jiang, L. Lai, D.-W. Li, Q.-L. Yu, J. Wang, C. Lin, Y. Liu, *J. Photochem. Photobiol. B.* **2012**, *109*, 1–11.
[3] D. Aristova, G. Volynets, S. Chernii, M. Losytskyy, A. Balanda, Y. Slominskii, A. Mokhir, S. Yarmoluk, V. Kovalska, *R. Soc. open Sci.* **2020**, *7*, 200453.
[4] S. Tayyab, S. R. Feroz, *Adv. Protein Chem. Struct. Biol.* **2021**, *123*, 193–218.
[5] T. E. Finn, A. C. Nunez, M. Sunde, S. B. Easterbrook-Smith, *J. Biol. Chem.* **2012**, *287*, 21530–21540.
[6] V. A. Kuzmin, T. D. Nekipelova, T. A. Podrugina, G. V Golovina, A. A. Kostyukov, V. V Temnov, I. A. Doroshenko, E. V Radchenko, V. A. Palyulin, N. S. Zefirov, *Photochem. Photobiol. Sci. Off. J. Eur. Photochem. Assoc. Eur. Soc. Photobiol.* **2016**, *15*, 1377–1384.
[7] G. J. van der Vusse, *Drug Metab. Pharmacokinet.* **2009**, *24*, 300–307.
[8] F. Moreno, M. Cortijo, J. González-Jiménez, *Photochem. Photobiol.* **1999**, *69*, 8–15.
[9] T. Kosa, T. Maruyama, M. Otagiri, *Pharm. Res.* **1997**, *14*, 1607–1612.
[10] K. D. Volkova, V. B. Kovalska, M. Y. Losytskyy, A. Bento, L. V. Reis, P. F. Santos, P. Almeida, S. M. Yarmoluk, *J. Fluoresc.* **2008**, *18*, 877–882.
[11] P. Caravan, *Acc.Chem.Res.* **2009**, *42*, 851–862.
[12] M. K. Thompson, D. M. J. Doble, L. S. Tso, S. Barra, M. Botta, S. Aime, K. N. Raymond, *Inorg. Chem.* **2004**, *43*, 8577–8586.
[13] D. Kong, C. Qin, P. Fan, B. Li, J. Wang, *Spectrochim. Acta. A. Mol. Biomol. Spectrosc.* **2015**, *140*, 372–381.
[14] G. L. Law, C. Man, D. Parker, J. W. Walton, *Chem. Commun.* **2010**, *46*, 2391–2393.
[15] A. Brandner, T. Kitahara, N. Beare, C. Lin, M. T. Berry, P. S. May, *Inorg. Chem.* **2011**, *50*, 6509–6520.
[16] S. Aime, E. Gianolio, E. Terreno, G. B. Giovenzana, R. Pagliarin, M. Sisti, G. Palmisano, M. Botta, M. P. Lowe, D. Parker, *J. Biol. Inorg. Chem.* **2000**, *5*, 488–497.
[17] D. C. Carter, J. X. Ho, *Adv. Protein Chem.* **1994**, *45*, 153–176.
[18] J. Li, J. Li, Y. Jiao, C. Dong, *Spectrochim. Acta Part A Mol. Biomol. Spectrosc.* **2014**, *118*, 48–54.
[19] J. R. Lakowicz, *Principles of Fluorescence Spectroscopy*, Springer, New York, **2006**.
[20] L. Alderighi, P. Gans, A. Ienco, D. Peters, A. Sabatini, A. Vacca, *Coord. Chem. Rev.* **1999**, *184*, 311–318.
[21] P. Gans, A. Sabatini, A. Vacca, *J. Solution Chem.* **2008**, *37*, 467–476.
[22] M. D. Meti, S. T. Nandibewoor, S. D. Joshi, U. A. More, S. A. Chimatadar, *J. Pharm. Anal.* **2015**, *5*, 249–255.
[23] X. Peng, W. Qi, R. Huang, R. Su, Z. He, *PLoS One* **2015**, *10*, e0118274.
[24] G. Zhang, N. Zhao, L. Wang, *J. Lumin.* **2011**, *131*, 2716–2724.
[25] K. Phopin, W. Ruankham, S. Prachayasittikul, V. Prachayasittikul, T. Tantimongcolwat, *Int. J. Mol. Sci.* **2019**, *21*, 249.
[26] C. Ràfols, S. Amézqueta, E. Fuguet, E. Bosch, *J. Pharm. Biomed. Anal.* **2018**, *150*, 452–459.
[27] S. He, J. W. Morse, *Geochim. Cosmochim. Acta* **1993**, *57*, 3533–3554.
[28] M. Damaghi, J. Wojtkowiak, R. Gillies, *Front. Physiol.* **2013**, *4*, 370.
[29] J. D. Kopple, K. Kalantar-Zadeh, R. Mehrotra, *Kidney Int. Suppl.* **2005**, *67*, S21–S27.
[30] F. J. Voskuil, P. J. Steinkamp, T. Zhao, B. van der Vegt, M. Koller, J. J. Doff, Y. Jayalakshmi, J. P. Hartung, J. Gao, B. D. Sumer, et al., *Nat. Commun.* **2020**, *11*, 3257.
[31] J. Buck, L. R. Levin, *Sensors* **2011**, *11*, 2112–2128.
[32] E. Boedtkjer, V. Matchkov, D. Boedtkjer, C. Aalkjaer, *Physiology* **2016**, *31*, 370–383.
[33] Y. Bretonniere, M. J. Cann, D. Parker, R. Slater, *Org. Biomol. Chem.* **2004**, *2*, 1624–1632.
[34] Y. Bretonnière, M. J. Cann, D. Parker, R. Slater, *Chem. Commun.* **2002**, 1930–1931.
[35] B. S. Murray, E. J. New, R. Pal, D. Parker, *Org. Biomol. Chem.* **2008**, *6*, 2085–2094.
[36] D. G. Smith, G. Law, B. S. Murray, R. Pal, D. Parker, K.-L. Wong, *Chem. Commun.* **2011**, *47*, 7347–7349.

[37] S. E. Bodman, S. J. Butler, *Chem. Sci.* **2021**, *12*, 2716–2734.
[38] D. Imperio, G. B. Giovenzana, G. L. Law, D. Parker, J. W. Walton, *Dalt. Trans.* **2010**, *39*, 9897–9903.
[39] S. J. Butler, B. K. McMahon, R. Pal, D. Parker, J. W. Walton, *Chem. - A Eur. J.* **2013**, *19*, 9511–9517.
[40] J. C. G. Bünzli, *Chem. Rev.* **2010**, *110*, 2729–2755.
[41] G. Tircsó, Z. Garda, F. K. Kálmán, Z. Baranyai, I. Pócsi, G. Balla, I. Tóth, *J. Inorg. Biochem.* **2013**, *127*, 53–61.
[42] S. Comby, S. A. Tuck, L. K. Truman, O. Kotova, T. Gunnlaugsson, *Inorg. Chem.* **2012**, *51*, 10158–10168.
[43] R. S. Dickins, T. Gunnlaugsson, D. Parker, R. D. Peacock, *Chem. Commun.* **1998**, 1643–1644.
[44] D. G. Smith, R. Pal, D. Parker, *Chem. – A Eur. J.* **2012**, *18*, 11604–11613.
[45] B. K. McMahon, D. Parker, *RSC Adv.* **2014**, *4*, 37649–37654.
[46] R. Pal, D. Parker, L. C. Costello, *Org. Biomol. Chem.* **2009**, *7*, 1525–1528.
[47] M. L. Aulsebrook, B. Graham, M. R. Grace, K. L. Tuck, *Coord. Chem. Rev.* **2018**, *375*, 191–220.
[48] M. H. V. Werts, R. T. F. Jukes, J. W. Verhoeven, *Phys. Chem. Chem. Phys.* **2002**, *4*, 1542–1548.
[49] R. S. Dickins, S. Aime, A. S. Batsanov, A. Beeby, M. Botta, J. I. Bruce, J. A. K. Howard, C. S. Love, D. Parker, R. D. Peacock, et al., *J. Am. Chem. Soc.* **2002**, *124*, 12697–12705.
[50] J.-C. G. Bünzli, *Coord. Chem. Rev.* **2015**, *293*, 19–47.

Chapter 6

General conclusions and future outlook

The new library of luminescent Eu(III) complexes synthetized and characterized in this PhD project shown promising and motivating properties for biosensing applications. All the complexes are water soluble, stable at physiological ionic strength and pH. The overall stability constants found are quite high and in accordance with values found in literature for similar complexes.

Both the thermodynamic and DFT studies, shown that the tri-acetate ligand form more stable europium complexes than the di-acetate ones. This is fundamental since Ln(III) ions present oxophylic character, and prefer bind ligands containing more oxygen donating atoms.

All complexes in aqueous solution are 8-fold coordinated, bearing two water molecules in the first coordination sphere and one 6-fold coordinating chiral ligand. These water molecules ca be easily displaced by a target bio-analyte, modulating then the luminescent intensity stemming from the optical probe. As far as the sensitization mechanism is concerned, the isoquinoline rings effectively sensitize only the Eu(III) ion. This is a crucial feature to consider during the design of the luminescent probes and the choice of the heteroaromatic antenna.

The only one component of the Eu(III) $^5D_0 \rightarrow {}^7F_0$ transition and the luminescence decay curves, properly fitted by a single exponential function, confirm the existence of only one main emitting species in solution. In addition, the total quantum yields shown by our optical probe, are in agreement with the values found in literature for cell imaging with either lanthanide or d-block complexes (around 10%).

All the Eu-complexes have been designed with 6–fold coordinating ligands with displaceable solvent molecules by target molecules present in the biological fluids.

The bio-analytes under investigation have been the components of the extracellular fluid at their typical concentration range. One of the promising response has been obtained for the sensing of the bicarbonate ion. The diacetate Eu(bisoQcd) complexes shown a logK values higher than 4, an unprecedented value in the literature. In addition, the luminescence response towards HCO_3^- is particularly selective in the 2-10 mM concentration range of the bio-analyte. This range of concentration is related to serious kidney disease (metabolic acidosis).

Another component that has been investigated was the serum albumin, for simplicity, the homologous Bovine Serum Albumin (BSA) was used. The Eu(bpcd)Cl (1R, 2R) and Eu(bisoQcd)OTf (1R, 2R) complexes revealed an opposite Eu(III) luminescence

response, despite the same experimental conditions. The Eu(bpcd) complex displayed a drastic decrease of the luminescence intensity during the progressive addition of the protein, while the Eu(bisoQcd) complex revealed a significant luminescence increase (≈80%). Docking studies shown that the luminescence changes observed for Eu(bisoQcd) complex interacting with BSA foresee the displacement of one water molecules from the metal center by the coordinating groups of the protein (the carboxylic group of the GLU17 residue). On the other hand, the luminescence changes in the case of the Eu(bpcd) complex have been explained by a protein/complex interaction which takes place on the surface of the protein, that influences the efficiency of the energy transfer from pyridine to lanthanide ion.

The diacetate and triacetate isoquinoline based complexes revealed to be promising for citrate signalling at its typical extracellular concentration. A significant enhance of the emission intensity ≈1.5 fold the initial luminescence emission has been detected for both Eu(bisoQcd) and Eu(isoQC3A) complexes, with higher probe-citrate binding constant for the diacetate complex. As concerns the detection of the other main components of the EF, a negligible contribution has been verified for phosphate, sulphate and L-lactate.

In regard of the results obtained, it would be interesting to perform further experiments, in order to complete the affinity study and the luminescent response with other bio-analyte and interfering molecules, for instance phosphate and ATP. In addition, CPL studies may be performed to observe the complex response in the presence of the bio-analytes.

Further outlook would be to test the probes in vivo, in order to check the cell viability and permeability, which would lead our luminescent probes closer to their concrete diagnosis application.

Annexes

I Eu(III) complex / BSA Interaction: MD data

II List of publications and communications

Annex I

The aminoacidic residues present on the external surface of this cavity, involved in the interaction with the pyridine-based complex, consist of several groups arising from four residues of phenylalanine (F227, F308, F325 and F329) and two residues of tyrosine (Y318 and Y331). In this superficial area also five negatively charged carboxylic groups are present [from three aspartic acids (D307, D311, D313) and two glutamic acids (E320, E332)]. This is in line with the possible interactions that Y(bpcd) can create with the protein.

Above all, the positive charge of the complex can lead to an electrostatic interaction with the negatively charged aspartic and glutamic acid side chains. The pyridine rings of the ligand can interact with Van der Waals forces to side groups of aromatic amino acids listed above. Since such amino acids (phenylalanine and tyrosine) contribute to a small protein fluorescence extent, their Eu(bpcd) complex interaction involvement could affect only marginally the BSA fluorescence spectrum (Figure I).

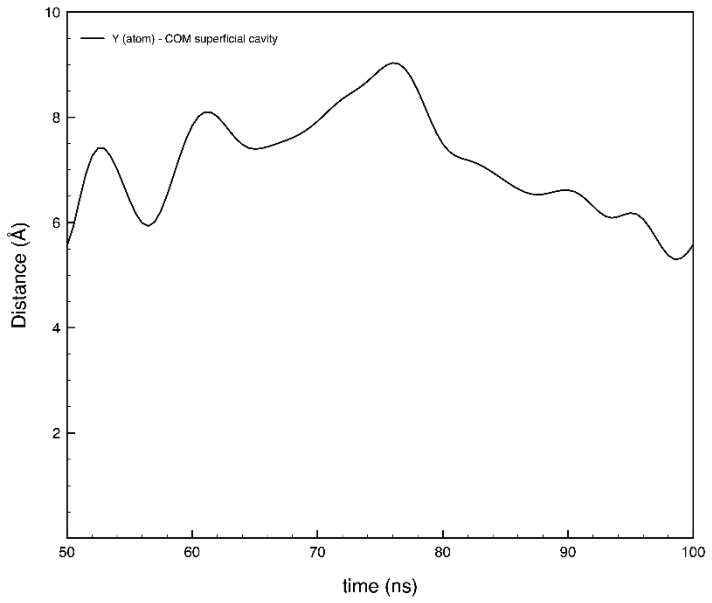

Figure I *Graphical representation of the distance between the Y atom of Y(bpcd) complex and the center of mass (COM) of the superficial cavity residues. These were selected according to a cut-off of 10 Å from the Y atom. The initial 50 ns were not shown for the sake of clarity, as the molecule explores the entire protein's surface*

Upon interaction, the metal ion does not lose the two bound water molecules, as shown in the Figure II a, where the graphical representation of the radial distribution function of the O(water)-Y pairs is reported. It results that the number of water molecules in the inner coordination sphere of the metal ion (at 2.6 Å) is around two, both in the simulation in bulk water and upon interaction with the protein. This is in good agreement with the analysis of the Eu(III) luminescence decay curves discussed in previously.

a

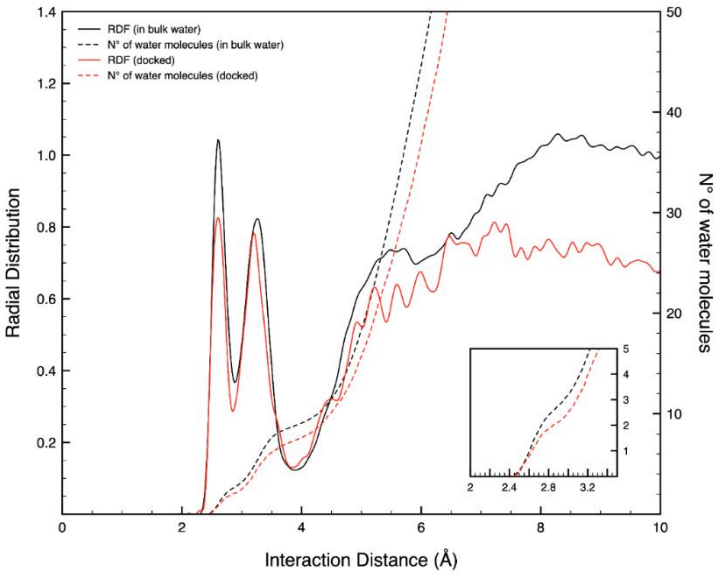

b

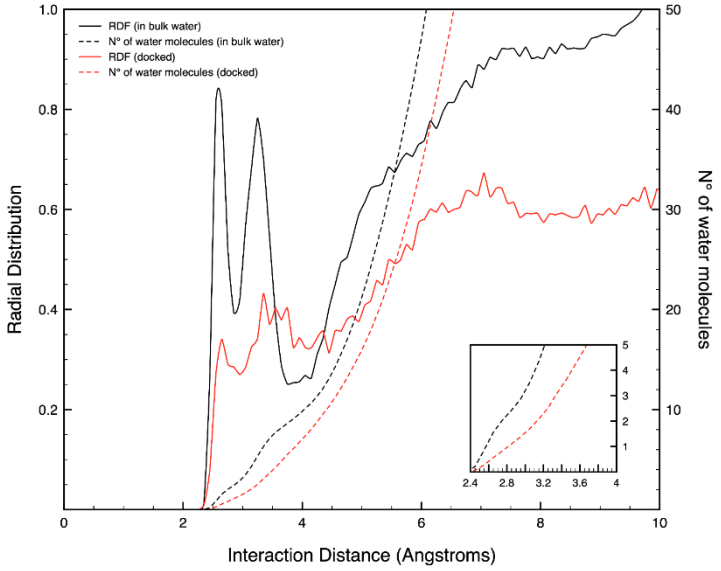

Figure II *Radial distribution function and the number of water molecules as a function of the interaction distance between Y(III) and water molecules, during a simulation in bulk water and upon interaction with BSA, black and red lines, respectively; for the complex with bpcd as a ligand (a) and bisoQcd (b)*

On the other hand, Y(bisoQcd) showed a selective interaction with the outer binding site containing the Trp residue 134, since it remained in this protein superficial area through all the simulation time (100 ns). In addition, as in the case of the Y(bpcd) derivative, no interaction occurs with the buried Trp213.

Focusing on the superficial binding site, the distance between Y(III) and Trp134 was constant (around 6.8 Å) over all simulation time (Figure III).

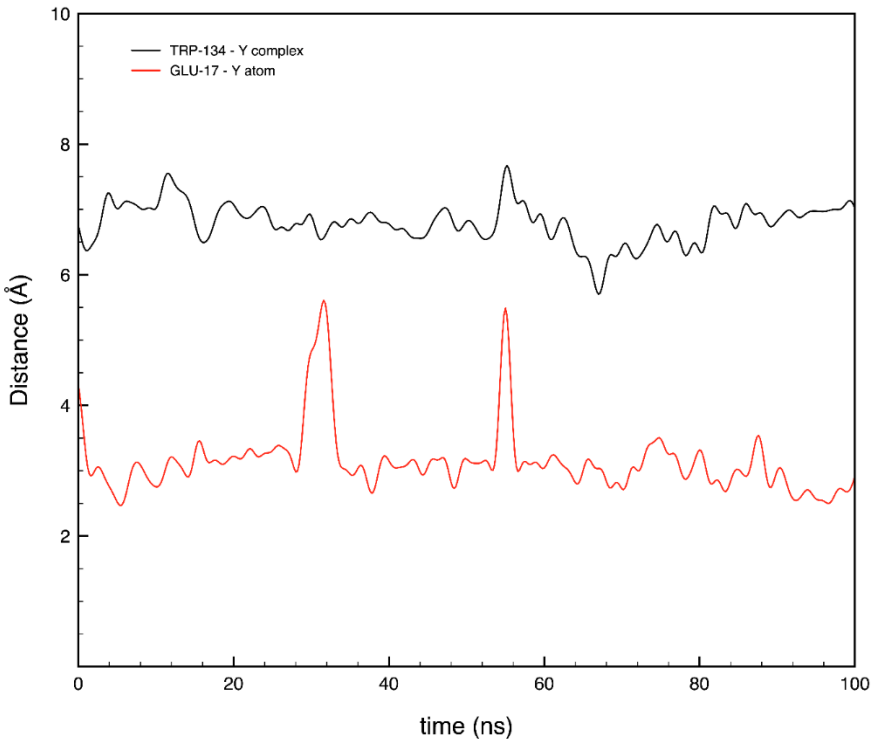

Figure III *Graphical representation of the distance between the side chain of Trp134 and the Y(III) (black plot), and E17 and Y(III) (red plot), in the case of Y(bisoQcd) complex*

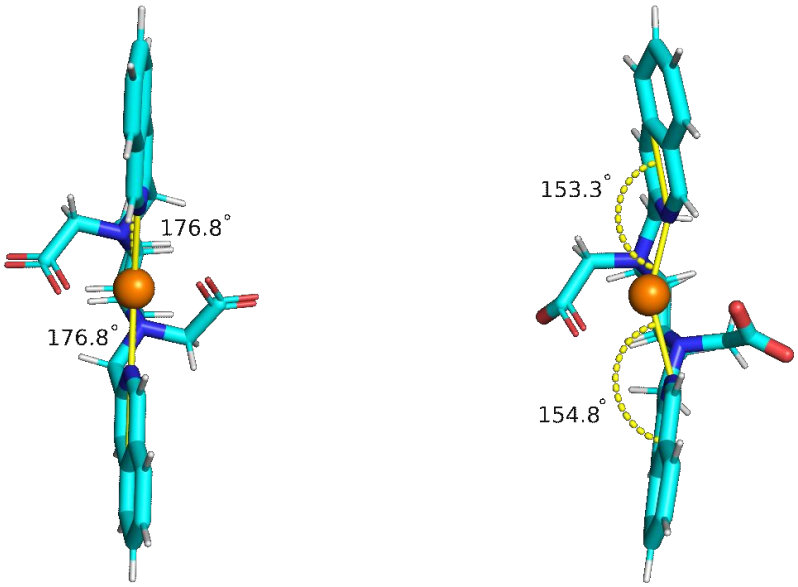

Figure IV *Representation of the geometry before (left) and after (right) the interaction with BSA for the Y(bisoQcd) complex*

Focusing on the complex geometry, only small differences in the orientation of the heteroaromatic fragments are noticed for Y(bisoQcd) upon interaction with BSA (Figure IV). In contrast, a significant change in the orientation of the pyridine rings was detected in the case of the Y(bpcd) complex. In this case, the lone pair of one pyridine nitrogen is not pointing precisely towards the metal ion (Figure V).

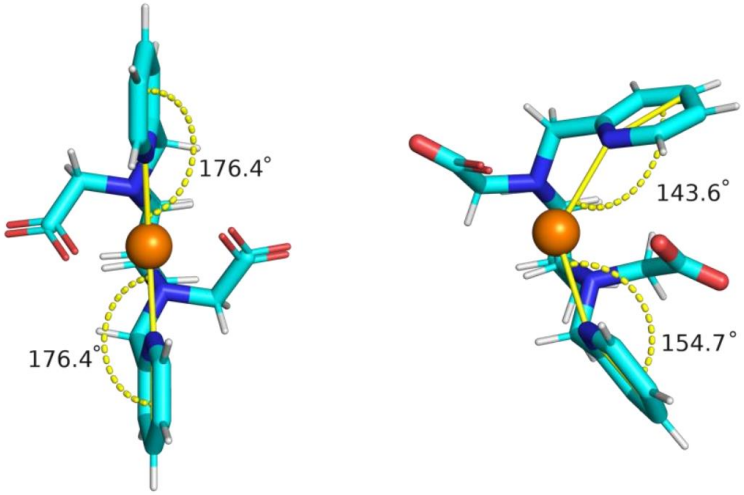

Figure V *Representation of the geometry before (left) and after (right) the interaction with BSA for the Y(bpcd) complex*

Annex II

PUBLICATIONS

2021 Processes, 9, 1873-1899

Y. Roque-Diaz, M. Sanadar, D. Han, M. López-Mesas, M. Valiente, M. Tolazzi, A. Melchior, D. Veclani

The Dark Side of Platinum Based Cytostatic Drugs: From Detection to Removal

2021 Dalton Transactions, 50, 4700-4712

C. De Rosa, A. Melchior, M. Sanadar, M. Tolazzi, A. Duerkop, F. Piccinelli

Isoquinoline-based Eu(III) luminescent probes for citrate sensing in complex matrix

2020 Inorganic Chemistry, 59, 12564–12577

C. De Rosa, A. Melchior, M. Sanadar, M. Tolazzi, A. Giorgetti, R. P. Ribeiro, C. Nardon, F. Piccinelli

Effect of the Heteroaromatic Antenna on the Binding of Chiral Eu(III) Complexes to Bovine Serum Albumin

COMMUNICATIONS

*** Presenting author**

14-23/09/2021 XXVII CONGRESSO NAZIONALE DELLA SOCIETÀ CHIMICA ITALIANA - Online, Italy

Participation grant by Division of Chemistry for the Technology of the Italian Chemical Society

Oral communication: M. Sanadar*, A. Melchior, M. Tolazzi, C. De Rosa, A. Duerkop, F. Piccinelli

A novel luminescent Europium (III) complexes for citrate detection

14-23/09/2021 XXVII CONGRESSO NAZIONALE DELLA SOCIETÀ CHIMICA ITALIANA - Online, Italy

Oral communication: S. Ruggieri*, F. Piccinelli, L. Di Bari, M. Sanadar, A. Melchior, A. Gualandi, C. Nardon

New chiral heteroleptic Eu(III)/Tb(III)/Yb(III)-based luminescent complexes designed for different applications

25-27/08/2021 2nd European NECTAR Conference - Lisboa, Portugal

Oral communication: M. Sanadar, M. Bettinelli, M. Tolazzi, F. Piccinelli, A. Melchior*

Thermodynamic and structural and aspects of Ln(III) complexes with N-donor heteroaromatic ligands and their interaction with bio-analytes

5-8/09/2021 XII CONGRESSO NAZIONALE ASSOCIAZIONE ITALIANA CHIMICA PER L'INGEGNERIA – Reggio Calabria, Italy

Poster: M. Sanadar*, A. Melchior, M. Tolazzi, C. De Rosa, A. Duerkop, F. Piccinelli

Europium(III) complexes as optical probes for bioanalytes sensing

16-18/06/2021 International Symposia on Thermodynamics of Metal Complexes – Online, Poland

Oral communication: M. Sanadar*, A. Melchior, M. Tolazzi, C. De Rosa, A. Duerkop, F. Piccinelli

Luminescent Eu(III) complexes as probes for citrate sensing in complex matrix

27-28/01/2021 XLII National Conference on Calorimetry, Thermal Analysis and Applied Thermodynamics – Online, Italy

Member of the organizing committee, Participation grant by The Italian Association for Thermal Analysis and Calorimetry

Oral communication: M. Sanadar*, A. Melchior, M. Tolazzi, C. De Rosa, F. Piccinelli

Calorimetric and fluorimetric interaction studies of Europium(III) complexes with Bovine Serum Albumin

27-28/01/2021 XLII National Conference on Calorimetry, Thermal Analysis and Applied Thermodynamics – Online, Italy

Member of the organizing committee, Participation grant by The Italian Association for Thermal Analysis and Calorimetry

Poster: M. Sanadar*, Y. Roque-Diaz, A. Melchior, M. Tolazzi, D. Veclani, P. Polese, M. Valiente

Platinum compounds adsorption on modified silica for water treatment

12-14/10/2020 PhD Week 2020, PhD Course in Environmental and Energy Engineering Science – Udine, Italy

Energy and Environmental Engineering Science PhD Best Poster Award

Poster: M. Sanadar*

Building luminescent sensors for on the fly bio-analysis

11-13/12/2018 School of Nanomedicine – Trieste, Italy

Poster: M. Sanadar*, M. Tolazzi, C. De Rosa, F. Piccinelli, A. Melchior

Luminescent lanthanide complexes for biomarkers sensing